Università degli Studi di Firenze

DOTTORATO DI RICERCA IN
Biochimica e Biologia Applicata

CICLO XXV

Dipartimento di Scienze Biomediche Sperimentali e Cliniche
COORDINATORE Prof.ssa Donatella Degl'Innocenti

Early-forming aberrant aggregates in protein deposition diseases: structural characteristics, interaction with molecular chaperones, ability to trigger inflammation

Settore Scientifico Disciplinare BIO/10

Dottorando
Dott.ssa Mannini Benedetta

Tutore
Prof. Chiti Fabrizio

Anni 2010/2012

To Argante and Corrado,
Dina and Edda

Table of Contents

SUMMARY

Protein aggregation into amyloid fibrils is the hallmark of many human pathologies, including Alzheimer's disease and Parkinson's disease. The aberrant assembly of peptides and proteins into fibrillar aggregates proceeds through oligomeric intermediates thought to be the primary pathogenic species in many of these protein deposition diseases. Since the first year of my PhD, I have been studying protein aggregation, focusing on misfolded protein oligomers formed by the N-terminal domain of the bacterial HypF protein from *E. coli* (HypF-N). These oligomers are a useful model system in the context of disease-associated protein aggregation because they have the same properties as the disease-related ones and are highly stable, allowing a detailed structural and functional investigation. Moreover, under two different conditions, HypF-N aggregates into two types of oligomers characterized by an opposite biological activity, since only one is toxic whereas the other is benign to cultured cells, facilitating the utilization of appropriate control nontoxic oligomers in our experiments.

In Chapter 2, the first one describing results in my thesis, the toxicity of HypF-N oligomers, as well as the aggregates formed by the amyloid-β peptide and the islet amyloid polypeptide, was tested in the presence of molecular chaperones, namely αB-crystallin, Hsp70, clusterin, α_2-macroglobulin and haptoglobin. Molecular chaperones play a pivotal role in the regulation of the proteome homeostasis, as they facilitate protein folding, inhibit protein aggregation, disaggregate pre-formed assemblies and promote clearance of misfolded aggregates. In this chapter we show that molecular chaperones also affect the structure and toxicity of protein misfolded oligomers. Indeed, measures of the cell viability showed that all the five chaperones are effective in suppressing the toxicity of oligomers formed by all three proteins. Infrared spectroscopy

and site-directed labeling experiments using pyrene ruled out a structural reorganization within the discrete HypF-N oligomers, even at the amino acid residue level. By contrast, analysis performed using confocal microscopy, SDS-PAGE and intrinsic fluorescence measurements revealed binding between the oligomers and the chaperones; atomic force microscopy (AFM) imaging indicated that large assemblies of oligomers are formed in the presence of the chaperones. This suggests that the chaperones bind to the oligomers and promote their assembly into larger species, with consequent decrease in their diffusional mobility and burial of hydrophobic surface.

In Chapter 3, with the aim of identifying the structural determinants responsible for the toxicity of misfolded oligomers, we created a set of HypF-N oligomeric variants by replacing one or more charged aminoacids with apolar aminoacids into the sequence of the wt protein, and allowing the mutated proteins to aggregate under different conditions. The resulting oligomeric species were characterized by different levels of cytotoxicity, as assessed by measurements of MTT reduction, tests with the apoptotic marker Hoechst and measurements of Ca^{2+} influx. The structural properties of the oligomeric variants was performed by evaluating the exposure of their hydrophobic surfaces to the solvent with ANS binding and by measuring their size by means of turbidimetry and light scattering measurements. A significant correlation was found between ANS binding and size of the oligomers, indicating that an increase of surface hydrophobicity causes an increase of the size of the oligomers. Moreover, both superficial hydrophobicity and size were found to influence the oligomer biological activity, cooperating in determining the levels of toxicity of the aggregates.

In Chapter 4, we used HypF-N toxic misfolded oligomers to investigate their interactions with transthyretin (TTR). This protein is a homotetrameric protein which can disassemble into its monomers, misfold and aggregate into fibrils whose growth is

considered the cause of TTR amyloidoses. Nevertheless, an anti-amyloidogenic effect that prevents Aβ aggregation *in vitro* has recently been proposed for TTR. We have therefore explored the ability of three different types of TTR, human TTR (hTTR), mouse TTR (mTTR) and an engineered monomer of human TTR (M-TTR), to suppress the toxicity of HypF-N oligomers. Cell viability tests showed that hTTR, and to a greater extent M-TTR, can avoid the cell damage induced by protein oligomers, whereas mTTR does not show any protective effect. To shed light on the different behavior of the TTRs and on the molecular mechanism by which they can exert their potential protective ability, we have investigated the molecular structure of HypF-N oligomers after the incubation with TTRs. Thioflavin T assay and pyrene site-directed labeling showed that all the three types of TTR cannot structurally re-arrange toxic HypF-N oligomers into a nontoxic form. Intrinsic fluorescence measurements and SDS-PAGE indicated that TTRs are able to bind to the oligomers. Following this binding, hTTR, and to a greater extent M-TTR, induced the formation of larger species, as shown by AFM and turbidimetry measurements. By contrast, the interaction with mTTR does not induce such formation of clusters. These data indicate that TTR suppresses the toxicity of HypF-N oligomers similarly to well established chaperones with an efficacy that correlates with its ability to disassemble into monomers.

Finally, in Chapter 5, we tested the ability of HypF-N oligomers to induce the inflammatory response. In fact, increasing evidence suggests that neurodegeneration associated to aggregation of proteins is the result of many causes. The uncontrolled immune response in the brain has recently been established to play a central role in the onset and progression of diseases, such as Alzheimer's disease and Parkinson's disease. For this reason we explored the inflammatory response to the injury caused by HypF-N toxic and not toxic misfolded oligomers, with particular attention to the role of Hsps,

Hsp70 and αB-crystallin, as immune signals and potential suppressors of HypF-N oligomer-mediated inflammation. The results, obtained by the evaluation of microglia activation in terms of cytokine-release, showed that both the toxic and the nontoxic oligomers triggered a pro-inflammatory response, as assessed through ELISA measurements of a set of cytokines. Interestingly, at concentrations in which the two types of oligomers share the ability of leaving unaltered the cellular viability evaluated by MTT tests, the nontoxic species were found to be stronger inducers of inflammation with respect to the toxic oligomers. Such immune property of the nontoxic aggregates could be linked to their lower level of internalization in microglia cells and to the consequent maintenance of their stimulus from outside the cells. In addition, the nontoxic oligomers and the assemblies of toxic oligomers neutralized by chaperones were found to have the ability to induce inflammation without affecting cellular viability.

In conclusion, the data presented in this thesis and collected entirely using misfolded protein oligomers by the model protein domain HypF-N have revealed (i) new structural determinants of protein oligomer toxicity, such as oligomer size and hydrophobic exposure and their interplay to determine toxicity, (ii) have revealed novel mechanisms by which molecular chaperones, including the emerging TTR, contribute to the maintenance of protein homeostasis and (iii) have shown how misfolded protein oligomers can be highly inflammatory, even in the absence of explicit toxicity.

Chapter 1

INTRODUCTION

1.1 Protein aggregation

1.1.1 Folding, misfolding and aggregation of proteins

Proteins are the fundamental constituents of living organisms, since they exert essential functions, participating in all the different processes that take place in the cells. These biological macromolecules are synthetized on cellular ribosomes as unstructured polypeptide chains that are able, in general, to spontaneously self-assemble into a compact three-dimensional structure, called "native state". The native structure of a protein is necessary to allow the fulfilment of its specific function and generally corresponds to the conformation that is most thermodynamically stable under physiological conditions [Dobson *et al*., 1998]. The process through which proteins reach the native structure is the folding process and consists in a stochastic search of the most energetically favourable conformation, passing through many conformations accessible to a polypeptide chain [Levinthal, 1968; Dobson *et al*., 1998; Fersht, 2000].

The importance of reaching and remaining in the folded state for a protein is underlined by the fact that cells have evolved mechanisms of control and regulation of the folding process [Dobson, 2003], such as molecular chaperones [Bukau and Horwich, 1998; Hartl and Hayer-Hartl, 2002], the heat shock response [Voellmy and Boellmann, 2007], the unfolded protein response [Kapoor and Sanyal, 2009], the endoplasmic reticulum associated degradation [Hoseki *et al*., 2010], the ubiquitin-proteasome system [Claessen *et al*., 2012], the autophagy [Bejarano and Cuervo, 2010] and enzymes that catalyse the restructuring of proteins [Schiene and Fischer, 2000].

A failure in the folding process, termed misfolding, can lead to relevant pathological conditions afflicting the mankind and generally referred to as "protein misfolding diseases". Misfolding episodes take place when a protein adopts an alternative conformation to the native one (Figure 1.1) and, as a consequence, it can appear no longer able to perform its normal function, such as in cystic fibrosis [Amaral, 2004], or unable to be translocated in its correct functional site, as in the early pulmonary emphysema [Lomas and Carrel, 2002]. In other cases, protein misfolding can induce the aggregation of proteins into highly organized fibrillar aggregates that deposit into the cells or, most commonly, in the extracellular space (Figure 1.1) [Chiti and Dobson, 2006]. These aggregates are called "amyloid fibrils" when they accumulate in the extracellular space, or "intracellular inclusions" when they form inside the cell [Westermark *et al*., 2005] and are associated with a broad range of human pathologies.

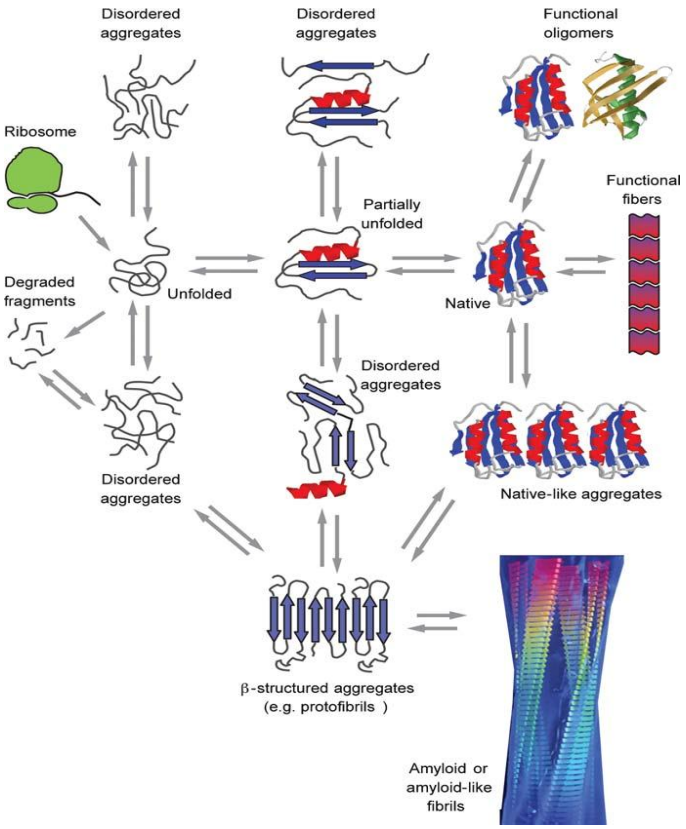

Figure 1.1. Schematic representation of some of the many conformational states that can be adopted by a polypeptide chain and of the means by which they can be interconverted. Amyloid fibrils are one of the possible aggregate forms. All of these different conformational states and their interconversions are carefully regulated in the biological environment, by using machineries such as molecular chaperones, degradation systems, and other quality control processes. Conformational diseases will occur when such regulatory systems fail. Figure taken from Chiti and Dobson, 2006.

The aggregation process leading to amyloid formation has many features of a "nucleated growth" mechanism. The time course of the conversion of a monomeric peptide or protein into its fibrillar form typically consists of a lag phase followed by a rapid exponential growth phase [Naiki *et al*., 1997; Serio *et al*., 2000; Pedersen *et al*., 2004]. The lag phase is considered to be the time required to allow the formation of "nuclei" and represents the rate-limiting step [Morris *et al*., 2009; Orte *et al*., 2008]. Once a nucleus is formed, fibril growth is thought to proceed rapidly by further association of either monomers or oligomers with the nucleus [Chiti and Dobson, 2006].

The formation of aggregates can start from any of the conformational states adopted by a monomeric protein (Figure 1.1), including the fully unfolded state, the folded state and the partially folded state, although this latter have the highest propensity to self-assemble [Bemporad *et al*., 2006; Chiti and Dobson, 2006]. The partially folded monomeric state can be found to be in rapid equilibrium with small soluble, unstructured oligomeric forms (Figure 1.1), interacting through hydrophobic surfaces exposed to the solvent that are normally buried in the native globular state. These oligomers, constituted by a few molecules and typically 2-5 nm in diameter, are transient, unstable and with heterogeneous conformations [Chiti and Dobson, 2006; Stefani, 2010]. The disordered oligomers undergo a structural reorganization into a β-sheet structure and a further association with each other to form amyloid protofibrils, which appear to be either isolated beads or beaded chains with the individual beads again having a diameter of 2-5 nm. Protofibrils can associate and act as precursor of longer protofilaments and mature fibrils, which represent the end product of the aggregation process (Figure 1.1) and are thermodynamically stable [Jahn and Radford, 2008].

It is well recognised that proteins unrelated to any amyloid disease aggregate *in vitro* into structures indistinguishable from the amyloid fibrils produced by disease-associated peptides and proteins [Gujiarro *et al*., 1998; Litvinovich *et al*., 1998; Chiti *et al*., 1999; Chiti *et al*., 2001; Fändrich *et al*., 2001; Gast *et al*., 2003; Pedersen *et al*., 2006]. Hence, the formation of highly organized amyloid aggregates appears to be a generic property of polypeptide chains, rather than a characteristic of a few proteins linked to pathological conditions [Dobson, 1999; Chiti *et al*., 1999].

1.1.2 Structural characteristics of amyloid fibrils

Amyloid fibrils share morphological, structural and tinctorial properties, despite they originate from different peptides and proteins [Dobson, 2003; Chiti and Dobson, 2006; Nelson and Eisenberg, 2006]. Images acquired through transmission electron microscopy (TEM) or atomic force microscopy (AFM) have shown that amyloid fibrils are rigid, long, unbranched and usually composed by 2-6 thinner filaments, called "protofilaments", each about 2-5 nm in diameter [Serpell *et al*., 2000]. These protofilaments twist together forming super-coiled fibrils generally 7-13 nm wide [Sunde and Blake, 1997; Serpell *et al*., 2000] or associate laterally to give origin to ribbons with a diameter ranging from 2-5 nm to 30 nm [Bauer *et al*., 1995; Saiki *et al*., 2005; Pedersen *et al*., 2006].

From a structural point of view, amyloid fibrils are characterized by a common X-ray diffraction pattern, typical of the cross-β structure consisting of parallel β-sheets whose strands are arranged perpendicularly to the long axis of the fibril [Eanes and Glenner, 1968; Sunde and Blake, 1997; Nelson and Eisenberg, 2006]. The β-sheet structure is confirmed by techniques such as circular dichroism, Fourier transform infra-red spectroscopy, solid-state NMR spectroscopy, X-ray microcrystallography and site-

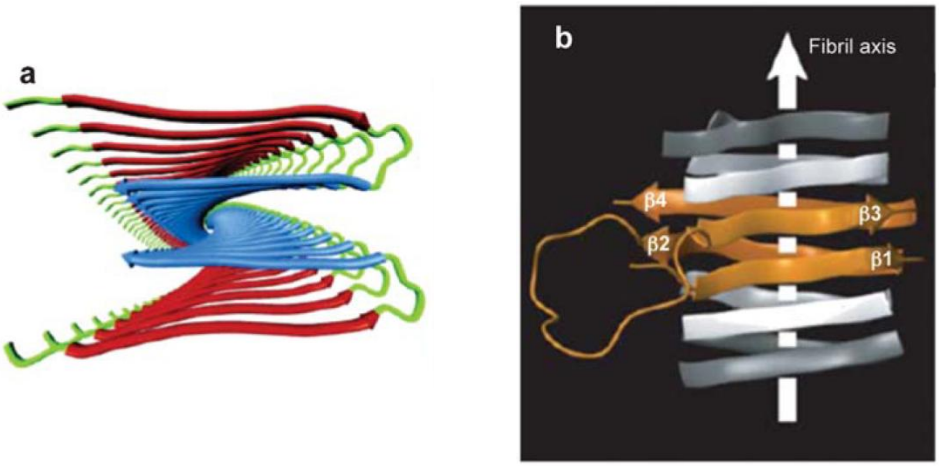

Figure 1.2. Molecular model of an amyloid fibril. (a) The protofilament of Aβ viewed down the long axis of the fibril. The segments 12-24 (red) and 30-40 (blue) are shown (Tycko, 2002). (b) The fibril from the C-terminal domain 218-289 of the fungal prion protein HET-s. The ribbon diagram shows the four β-strands (orange) (residues 226-234, 237-245, 262-270 and 273-282) and the long loop between β2 and β3 from one molecule. Flanking molecules along the fibril axis (gray) are shown (Ritter *et al.,* 2005).

directed spin labeling coupled to EPR [Bouchard *et al*., 2000; Balbach *et al*., 2002; Tycko, 2003; Jaroniec *et al*., 2004; Kajava *et al*., 2005; Ritter *et al*., 2005; Luca *et al*., 2007; Vilar *et al*., 2008; Nelson *et al*., 2005; Sawaya *et al*., 2007; Török *et al*., 2002] allowing to obtain information on the cross-β architecture of amyloid fibrils at molecular or even atomic level (Figure 1.2).

Amyloid fibrils also display the ability to bind specific dyes such as thioflavin T (ThT) and Congo red (CR) [Klunk *et al*., 1989; LeVine III, 1995; Nilsson, 2004]. Upon binding of ThT to amyloid fibrils, it is possible to observe in the ThT excitation spectrum a red-shift from 336 nm to 450 nm and the appearance of a new peak in its emission spectrum centred at around 485 nm, whose intensity is proportional to the extent of binding to the aggregates [LeVine III, 1995]. Fibrils stained with CR are characterized by a green birefringence under cross-polarized light [Missmahl and Hartwig, 1953].

1.1.3 Amyloid fibrils and their relevance to human diseases

Amyloid fibrils are the hallmark of a wide range of human diseases (Table 1.1), which can be divided into (i) neurodegenerative disordes, characterized by protein aggregation in the brain, (ii) nonneuropathic localised amyloidoses, in which aggregation involves a single type of tissue other than the brain, and (iii) nonneuropathic systemic amyloidoses, in which protein deposits are found in multiple tissues [Chiti and Dobson, 2006]. Most of these pathologies can be either sporadic or hereditary. When they have a sporadic etiology, they are generally due to the age-related decline of the cellular machinery in charge of the maintenance of the proteome homeostasis. The familial forms are related to mutations that dramatically increase aggregation rates of proteins and are usually characterized by early onset and aggressive symptomatology [Chiti and Dobson, 2006]. Prion diseases can also be transmissible, since an infectious etiology has been found [Prusiner, 1982]. Other diseases, such as hemodialysis related amyloidosis, originate from medical treatment [Chiti and Dobson, 2006].

The peptides and proteins forming amyloid fibrils have very different structural properties but are usually small in size [Ramshini *et al*., 2011]. Some of them are proteins, such as lysozyme; others are peptides, such as the islet amyloid polypeptide (IAPP), fragments of larger proteins produced by a specific cleavage, such as the amyloid β peptide (Aβ), or by degradation, such as polyQ stretches [Stefani and Dobson, 2003; Chiti and Dobson, 2006].

The causative relation between formation of amyloid fibrils or their precursor oligomers and the disease symptoms is widely accepted on the basis of numerous studies and of the post-mortem observation of amyloid aggregates in patients.

Table 1.1. Diseases associated with the formation of extracellular amyloid fibrils or intracellular inclusions with amyloid-like properties.

Disease	Aggregating protein or peptide	Disease	Aggregating protein or peptide
Neurodegenerative diseases		**Nonneuropathic systemic amyloidoses**	
Alzheimer's disease[a]	amyloid β peptide	AL amyloidosis[a]	immunoglobulin light chains or fragments
Spongiform encephalopaties[a,c]	prion protein and fragments thereof	AA amyloidosis[a]	fragments of serum amyloid A protein
Parkinson's disease[a]	α-synuclein	Familial Mediterranean fever[a]	fragments of serum amyloid A protein
Dementia with Lewy bodies[a]	α-synuclein	Senile systemic amyloidosis[a]	wild-type transthyretin
Frontotemporal dementia with Parkinsonism[a]	tau	Familial amyloidotic polyneuropathy[b]	mutants of transthyretin
Amyotrophic lateral sclerosis[a]	superoxide dismutase I	Hemodialysis-related amyloidosis[a]	β_2-microglobulin
Hungtington's disease[b]	hungtingtin with polyQ expansion	ApoAI amyloidosis[b]	N-terminal fragment of apolipoprotein AI
Spinocerebral ataxias[b]	ataxins with polyQ expansion	ApoAII amyloidosis[b]	N-terminal fragment of apolipoprotein AII
Spinocerebral ataxia 17[b]	TATA box binding protein with polyQ expansion	ApoAIV amyloidosis[a]	N-terminal fragment of apolipoprotein AIV
Spinal and bulbal muscular atrophy[b]	androgen receptor with polyQ expansion	Finnish hereditary amyloidosis[b]	fragments of gelsolin mutants
Hereditary dentatorubral-pallidoluysian atrophy[b]	athrophin-1 with polyQ expansion	Lysozyme amyloidosis[b]	mutants of lysozyme
Familial British dementia[b]	ABri	Fibrinogen amyloidosis[b]	variants of fibrinogen α-chain
Familial Danish dementia[b]	ADan	Icelandic hereditary cerebral amyloid angiopathy[b]	mutant of cystatin C
Nonneuropathic localised diseases			
Type II diabetes[a]	islet amyloid polypeptide	Calcifying epithelial odontogenic tumors[a]	unknown
Medullary carcinoma of the thyroid[a]	calcitonin	Pulmonary alveolar proteinosis[b]	lung surfactant protein C
Atrial amyloidosis[a]	atrial nutriuretic factor	Inclusion-body myositis[a]	amyloid β peptide
Hereditary cerebral haemorrhage with amyloidosis[b]	mutants of amyloid β peptide	Cutaneous lichen amyloidosis[a]	keratins
Pituitary prolactinoma	prolactin	Cataract[a]	γ-crystallins
Aortic medial amyloidosis[a]	medin	Corneal amyloidosis associated with trichiasis[a]	lactoferrin

[a] Predominantly sporadic although in some of these diseases hereditary forms associated with specific mutations are well documented
[b] Predominantly hereditary although in some of these diseases sporadic cases are documented
[c] 5% of cases are infectious (iatrogenic)

An increasing number of studies have shown that the pathogenic species in protein deposition diseases are not the mature fibrils, but the precursor species forming before the fibrils, such as oligomers and structured protofibrils [Bucciantini *et al*. 2002; Billings *et al*., 2005; Cleary *et al*., 2005; Lesnè *et al*., 2006; Haass and Selkoe, 2007; Koffie *et al*., 2009]. Nevertheless, in some cases amyloid fibrils are able to cause cellular dysfunction because they can trigger the inflammatory response, a detrimental phenomenon if it is chronic, and because they act as sources of more toxic and soluble low molecular weight aggregates [Gharibyan *et al*., 2007; Jan *et al*., 2011; Martins *et al*., 2008; Novitskaya *et al*., 2006; Selkoe, 2011; Wogulis *et al*., 2005; Stefani, 2010].

1.2 Misfolded protein oligomers

1.2.1 Oligomers and disease

It has been shown that the severity of cognitive impairment in Alzheimer's disease correlates with the levels of low-molecular-weight species of the Aβ peptide rather than with the amount of amyloid fibrils from the same peptide [Lue *et al*., 1999; McLean *et al*., 1999; Wang *et al*., 1999]. Soluble oligomeric forms of Aβ, including trimers and dimers, were found to be both necessary and sufficient to disrupt learned behavior [Cleary *et al*., 2005]. Moreover, transgenic mice show deficits in cognitive learning before the accumulation of significant amount of amyloid plaques [Moechars *et al*., 1999; Larson *et al*., 1999; Billings *et al*., 2005; Lesné *et al*., 2006]. Yet, in mice models of Alzheimer disease, synapse loss was found to be higher near senile plaques from which oligomers are released [Koffie *et al*., 2009]. Lastly, genetic evidence provides support to the toxicity of the oligomers; indeed the "Artic" (E693G) mutation of the amyloid β precursor protein, associated with a heritable early-onset manifestation of Alzeimer's disease, has been found to enhance protofibril, but no fibril, formation *in*

vitro [Nilsberth *et al*., 2001]. Similar arguments hold for α-synuclein and Parkinson's disease [Kitada *et al*., 1998; Masliah *et al*., 2000; Winner *et al*., 2011], as well as TTR and its associated amyloidoses [Sousa *et al*., 2001].

Numerous experimental data have shown that oligomers formed by proteins unrelated to any disease, such as the N-terminal domain of HypF from *E. coli* (HypF-N), the SH3 domain from bovine phosphatidylinositol 3′ kinase (PI3-SH3) and apomyoglobin from sperm whale, can be highly toxic to cultured cells, whereas the monomeric native states and the amyloid-like fibrils (all formed *in vitro*) display very little, if any, toxicity [Bucciantini *et al*., 2002; Sirangelo *et al*., 2004]. Therefore, oligomer toxicity seems to be a property linked to structural characteristics of the pre-fibrillar aggregates and independent of the protein forming them.

1.2.2 Dynamic and heterogeneous nature of oligomers

The oligomers are characterized by a substantial instability and heterogeneity making a challenge to obtain molecular details at the residue level [Stefani, 2010; Bemporad and Chiti, 2012]. Nevertheless, a number of approaches and techniques have been recently introduced and allowed a deep molecular characterization of the oligomers [Bemporad and Chiti, 2012].

The aggregation process gives rise to the appearance of a wide range of oligomeric species structurally heterogeneous and in an ever-changing state of rearrangement. The description of these species is, therefore, strictly related to the time parameter and to the starting conditions. When aggregation starts from fully or largely unfolded monomers, the initial oligomers, forming during the nucleated conformational conversion, exhibit a large variety of conformations, with monomers still characterized by a disordered structure (Figure 1.3). Indeed, early aggregates with unstable β-sheet structure and a

poor level of order have been described for $A\beta_{40}$ [Lee *et al*., 2011; Qi *et al*., 2008], α-synuclein [Dusa *et al*., 2006] and the PI3-SH3 domain [Carulla *et al*., 2009]. If the aggregation process take origin from native-like state, the early aggregates are characterized by oligomers retaining monomers in a native-like conformation [Banci *et al*., 2005; Olofsson *et al*., 2004; Pagano *et al*., 2010]. It is therefore clear that the early forming species are reminiscent of the monomeric state from which they originate and are far from the amyloid structure, as shown also by their inability to bind amyloid specific dyes [Plakoutsi *et al*., 2005; Lee *et al*., 2011].

As the aggregation proceeds, the aggregates are subjected to a continuous structural reorganization and acquire amyloid-like properties, such as an extensive β-sheet content and ability to bind ThT and CR [Bemporad and Chiti, 2012]. Moreover, they increase in dimensions, compactness, stability, hydrophobic burial and order, still retaining a non fibrillar morphology (Figure 1.3), as it has been reported for $A\beta_{40}$ and $A\beta_{42}$ [Bitan *et al*., 2003; Lee *et al*., 2011; Qi *et al*., 2008], α-synuclein [Kaylor *et al*., 2005] and the human muscle acylphosphatase [Calamai *et al*., 2005]. In addition, they decrease in dynamic fluctuations and oligomer surface per number of monomers [Bemporad and Chiti, 2012]. Such conversion form unstructured or native-like oligomers into amyloid oligomers is inevitably accompanied by the generation of a variety of oligomeric species that differ in the extension of the β-sheet content, giving origin to a complex scenario of multiple species.

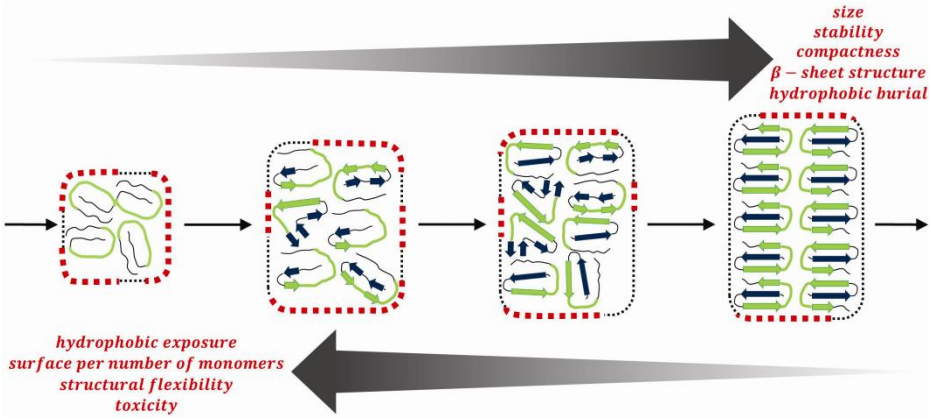

Figure 1.3. A schematic representation of the structural rearrangements occurring during oligomer formation. For simplicity, only aggregation starting from fully or largely unfolded monomers is considered. Amyloidogenic/hydrophobic segments are in green. The oligomer surface is drawn as a thin black when amyloidogenic/hydrophobic segments are buried and as a thick red dotted line when they are exposed to the solvent. While aggregation proceeds (left to right), a set of structural rearrangements take place and leads to growth of thin filaments, which eventually originate amyloid fibrils: the top and bottom arrows show the parameters that increase and decrease, respectively. Image taken from Bemporad and Chiti, 2012.

The heterogeneous and dynamic nature of the oligomers is responsible for the differences in their structure and morphology, phenomenon called polymorphism [Kodali and Wetzel, 2007; Stefani, 2010]. Oligomer polymorphism concerns their size, shape, compactness, stability and secondary and tertiary structure content [Bemporad and Chiti, 2012]. In addition to these characteristics, it is important to note that different kind of oligomers can coexist at the same time in solution [Goldsbury *et al*., 2005; Gosal *et al*., 2005; Jain and Udgaonkar, 2011; Mastrangelo *et al*., 2006; Relini *et al*., 2010] and even *in vivo* [Winner *et al*., 2011]. The importance of oligomer polymorphism reflects in the biological activity of the oligomers. Indeed, it has been shown that expression of different mutants of Aβ in *Drosophila* qualitatively leads to different pathologies [Iijima *et al*., 2008] and that different oligomers of α-synuclein and Aβ cause toxicity in cell cultures through different mechanisms [Danzer *et al*.,

2007; Deshpande *et al*., 2006]. Finally, polymorphism is fundamental in determining the propagation of prion strain infectivity [Jones and Surewicz, 2005].

1.2.3 Structural determinants and mechanisms of oligomer cytotoxicity

It has been observed that different oligomers formed by the same protein present different levels of cytotoxicity and that oligomers originated by different proteins are able to affect the cellular viability to the same extent, indicating that the toxicity of these species is due to their misfolded nature rather than to specific features of their amino acid sequences. The increasing number of studies, targeted to elucidate the fine oligomer structure, has allowed to shed light on the structural determinants of oligomer toxicity, i.e. the structural elements that are responsible for the ability of protein oligomers to interact with the cells and cause their dysfunction [Bemporand and Chiti, 2012].

The degree of hydrophobic surface exposure seems to play an important role in oligomer-mediated toxicity. It has been observed that the increase of hydrophobic exposure in $A\beta_{40}$ aggregates correlates with their ability to affect model membrane fluidity [Kremer *et al*., 2000]; such a positive correlation was also found in homopolymeric amino acid stretches between hydrophobicity and cytotoxicity of their aggregates [Oma *et al*., 2005]. In a recent study, two types of spherical oligomers formed by the HypF-N protein, similar in size, morphology and ThT binding, were found to have very different toxicities on cell cultures, with one species found to be nontoxic [Campioni *et al*., 2010]. Through the technique of the site-directed labeling with the fluorescent probe pyrene, it was found that the three most hydrophobic regions of the protein sequence are structured and buried in the nontoxic oligomers, whereas in the toxic oligomers the same regions are more solvent exposed and flexible [Campioni

et al., 2010]. Moreover, it has been shown that prefibrillar aggregates of the E22G variant of the $A\beta_{42}$ peptide bind strongly to 1-anilinonaphthalene 8-sulfonate (ANS), an indicator of hydrophobic exposure, and that changes in this property correlate significantly with changes in their cytotoxicity [Bolognesi *et al*., 2010]. In the same work, investigation on other protein systems indicated that this is a shared property of misfolded species. Another study has demonstrated that the degree of toxicity of highly amyloidogenic proteins expressed intracellularly increases with the exposure to the solvent of hydrophobic regions on the aggregates surface [Olzscha *et al*., 2011]. Recently, it has been reported that the interaction between Aβ and antibodies grafted with small hydrophobic portions of Aβ itself prevents amyloid formation by converting monomers and/or fibrillar intermediates into small complexes that are unstructured and benign on cell cultures [Ladiwala *et al*., 2012].

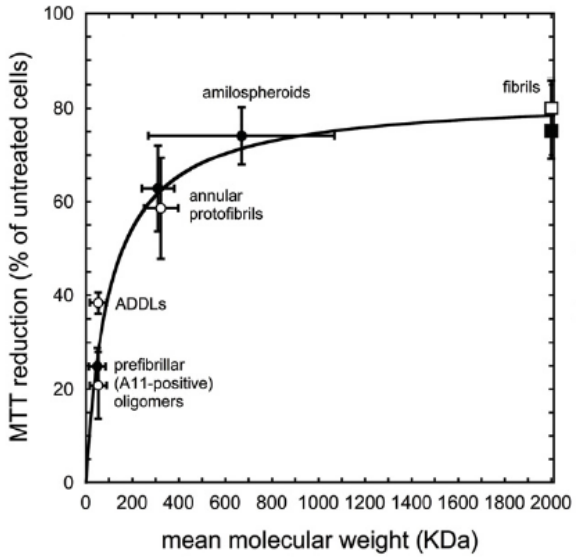

Figure 1.4. Toxicity versus size of $A\beta_{40}$ (filled circles) and $A\beta_{42}$ (empty circles) aggregates. Toxicity is measured by determining MTT reduction by cultured cells following their exposure to oligomers added to the extracellular medium. Aggregate toxicity was expressed as percentage of MTT reduction relative to untreated cells, where 0% and 100% values are two extremes of full cell death and full viability, respectively. All data were obtained at a peptide concentration in the range of 2.0-2.7 mM and aggregate size was expressed as mean molecular weight. All data points were fitted to a hyperbolic function of the form y = a * x/(b + x). Image taken from Bemporad and Chiti, 2012.

Lately, particular attention has been paid to the size of the oligomers as a structural determinant of cytotoxicity. Indeed, it was found that $A\beta_{42}$ pre-fibrillar aggegates of different sizes give rise to an inverse correlation between oligomer size and neuronal toxicity, with the smallest species showing the highest ability in causing cell dysfunction [Cizas *et al*., 2010]. In addition, it was found that three classes of small aromatic molecules can inhibit $A\beta_{42}$ oligomer toxicity by converting the small oligomers into large aggregates, fibrils, and monomers, respectively [Ladiwala *et al*., 2011]. Interestingly, the formation of larger assemblies of toxic oligomeric species of Aβ induced by other molecules, such as molecular chaperones has been found to result in a suppression of their toxicity [Ojha *et al*., 2011]. Finally, through the analysis of the toxicity levels of many oligomeric species of Aβ it has been observed that the cytotoxicity decreases with the increase of oligomer size (Figure 1.4) [Bemporad and Chiti, 2012].

The higher ability of small soluble oligomers to cause cellular damage may reflect their greater diffusion capability and higher hydrophobic surface per number of monomers with respect to larger assemblies. In agreement with this hypothesis, the fibrils forming at the end of the aggregation process are characterized by a lower level of toxicity with respect to their precursors, as they display hydrophobic burial and mass increase [Haass and Selkoe, 2007; Keshet *et al*., 2010].

The mechanisms by which oligomers exert their toxicity is not clear but a prominent hypothesis suggests that the aggregates may expose flexible and hydrophobic regions on their surface that can mediate aberrant interactions with other proteins or cell membranes. Indeed, the toxicity of intracellularly forming aggregates was attributed to their ability to interact and alter the function of a number of cellular proteins [Olzscha *et al*., 2011], whereas the ability to cause cellular damage of exogenously added oligomers

was found to result from a disruption of cell membranes and a consequent uptake of calcium (Figure 1.5) [Campioni *et al*., 2010; Zampagni *et al*., 2011].

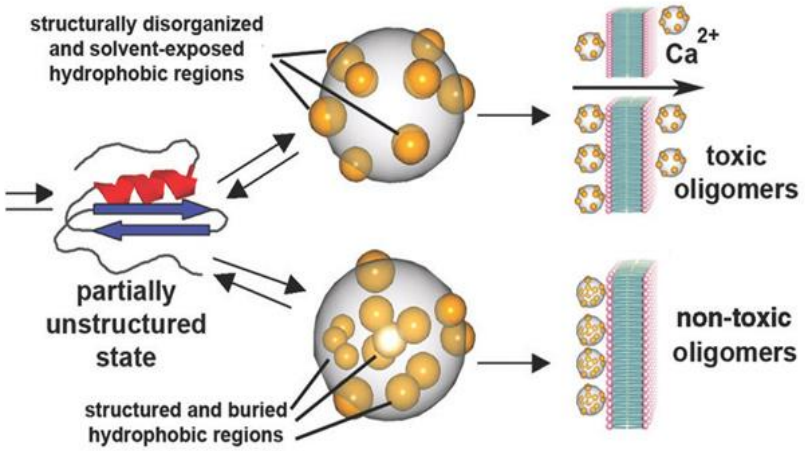

Figure 1.5. Schematic representation of two different types of oligomers generated incubating HypF-N in different conditions of aggregation. Toxic oligomers (on top) characterised by a lower degree of packing and higher solvent exposure of the hydrophobic regions than the ones of the non-toxic species (bottom) are shown. Probably, these characteristics allow the interaction between toxic oligomers and membrane and subsequently dysregulation of Ca^{2+} levels. Image taken from Campioni *et al.,* 2010.

1.3 Homeostasis of the proteome

1.3.1 Protein homeostasis network

Protein homeostasis, or proteostasis, is the cellular process that governs the "life of proteins", as it encompasses regulation and control of the translation, folding, translocation to different intracellular compartments, assembly or disassembly, and clearance of proteins [Balch *et al*., 2008]. Clearly, the maintenance of the proteome in its functional state has a fundamental importance for living cells and, for this reason,

several dedicated systems have been evolved. In this section a brief description of such systems will be given.

Molecular chaperones include, for example, the families of the Hsp100s, Hsp90s, Hsp70s, Hsp60s, Hsp40s and the small heat shock proteins (sHsps). They can act in the cytosol or in specific cellular compartments such as the endoplasmic reticulum (ER) or the mitochondria [Young *et al*., 2004; Bukau *et al*., 2006]. All molecular chaperones interact promiscuously with a broad range of unfolded proteins, recognizing an increased exposure of hydrophobic amino acids [Bukau *et al*., 1996; Sharma *et al*., 2008; Viitanen *et al*., 1992; Walter and Buchner, 2002]. Generally, they do not provide structural information for folding, but avoid unwanted molecular interactions, through controlled binding and release of nonnative proteins that involves, for some of them, ATP hydrolysis. Molecular chaperones also prevent the aberrant aggregation of unfolded, partially folded and misfolded proteins [Broadley *et al*., 2009], are able to solubilize and reactivate aggregated proteins [Weibezahn *et al*., 2005] and mediate the degradation of misfolded proteins [Pickart and Cohen, 2004].

Recent evidence has shown that extracellular counterparts to the intracellular molecular chaperones exist and are referred to as extracellular chaperones (ECs). Indeed, a series of glycoproteins, such as clusterin [Humphreys and Carver, 1999], haptoglobin [Yerbury *et al*., 2005] and α_2-macroglobulin [French *et al*., 2008] have been found to be secreted and to act in a chaperone-like manner [Wilson *et al*., 2008]. In most cases, ECs share functional similarities with the sHsps, as they are able to stabilize misfolded proteins preventing their aggregation, but cannot refold independently proteins as they lack ATPase activity [Wyatt *et al*., 2013].

A universal and ancient mechanism where molecular chaperones and other proteins work in an integrated process is the heat shock response (HSR), so called because it was

initially described as an enhanced transcription of specific genes triggered by an increase in the temperature [Ritossa, 1962], and later recognized to be prompted by a variety of stresses, including oxidative stress, heavy metals, ethanol or other toxic substances [Courgeon *et al*., 1984; Heikkila *et al*., 1982; Michel and Starka, 1986; Yura *et al*., 1984]. Proteins involved in the HSR exert several and different functions, but they are predominantly molecular chaperones [Ellis *et al*., 1989; Young *et al*., 2004]. A related process, originating from the accumulation of misfolded proteins in the ER, is the unfolded protein response (UPR) [Walter and Ron, 2011].

Improperly folded proteins are not allowed to leave the ER and are retrotraslocated into the cytosol for proteasomal degradation, a process called ER-associated degradation (ERAD) [Smith *et al*., 2011]. These proteins, once in the cytosol, are degraded by the ubiquitin-proteasome system (UPS) [Claessen *et al*., 2012].

Protein degradation through UPS is the major pathway of non-lysosomal proteolysis of intracellular short-lived, mislocated, misfolded, mutant or damaged proteins [Sherman and Goldberg, 2001]. Firstly, a series of enzyme-mediated reactions identifies and covalently links abnormal proteins with multiple ubiquitin molecules as a signal for degradation. Then, ubiquitin-protein conjugates are recognized and degraded by the proteasome, which is a multisubunit protease [DeMartino and Slaughter, 1999]. The degradation products are short peptide fragments and amino acids that can be recycled to produce new proteins [Pickart, 2000].

The degradation of intracellular components occurs thanks to autophagy, that mediates the degradation of intracellular components, such as single macromolecules and organelles, inside lysosomes [Mizushima *et al*., 2008], guaranteeing their renewal and, therefore, contributing to basal homeostasis [Bejarano and Cuervo, 2010].

All of the systems described here are strictly connected and interdependent on each other, and a continuous balance among them is necessary in order to ensure the homeostasis of the proteome. The importance of studying these systems in the context of a complex network that preserves cellular functionality is now emerging. Indeed, the comprehension of the mechanisms that govern the co-dependence of these systems could help to shed light on situations in which the proteostasis machinery fails [Morimoto and Cuervo, 2009].

1.3.2 Protein homeostasis and protein deposition diseases

Deficiencies in the protein homeostasis can lead to a broad variety of human pathologies, including those associated with misfolding and aggregation of proteins (Figure 1.6) [Selkoe, 2003; Chiti and Dobson, 2006; Muchowski and Wacker, 2005]. Upon aging a decline of the proteostatic controls naturally occurs, due to changes in the transcriptional levels of chaperones, post-translational modifications, increase in protein oxidation, decrease in the protein degradation rate, etc. [Balch *et al*., 2008; Martinez-Vicente *et al*., 2005]. The age-related deterioration of the proteostasis can in part explain the reason why many diseases are age-dependent [Lu *et al*., 2004; Zhang *et al*., 2004; Massey *et al*., 2006; Erickson *et al*., 2006; Derham and Harding, 1997].

Numerous studies have shown that chaperones and components of the ubiquitin-proteasome system associate with inclusion bodies or extracellular plaques characteristic of protein deposition diseases, suggesting a general activation of the cellular quality control machinery in an attempt to face the accumulation of misfolded species [Barral *et al*., 2004; Wyatt *et al*., 2013]. The homeostatic capacity of the cells can be overwhelmed by the increasing amounts of misfolded proteins [Barral *et al*., 2004; Gidalevitz *et al*., 2006] and, concomitantly, by a progressive reduction of the

efficiency of the quality control network, enhancing the imbalance and allowing further accumulation of toxic misfolded proteins.

Moreover, disease processes themselves might cause, or worsen, chaperone deficiency. Indeed, it has been suggested that aggregate deposits are able to sequester molecular chaperones in a non-functional state, inhibiting their essential function in cellular processes [Schaffar *et al*., 2004; Barral *et al*., 2004; Satyal *et al*., 2000]. In addition, studies report that several cellular models of misfolding diseases do not promptly activate the cytosolic stress response upon overexpression of disease proteins [Duennwald and Lindquist, 2008; Magrane *et al*., 2005; Tagawa *et al*., 2007; Hay *et al*., 2004; Cowan *et al*., 2003]. Similarly, a malfunctioning of the extracellular chaperone machinery has been observed to inevitably affect plasma protein solubility [Poon *et al*., 2002; Pavliček and Ettrich, 1999; Yerbury *et al*., 2005].

If an age-related or disease-related decrease in chaperone activity contributes to pathology, restoring or maintaining proteostasis process should postpone or even prevent disease onset [Balch *et al*., 2008; Broadley and Hartl, 2009]. Indeed, a great number of studies have been done in agreement with this idea. It has been demonstrated that aggregation-mediated proteotoxicity was ameliorated by delaying the ageing process in *Caenorhabditis elegans* models of Huntington's and Alzheimer's diseases, acting at the level of proteostasis regulators of chaperones [Morley *et al*., 2002; Parker *et al*., 2005; Cohen *et al*., 2006]. The overexpression of certain chaperones, including Hsp70s and Hsp40s, suppresses aggregation-associated damage in numerous neurodegenerative disease models [Auluck *et al*., 2002; Tam *et al*., 2006; Kitamura *et al*., 2006; Behrends *et al*., 2006]. It has been reported that in transgenic mouse models of Alzheimer's diseases the sHsp αB-crystallin has a cytoprotective effect, since it neutralizes the toxic Aβ oligomers [Ojha *et al*. 2011]. Also extracellular chaperones

have been shown to interact with oligomeric species [Yerbury *et al*., 2007; Yerbury *et al*., 2009] with benefic results for cells. Indeed, cerebrospinal fluid (CSF) samples from patients with Alzheimer's disease were found to be more toxic to cultured neuroblastoma cells than normal CSF; interestingly, the addition of extracellular chaperones, such as clusterin, α_2-macroglobulin and haptoglobin, suppressed this toxicity and the effect coincided with more efficient cellular uptake of Aβ [Yerbury and Wilson, 2010].

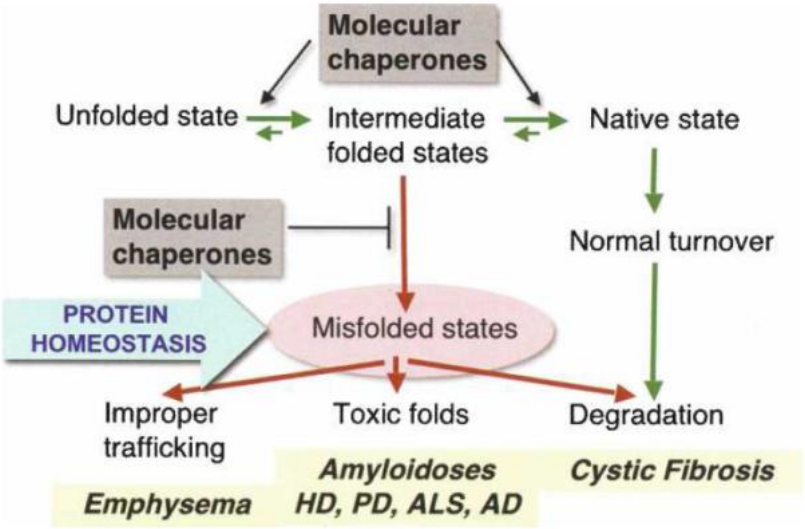

Figure 1.6. Interplay between protein quality control (transitions from unfolded to intermediates to native and to misfolded states) and clearance mechanisms in protein conformation disease. Chaperones have a critical role to suppress the appearance of misfolded species and to enhance protein folding. The imbalance of misfolded species is associated with human disease. Images taken from Morimoto, 2008.

1.4 Multifactorial origin of neurodegeneration

1.4.1 Immune system in the central nervous system

It has been suggested that neurodegeneration associated with protein deposition diseases, such as Alzheimer's disease and Parkinson's disease, is a multifactorial

phenomenon [Mangialasche *et al*., 2010; Roodveldt *et al*., 2008]. Among the factors that have been proposed to affect these pathologies, the uncontrolled inflammatory response in the brain has arisen to a central role [Amor *et al*., 2010].

The central nervous system (CNS) is considered an "immune privileged" organ since it has developed strategies to limit the immune activation within the tissue itself, probably to avoid strong inflammatory reactions that can damage delicate, non-regenerating cells such as neurons and oligodendrocytes [Ransohoff and Brown, 2012]. Firstly, it lacks of antigen-presenting cells that act as messengers between the innate and adaptive immunity in the periphery (performing antigen uptake, migration to draining lymph nodes and presentation to naive T cells) [Ransohoff and Brown, 2012]; secondly, it is surrounded by the blood-brain barrier (BBB), that limit the entry of immune elements [Carson *et al*., 2006]; finally, it is characterized by an anti-inflammatory environment, with a high presence of inflammation-suppressive cytokines, such as interleukin-10 (IL-10), and gangliosides, which can be toxic to T cells [Strle *et al*. 2001; Irani, 1998].

Microglia and astrocytes represent the innate immune component in the CNS parenchyma [Aloisi, 2001; Dong and Benveniste, 2001] and deal directly with pathogens and tissue damage acting as the fundamental first line of defence [Ransohoff and Brown, 2012]. These cells cannot directly initiate adaptive responses, but can recruit cells of the adaptive immune system by secreting various cytokines and chemokines that induce adhesion molecules on the BBB [Amor *et al*., 2010].

Microglia and astrocytes constantly survey the microenvironment and produce factors that influence surrounding neurons. Under physiological conditions, these cells exhibit a deactivated phenotype that is associated with the production of anti-inflammatory and neurotrophic factors [Streit, 2002]. They can switch to an activated

status when they recognize highly conserved structural motifs, either from pathogens (pathogen-associated molecular patterns, or PAMPs) or from damaged or stressed tissues (danger-associated molecular patterns, or DAMPs). PAMPs include bacterial, viral and protozoal products, such as protein, lipid, nucleic acid and carbohydrate [Ransohoff and Brown, 2012]. DAMPs are endogenous signals, encompassing HSPs, uric acid, chromatin, adenosine and ATP, fibrinogen and aggregated, modified or misfolded proteins [Amor *et al*., 2010]. The recognition is mediated by pattern-recognition receptors, such as the Toll-like receptors (TLRs), which are located on the plasma membrane or in endosomal compartments [O'Neill, 2004]. Upon activation, microglia and astrocytes release a variety of immune regulators, such as cytokines and chemokines, promoting an inflammatory response directed to tissue repair [Glass *et al*., 2010].

In a prototypical scenario, the engagement of TLRs evokes transcriptional activation of genes encoding interleukin-1 (IL-1) family cytokines. Pro-forms of the resulting peptides, for example pro-IL-1β, remain cytoplasmic until cleaved enzymatically by activated caspase-1 [Martinon and Tschopp, 2004]. The release of biologically active IL-1β elicits production of a secondary inflammatory cytokine cascade by both microglia and astrocytes [Chakraborty *et al*., 2010]. For example, IL-1β can induce expression of tumor necrosis factor-α (TNF-α) and interleukin-6 (IL-6) [Ransohoff and Brown, 2012].

Microglial cells are also the resident phagocytes of the brain [Perry and Gordon, 1988]. Phagocytosis contributes to the maintenance of the integrity of the tissue, through the clearance of apoptotic cells and the promotion of the damage resolution. This process is also exploited to remove extracellular protein aggregates [Rogers *et al*., 2002; Zhang *et al*., 2005]. Regarding astrocytes, they act in buffering CNS potassium

ions, removing and recycling potentially toxic glutamate, adjusting water balance, and modulating synaptic activity and blood flow [Nash *et al*., 2011].

1.4.2 Inflammatory response and protein deposition diseases

Inflammation has been found to be linked to certain neurodegenerative disorders including Alzheimer's disease, Parkinson's disease and multiple sclerosis [Raine, 1994; Banati *et al*., 1998; McGeer *et al*., 1988]. The inflammatory response protects the tissue, promoting the insult resolution. However, when chronically sustained because of a persistent stimulation, it may become harmful and self-damaging. An over-activation of microglia and astrocytes is inevitably present in brains affected by neuropathologies and it has been observed in Parkinson's disease [Kim and Joh, 2006], Alzheimer's disease [McGeer *et al*., 2006] and Huntington's disease [Masters and O'Neill, 2011].

Following activation, microglia cells change their morphology, express MHC antigens and become phagocytic [Hayes *et al*., 1987]. They secrete pro-inflammatory cytokines that amplify the inflammatory response by activating and recruiting other cells to the lesion, express chemokines and release nitric oxide, which mediates apoptosis [Dickson *et al*., 1993; Griffin *et al*., 1989]. Chronic microglia activation may lead to the recruitment of cells of the adaptive immune system into the CNS, resulting in neuronal damage [Amor *et al*., 2010]. This process is particularly harmful in the brain, since neurons are generally irreplaceable [Kim and Joh, 2006].

An increasing number of studies have reported that amyloidogenic proteins/peptides and misfolded aggregates are potent immunostimulatory [reviewed in Masters and O'Neill, 2011]. Importantly, the microglial activation and inflammatory processes are thought to be largely caused by the aberrant protein oligomers accumulating throughout the pathological aggregation process [Roodveldt *et al*., 2011; Amor *et al*., 2010].

Interestingly, it has been proposed that the innate immune system universally recognizes hydrophobicity as a damage-associated pattern, evolving its TLRs in order to react with the exposed hydrophobic portions of molecules [Seong and Matzinger, 2004]. Indeed, the TLRs are highly promiscuous and bind to a very large number of ligands. These ligands are structurally different, but most of them are either normally hydrophobic or prone to exposing large hydrophobic areas when they are damaged or modified [Seong and Matzinger, 2004].

1.4.3 Heat shock proteins as immune mediators

Many studies have documented induction of Hsps in nerve cells and glia as the result chronic neurodegeneration and neuroinflammation. The inducible form of Hsp70 accumulates in astrocytes, oligodendrocytes and microglia, following a variety of stresses [Richter-Landsberg and Goldbaum, 2003]. The expression of Hsp60 has been

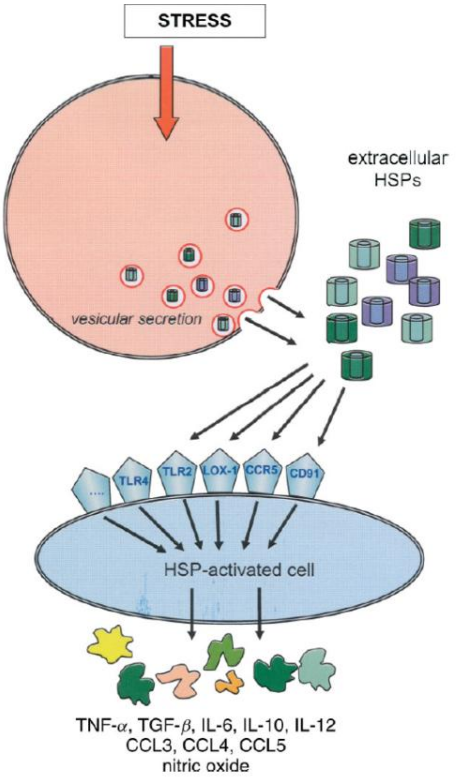

Figure 1.7. Extracellular Hsps as mediators of inflammation. By controlled vesicular exocytosis, a variety of Hsps are secreted in response to stress by different cells. A growing number of surface receptors, including CD91, scavenger receptors, pattern-recognition receptors, CD40 and the chemokine receptor CCR5, relay signals given by extracellular Hsps and trigger production of a range of molecules with diverse functions in innate and adaptive immune responses. Adapted from van Noort, 2008.

observed as a consequence of inflammatory cytokine stimuli in oligodendrocytes and astrocytes, and of inflammatory lesions during multiple sclerosis [Bajramovic *et al*., 2000]. In addition, during neuroinflammation in multiple sclerosis and Alzheimer's disease, oligodendrocytes have been found to produce the sHsp αB-crystallin [van Noort *et al*., 1995; Renkawek *et al*., 1994].

Evidence is now emerging that Hsps not only accumulate in brain cells following stress, but are secreted and act as extracellular signals for receptor-mediated signaling in a similar manner to other soluble mediators of inflammation [Calderwood *et al*., 2007] (Figure 1.7). The release of Hsps in the extracellular space seems to be a physiological phenomenon, since it occurs even under mild forms of stress *in vivo*. For example, Hsp70 is induced as an extracellular mediator in the CNS during exercise in humans [Lancaster *et al*., 2004]. In addition, Hsp60, Hsp70 and αB-crystallin have been observed in the cerebrospinal fluid of patients suffering from neurodegenerative disorders, but also in healthy controls [Ousman *et al*., 2007; Lancaster *et al*., 2004; Lai *et al*., 2006]. In agreement with this findings, several surface receptors have been found to recognize extracellular Hsps, and even fragments of Hsps [Habich *et al*., 2006; Wang *et al*., 2005].

Interestingly, exogenous Hsps, including Hsp32, Hsp70, Hsp90 and αB-crystallin, are able to activate microglia [Calderwood *et al*., 2007; Kakimura *et al*., 2002; Kakimura *et al*., 2001; Bhat and Sharma, 1999]. *In vitro* treatment of microglia with such Hsps generally induces production of nitric oxide, several cytokines including TNFα, TGFβ and IL-6 and chemokines [van Noort, 2008]. The microglial activation has also been observed *in vivo* by injecting exogenous Hsp90 into the hippocampus of rats [Takata *et al*., 2003]. Moreover, in several cases, microglial activation by exogenous

Hsps has been demonstrated to result in increased uptake and clearance of amyloid peptide aggregates [Kakimura *et al*., 2002; Kakimura *et al*., 2001; Takata *et al*., 2003].

Due to their anti-inflammatory effects, Hsps have been evaluated as therapeutic agents in a variety of human inflammatory diseases, such as rheumatoid arthritis [Vanags *et al*., 2006; van Eden, 2008; Panayi and Corrigall, 2008], psoriasis [Williams *et al*., 2008], diabetes [Huurman *et al*., 2008] and multiple sclerosis [Broadley *et al*., 2009].

1.5 The model protein HypF-N

1.5.1 Structural properties of HypF-N

HypF-N is the N-terminal domain of the prokaryotic hydrogenase maturation factor HypF of *Escherichia coli*, a large multi-domain protein of about 82 kDa that is in charge of assisting the folding of [NiFe]-hydrogenases, enzymes involved in the hydrogen metabolism of prokaryotes [Colbeau *et al*., 1998]. HypF is constituted by an N-terminal acylphosphatase-like domain (residues 1-91), a sequence motif shared with enzymes catalysing O-carbamoylation reactions (residues 473-479) and two zinc-finger motifs similar to those found in the DnaJ chaperone (residues 109-134 and 159-184) [Casalot and Rousset, 2001]. The N-terminal domain is homologous in the sequence and structure to the acylphosphatase-like structural family. Acylphosphatases (AcPs) are small enzymes that catalyse the hydrolysis of carboxyl-phosphate bonds in acylphosphates [Stefani and Ramponi, 1995]. In spite of sharing about 22% and 50% of its sequence with human and *E. coli* AcP, respectively, HypF-N does not show any catalytic activity typical of AcPs [Chiti *et al*., 2001].

The native structure of this domain has been resolved by X-ray crystallography [Rosano *et al*., 2002] and displays a ferredoxin-like fold with a α/β topology, consisting

of a βαββαβ secondary structure (Figure 1.8). The domain is about 43x28x27 Å in size [Rosano *et al*., 2002] and has a compact and globular structure, targeted to avoid aggregation from its native state. Indeed, in order to disfavour intermolecular interactions, the protein presents very short or highly twisted edge β-strands, a β-bulge (71-72), a proline residue (Pro78) and a cluster of charged residues (Asp72, Glu75-Arg76-Glu77), all structural properties that prevent interactions between different molecules [Rosano *et al*., 2002].

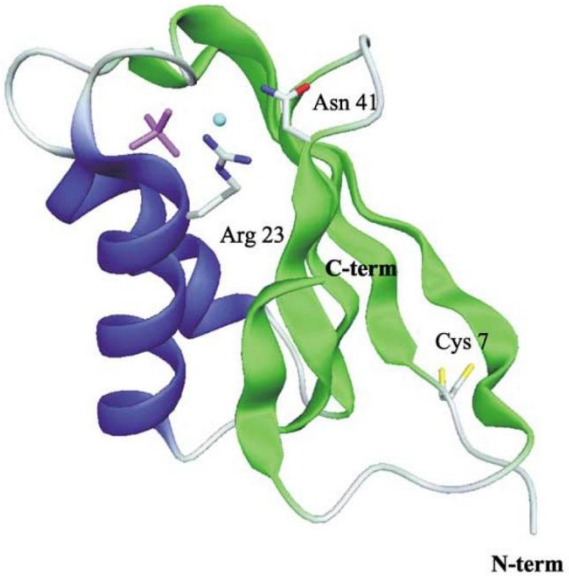

Figure 1.8. Ribbon representation of HypF-N structure. The secondary structure elements are displayed in blue (α-helices) and green (β-strands) colours. The putative active site is also shown with the conserved residues Arg23 and Asn41, the bound phosphate (purple sticks) and the bound chloride ion (light blue sphere). The Cys7 residue shown in figure was found to adopt two alternative conformations both able to form right-handed disulfides with a neighbouring molecule in the crystal. The figure was taken from Rosano *et al.*, 2002.

1.5.2 Aggregation of HypF-N *in vitro*

Conditions that partially destabilize the native structure of HypF-N can induce its aggregation *in vitro*, and encompass low and high pH, mutations and the presence of a moderate amount of trifluoroethanol (TFE) [Chiti *et al*., 2001; Relini *et al*., 2004; Marcon *et al*., 2005; Campioni *et al*., 2008; Calloni *et al*., 2008; Ahmad *et al*., 2010].

A first work reported the formation of amyloid-like fibrils by incubating the protein in citrate buffer at pH 3.0 or in acetate buffer at pH 5.5 with 30% (v/v) TFE [Chiti at al., 2001]. Electron microscopy images showed the presence of 7-9 and 12-20 nm wide fibrils in the samples incubated for 1 month at acidic pH, whereas in TFE the majority of the fibrils was 3-5 nm and 7-9 nm in width [Chiti at al., 2001]. In addition to the fibrillar morphology, these aggregates were found to bind to ThT and CR, resembling the amyloid-like properties [Chiti *et al*., 2001]. The aggregation process in 30% TFE was further investigated using AFM (Figure 1.9) and resulted to be a hierarchical path [Relini *et al*., 2004]. Initially globular structures with a height of 2-3 nm consistent with that of a small oligomers form; after 3 days of incubation in the aggregating conditions, the globules self-assemble into beaded chains with crescent-like appearance; these latter originate large rings after 5 days; subsequently the annular structures convert into ribbon-like fibers by opening and reorganizing their constituent globular units; for further assembly, after 8 days, supercoiled fibrils formed by a different number of protofilaments appear, and after eleven days the large majority of the structures observed are tangles of fibrils having a width of 3.5, 5.0 and 8.5 nm [Relini *et al*., 2004], in agreement with previously reported TEM observations [Chiti *et al*., 2001]. These fibrils show a cross-β structure in the X-ray diffraction pattern, typical of amyloid fibrils [Relini *et al*., 2004].

Oligomeric aggregates and fibrils were also able to form in 6-12% TFE [Marcon *et al*., 2005]. In these mildly denaturing conditions, HypF-N was found to be initially in a predominantly native-like conformation, with the partially folded state being poorly populated. A kinetic analysis revealed that molecules accessing such a partially folded state were able to originate the aggregation process. In the context of a physiological environment, this finding is significantly relevant, since it underlines the need of the

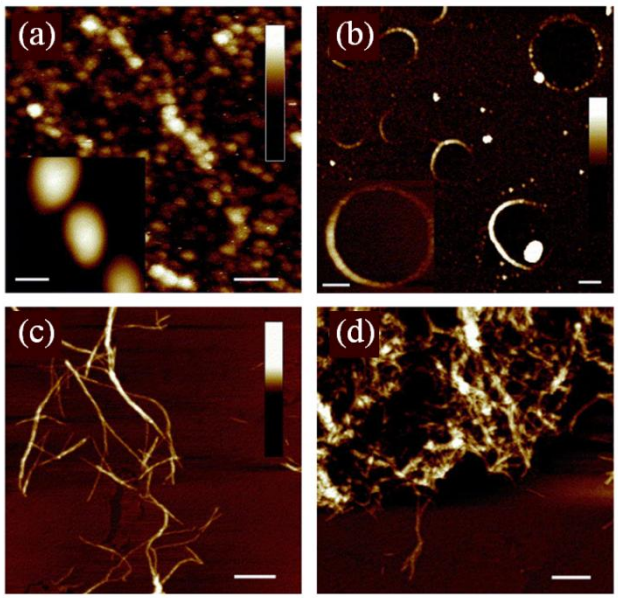

Figure 1.9. TM-AFM images of HypF-N aggregates formed in the presence of 30% (v/v) TFE at pH 5.5. (a) After few hours of incubation, globular aggregates are observed. The scale bar represents 100 nm. Inset: STM image of globular aggregates. The scale bar represents 10 nm. (b) After three days of incubation, crescents and rings are observed. Inset: observation of a ring at higher resolution. The scale bars represent 400 nm. (c) Supercoiled fibrils observed after 8 days of incubation. (d)Tangles of the mature fibrils that represent the large majority of the structures observed after 11 days of incubation. Scale bars represent 500 nm (c-d). Images adapted from Relini *et al.*, 2004.

cells to constantly fight the propensity to aggregate for even the most stable proteins [Marcon *et al*., 2005].

The HypF-N aggregation process under acidic pH condition was investigated from the structural characterization of the amyloidogenic precursor state adopted by the protein to the description of the resulting aggregates. At low pH, precisely pH 1.7, HypF-N was found to be largely unfolded but still contain significant secondary structure elements and hydrophobic clusters [Campioni *et al*., 2008]. By increasing the ionic strength of the solution the aggregation of this precursor state was induced and amyloid-like protofibrils were detected in the samples, as revealed by ThT fluorescence and AFM [Campioni *et al*., 2008; Calloni *et al*., 2008; Campioni *et al*., 2012].

The NMR analysis of the pH-denatured precursor state allowed to identify the regions of the sequence that form hydrophobic interactions and adopt secondary structure. Indeed, it was found that the regions spanning residues 23-34, 56-64, and 81-82 form hydrophobic clusters, whereas the regions spanning residues 26-30, 56-61 and

46-49 form α-helical structure. These latter regions correspond largely in the native conformation to helix α1, helix α2 and strand β3, respectively [Calloni *et al*., 2008]. By creating a set of variants, the regions of the sequence that play key roles in the conversion of the pH-denatured state of HypF-N into ThT-binding and β-sheet containing protofibrillar species were also identified (approximately residues 9-15, 27-35, 46-48, and 58-60). These groups of residues correspond to the regions of the sequence that have the highest intrinsic aggregation propensity [Calloni *et al*., 2008].

The conversion of HypF-N into amyloid-like oligomers under conditions of acidic pH has been recently studied under the influence of different salts [Campioni *et al*., 2012]. The AFM results show that, irrespective of the salt used, the aggregation process lead to the formation of bead-like oligomers with similar morphologies and heights. By contrast, the content of secondary structure and the exposure of hydrophobic clusters of the monomeric precursor state is greatly affected by the anions constituting the salts [Campioni *et al*., 2012].

A partially folded state of HypF-N, which subsequently assembles to form stable soluble oligomers, has been observed in condition of alkaline pH and low concentrations of TFE [Ahmad *et al*., 2010]. These aggregates are able to CR and ThT, contain extensive β-sheet structure and have a morphology similar to the HypF-N oligomers formed at low and nearly neutral pH [Ahmad *et al*., 2010].

1.5.3 Aggregation of HypF-N *in vivo*

The aggregation process of HypF-N was also investigated *in vivo*, where several additional factors able to affect substantially the aggregation are present. In *E. coli* cells, wild-type HypF-N does not aggregate; conversely HypF-N variants engineered in order to destabilize the native structure precipitate into inclusion bodies after expression

[Calloni *et al*., 2005]. The aggregation of unstable mutants can be avoided by the insertion of mutations that increase the net charge and therefore reduce the polypeptide chain propensity to aggregate. Interestingly, the aggregating variants were found to be less stable than the soluble variants, indicating that the aggregation of this protein *in vivo* also requires partial unfolding of the native state [Calloni *et al*., 2005].

In a recent study, by expressing wild-type HypF-N and 21 folding-incompetent mutants in *E. coli*, a significant inverse correlation was found between the solubility of the variants and their intrinsic propensity to form amyloid fibrils, suggesting that the physicochemical parameters (such as hydrophobicity, β-sheet propensity and charge) recognized to affect amyloid formation by fully or partially unfolded proteins *in vitro* are generally valid for situations *in vivo* [Winkelmann *et al*. 2010].

1.5.4 Cytotoxicity of oligomeric species formed by HypF-N

As described above, the oligomeric species forming during the aggregation pathway of HypF-N share structural properties with the diseases related ones [Chiti *et al*., 2001; Relini *et al*., 2004; Marcon *et al*., 2005; Campioni *et al*., 2008]. Moreover, they are cytotoxic to cell cultures and animal models in the same manner of the pathology-related pre-fibrillar aggregates [Bucciantini *et al*., 2002; Cecchi *et al*., 2005; Baglioni *et al*., 2006; Campioni *et al*., 2010; Zampagni *et al*., 2011].

Pre-fibrillar aggregates formed in 30% TFE have been found to reduce the viability of cell cultures, using the 3-(4,5-dimethylthiazol-2-yl)-2,5-diphenyltetrazolium bromide (MTT) reduction inhibition assay (Figure 1.10), a generic indicator of cellular stress, and the trypan blue internalization assay [Bucciantini *et al*., 2002]. The levels of cell impairment caused by HypF-N oligomers were very similar to those reported for the disease-associated proteins, such as α-synuclein, $A\beta_{1-42}$ and transthyretin [Bucciantini *et*

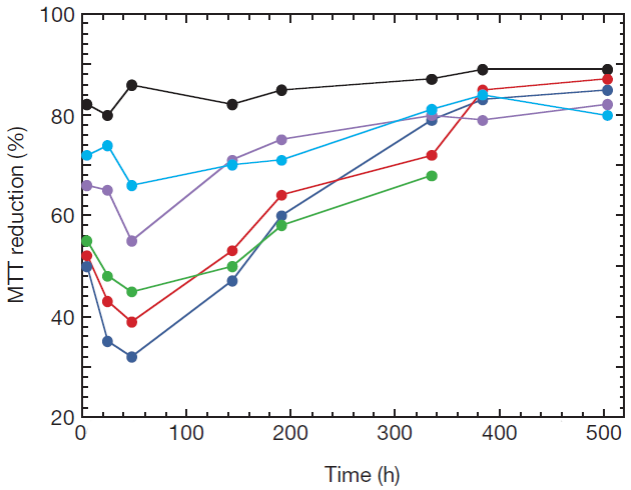

Figure 1.10. Differential cytotoxicity of protofibrillar and fibrillar HypF-N aggregates. (a) Cell viability was checked by the MTT inhibition reduction test, after addition to the cell medium of either 20 μM native protein (●) or different concentrations of aggregates formed at different times of incubation at pH 5.5 in the presence of 30% (v/v) TFE: 20 μM (●), 5 μM (●), 1 μM (●), 0.2 μM (●) and 0.04 μM (●). Values are relative to untreated cells. Figure adapted from Bucciantini *et al.*, 2002.

al. 2002]. In addition, the toxic effects were not observed when the cells were exposed to HypF-N aggregates incubated for several days in the aggregating condition and containing fibrillar species (Figure 1.10).

HypF-N oligomers were found to cause an increase of reactive oxygen species (ROS) and free Ca^{2+} levels inside the cells, phenomena that can lead to apoptosis or necrosis, as shown in several studies [Bucciantini *et al*., 2004; Bucciantini *et al*., 2005; Cecchi *et al*., 2005]. These events are triggered by the ability of oligomers to interact and disrupt the cell membranes; indeed, it has been found that HypF-N formed in 30% TFE were able to permeabilize synthetic membranes [Relini *et al*., 2004; Canale *et al*., 2006] and even plasma membranes of cultured cells [Bucciantini *et al*., 2004; Bucciantini *et al*., 2005; Cecchi *et al*., 2005]. An important mechanism in determining membrane permeabilization and calcium influx was identified in the activation of the glutamatergic channels, NMDA and AMPA receptors, following their interaction with HypF-N oligomers, with unspecific membrane permeabilization occurring later [Pellistri *et al*., 2008]. Noteworthy, a loss of cholinergic neurons was observed when

HypF-N pre-fibrillar aggregates were injected into rat brains [Baglioni *et al*., 2006], indicating that these species are toxic also in higher organisms.

The recent finding that different types of HypF-N oligomers have different abilities to cause cellular impairment, with one species being nontoxic, has provided a unique opportunity to study and compare the structure and activity of toxic and nontoxic oligomeric aggregates [Campioni *et al*., 2010]. The toxic HypF-N oligomeric species were formed in 12% TFE and termed type A oligomers, whereas the nontoxic species were generated at low pH and called type B.

Type A oligomers were found to decrease cellular viability in human neuroblastoma cells (SH-SY5Y) and mouse endothelial cells (Hend), as detected by MTT test, whereas type B were benign to these cells [Campioni *et al*., 2010]. Furthermore, type A oligomers penetrated the plasma membrane, induced a calcium influx into the cytosol, increased intracellular ROS production and lipid peroxidation, resulting in the activation of the apoptotic pathway, as indicated by the substantial increase of caspase-3 level and by the staining with the apoptotic marker Hoechst 33342. By contrast, type B oligomers were unable to cause such effects [Campioni *et al*., 2010; Zampagni *et al*., 2011]. Lately, it has been observed that type A oligomers, unlike type B, colocalize with post-synaptic densities in primary rat hippocampal neurons, induce impairment of long term potentiation in rat hippocampal slices and impair spatial learning of rats in the Morris Water Maze test, mimicking the synaptotoxicity of Aβ aggregates [Tatini *et al*., unpublished].

As described above, the interaction of the oligomers with cell membranes is a primary event resulting in cytotoxicity and, therefore, the prevention of such interaction mediated by the shielding of glycosaminoglycans bound to cell membranes [Saridaki *et al*., 2012] results in a loss of toxicity of type A oligomers.

Further investigations have shown that oligomer cytotoxicity depends on the contributions of the physicochemical properties of both the aggregates and the cell membrane with which they interact [Evangelisti *et al*., 2012]. Indeed, by increasing the content of cholesterol and decreasing the one of ganglioside GM1 in cell membrane, type A oligomers become essentially benign, whereas type B oligomers become toxic [Evangelisti *et al*., 2012].

1.5.5 Structural determinants for HypF-N oligomer cytotoxicity

The different biological properties of HypF-N type A and type B oligomers described in the previous section were found to arise from differences in the structure of the two types of aggregates [Campioni *et al*., 2010]. Type A oligomers were formed by incubating HypF-N for 4 hours in 50 mM acetate buffer, 12% (v/v) TFE, 2 mM DTT, pH 5.5 (condition A), whereas type B aggregates are generated by incubating the protein for 4 hours in a solution of 20 mM trifluoroacetic acid (TFA), 330 mM NaCl, pH 1.7 (condition B).

The two types of oligomers appeared to be indistinguishable measuring their ability to bind to ThT and analysing their morphology through AFM [Campioni *et al*., 2010]. In order to shed light on the structural characteristics responsible for the different behavior of the oligomers, 18 HypF-N variants carrying a single cysteine residue located at different positions along the polypeptide chain were created and labelled with the fluorescent probe *N*-(1-pyrene)maleimide (PM). PM can be used to obtain information on the proximity between two labelled residues located on different protein molecules, because of its property to originate excited-state dimers, also called excimers [Betcher-Lange and Lehrer, 1978; Hammarström *et al*., 1997; Hammarström *et al*., 1999; Krishnan and Lindquist, 2005]. Excimers form when the distance between two

PM molecules is less than 10 Å; as a consequence, in the fluorescence emission spectrum, an excimer peak, indicated by the appearance of broad band at level of the 440-470 nm region, is observed. Conversely, when the probes are distant, such a band is absent [Birks, 1967; Förster, 1969; Betcher-Lange and Lehrer, 1978; Hammarström *et al*., 1997; Hammarström *et al*., 1999; Krishnan and Lindquist, 2005].

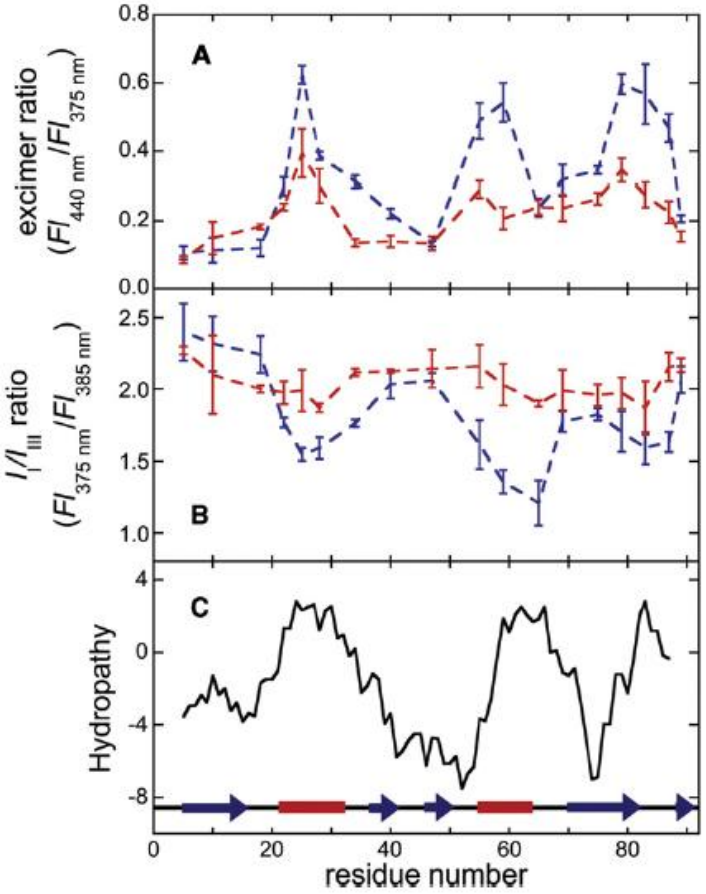

Figure 1.11. Structural differences between toxic and nontoxic oligomeric aggregates of HypF-N. (a) Excimer ratio of PM (related to the degree of structure formation) versus number of labeled residue for toxic (red lines) and nontoxic (blue lines) oligomers of HypF-N. (b) I_I/I_{III} ratio of pyrene (a correlate of the degree of solvent exposure) versus number of labeled residue for toxic (red lines) and nontoxic (blue lines) oligomers. (c) Hydropathy profile of the HypF-N sequence. The three panels show that in nontoxic aggregates, unlike the toxic aggregates, the three hydrophobic regions of the sequence are structured and buried inside the oligomers. Image adapted from Campioni *et al.*, 2010.

Each labelled mutant was then allowed to aggregate in condition A and in condition B and the PM fluorescence emission spectra of the resulting samples were acquired. From these spectra, the ratio of the excimer to monomer fluorescence intensities (FI_{440} /FI_{375}) was obtained for each labelled position (Figure 1.11). This approach revealed that the regions involved in the formation of the structural core of the aggregates are the same in the two types of oligomers and correspond to the three major hydrophobic regions of the HypF-N sequence (Figure 1.11). However, the excimer ratio profile resulting from type B oligomers was characterized by higher values with respect to the ones obtained for type A aggregates, indicating a more compact structure and a tight packing of the type B aggregates with respect to type A oligomers.

In addition, type A aggregates were found to have a stronger affinity for the fluorescent probe ANS than the type B oligomers, suggesting that the degree of exposure to the solvent of hydrophobic surface is greater in the toxic species. In conclusion, the ability of the oligomers to cause cellular dysfunction was linked to the level of structural flexibility and solvent-exposure of the hydrophobic residues of the oligomers. These structural properties allow the oligomeric species to interact and damage cell membranes, leading ultimately to cell death [Campioni *et al*., 2010].

1.6 Aim of the thesis

For the experimental work presented in this thesis we took advantage of the ability of HypF-N to form oligomeric intermediates with structural and functional properties that resemble those associated with protein deposition diseases and that are, in addition, relatively easy to form, stable, amenable to structural analysis and producible in two forms, toxic and nontoxic. In the first chapter dedicated to the results (Chapter 2), we show that chaperones, such as αB-crystallin, Hsp70, α_2-macroglobulin, clusterin and

haptoglobin, are able to neutralize the toxicity of the oligomers and that such behavior derives from their ability to interact with the oligomers and promote their further assembly, in the absence of any disaggregation or structural reorganization of the aggregates. In addition to showing a novel mechanism used by chaperones to control protein homeostasis and to suggesting strategies against protein depositions diseases, these results put forward oligomer size as a structural determinant of protein oligomer toxicity.

In Chapter 3 we show that an increase of the surface hydrophobicity of the oligomers can have the unexpected result of lowering the toxicity of the aggregates and that this phenomenon arises from the ability of the hydrophobic surface to promote the formation of larger assemblies, resembling the mechanism used by molecular chaperones and described in Chapter 2. In addition, the data confirm the essential role of the size in determining the oligomeric ability of damaging cells. Most importantly, we illustrate that the level of toxicity of the aggregates is explicable on the basis of superficial hydrophobicity and size, only if these two parameters are considered together as forces that act and cooperate simultaneously.

In Chapter 4 we present results on the ability of TTR to suppress the toxicity of HypF-N oligomers by binding and inducing the formation of larger clusters of aggregates, similarly to well established chaperones. The results confirm the efficacy of such mechanism detoxifier of misfolded oligomers and underline again the dimension as structural parameter affecting oligomer toxicity. Moreover, the chaperone-like activity has to be enrolled among the functions of TTR.

Finally, in Chapter 5 results on the ability of HypF-N oligomers to trigger a pro-inflammatory response will be presented. Interestingly, the nontoxic species were found to be stronger inducers of inflammation with respect to the toxic oligomers. In addition,

the nontoxic oligomers and the assemblies neutralized by chaperones exert the ability to induce inflammation without affecting cellular viability. These first results, although they need to be further proved, suggest that the inflammation process should not be underestimated in approaching to degenerative diseases.

Chapter 2

MOLECULAR MECHANISMS USED BY CHAPERONES TO REDUCE THE TOXICITY OF ABERRANT PROTEIN OLIGOMERS

2.1 Introduction

The ability of living systems to maintain their peptides and proteins in soluble, native and functional states is the result of a wide variety of physicochemical and conformational characteristics of these macromolecules that have been selected by evolution [Dobson, 2003; Monsellier and Chiti, 2007] and it is also attributable to an array of dedicated biological mechanisms that together ensure protein homeostasis [Balch *et al*., 2008; Powers *et al*., 2009], as described in section 1.3. The cellular machinery dedicated to the maintenance of proteostasis includes ribosomes, molecular chaperones, the ubiquitin-proteasome system, the heat shock response, the unfolded protein response, endoplasmic reticulum associated degradation, autophagy, etc. [Voellmy and Boellmann, 2007; Kapoor and Sanyal, 2009; Kubota, 2009; Hoseki *et al*., 2010; Bejarano and Cuervo, 2010]. The failure of this machinery to function effectively causes a wide variety of pathological conditions, included those associated with the misfolding of proteins that can lead to aggregate accumulation both in the cytosol and in the extracellular space [Selkoe, 2003; Chiti and Dobson, 2006].

Molecular chaperones are proteins that play a central role in the avoidance of protein misfolding and aggregation [Bejarano and Cuervo, 2010; Morimoto, 2008; Young *et al*., 2004; Weibezahn *et al*., 2005; Hartl *et al*., 2011]. Most known chaperones are intracellular and act in the cytosol or in specific cellular compartments such as the ER or the mitochondria [Young *et al*., 2004; Bukau *et al*., 2006], but some chaperones

are secreted and are collectively referred to as extracellular chaperones [Wilson *et al*., 2008]. The variety of molecular chaperones are known to have a range of different functions, including assisting in the folding process of newly synthesised proteins or temporarily misfolded proteins [Young *et al*., 2004], inhibiting the aggregation of unfolded, partially folded and misfolded proteins [Broadley *et al*., 2009], causing the disaggregation of small aberrant protein aggragates [Weibezahn *et al*., 2005] and mediating the degradation of misfolded proteins [Pickart and Cohen, 2004]. However, little is known about about their ability to suppress the toxicity of aberrant protein oligomers, which are considered the major deleterious species in protein misfolding diseases.

In this study we have examined the effects of five chaperones (human αB-crystallin and Hsp70 as intracellular chaperones, and human clusterin, haptoglobin and α_2-macroglobulin as extracellular chaperones) on the toxicity of extracellularly added oligomers formed by three different peptides/proteins $A\beta_{42}$, IAPP and HypF-N. We have focused our attention on small oligomers as these are highly toxic and thought to be the major deleterious species in a range of protein misfolding diseases [Chiti and Dobson, 2006; Selkoe, 2008]. We show that all five chaperones suppress completely, or decrease markedly, the toxicity of all oligomers examined here, with significant effects observed even at molar ratios of protein:chaperone as low as 500:1. In the light of these observations we have carried out experiments to elucidate whether the chaperones cause a structural modification of the oligomers at the single residue level, their gross disaggregation or their further assembly; we will show that the chaperones bind to the oligomers and promote their clustering into larger aggregates, providing an explanation to why they are efficient at such low concentrations.

2.2 Results

The cellular biology experiments here described were acquired in collaboration with the group of Prof. Cristina Cecchi of the University of Florence. AFM measurements were performed by the group of Prof. Annalisa Relini of the University of Genoa. This work have been published in June 2012 by Proceedings of the National Academy of Sciences of the United States of America [Mannini *et al*., 2012].

2.2.1 Chaperones suppress the toxicity of oligomers formed by different proteins

Toxic oligomers were generated from three different peptides/proteins, $A\beta_{42}$, IAPP and HypF-N, as described previously [Lambert *et al*., 2001; Cecchi *et al*., 2008; Campioni *et al*., 2010]. They were incubated in the cell culture medium for 1 hour and then added to SH-SY5Y cultured cells, at 12 μM monomer concentration. All three types of oligomers were found to decrease the MTT reduction of the SH-SY5Y cells by 30-40%, demonstrating their toxic nature (Figure 2.1A-C). They were then subjected to the same procedure but incubated for 1 hour in the cell culture medium containing either αB-crystallin, Hsp70, clusterin, haptoglobin or α_2-macroglobulin prior to addition to SH-SY5Y cells (protein:chaperone molar ratios were 5:1, 5:1, 10:1, 15.1 and 100:1, respectively). In each case the cells were found to reduce MTT to levels similar to untreated cells or to cells treated with the native proteins (Figure 2.1A-C). By contrast, when the three types of oligomers were incubated in cell culture medium for 1 hour with hen egg white lysozyme (HEWL) or bovine serum albumin (BSA), proteins that are not expected to possess chaperone properties, the oligomers were found to maintain their toxicity (Figure 2.1A-C).

These results therefore indicate that all the five chaperones examined here can suppress or decrease markedly the toxicity of oligomers formed by three different peptides and proteins, with such generic suppression being specific for chaperones relative to other proteins.

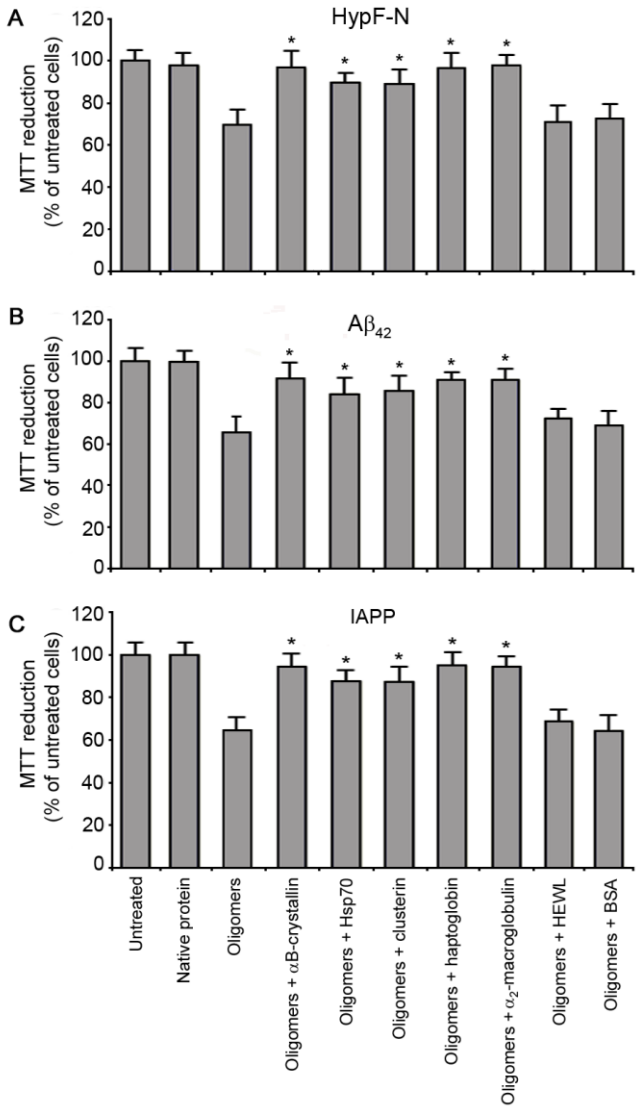

Figure 2.1. Suppression of protein oligomer toxicity by chaperones. Preformed oligomers of HypF-N (A), $A\beta_{42}$ (B) and IAPP (C) were resuspended in the cell culture medium, incubated for 1 hour at a corresponding monomer concentration of 12 μM in the absence or presence of the indicated chaperones and control proteins (protein:chaperone molar ratios were 5:1, 5:1, 10:1, 15:1 and 100:1, respectively; protein:HEWL and protein:BSA molar ratio was 5:1) and then added to SH-SY5Y cells. Cell viability was expressed as percent of MTT reduction in treated cells with respect to untreated cells (taken as 100%). The values shown are means ± SD of three independent experiments carried out in triplicate. An asterisk indicates a significant difference ($p \leq 0.01$) relative to the experiment without chaperones.

2.2.2 Chaperones reduce protein oligomer toxicity even at very low concentration

In order to investigate the means by which chaperones suppress the toxicity of protein oligomers and the resulting effects on the cells, we chose to focus on oligomers formed by one specific protein, HypF-N. Under different experimental conditions, HypF-N aggregates into toxic (type A) or nontoxic (type B) oligomeric forms, which are morphologically similar and bind ThT to similar levels, making it possible to have a powerful control system [Campioni *et al*., 2010]. In addition, differences in structure of toxic and nontoxic oligomers have been detected by means of fluorescence spectra of PM-labelled oligomers [Campioni *et al*., 2010], providing a valuable spectroscopic method for probing the conformational changes experienced by the oligomers following their exposure to chaperones (see below).

The experiments described above for toxic (type A) HypF-N oligomers were repeated by varying the concentrations of each of the five chaperones in the 1 hour pre-incubation solution, while maintaining constant the HypF-N concentration. The results show that the ability of each of the five chaperones to suppress the toxicity of HypF-N oligomers decreased with the chaperone concentration (Figure 2.2). However, all chaperones had significant effects even at HypF-N:chaperone molar ratios of 500:1, becoming ineffective only at molar ratios of 2000:1 (Figure 2.2). Given the size of HypF-N oligomers observed with atomic force microscopy (2-6 nm) it can be estimated that HypF-N oligomers do not contain more than 10-20 molecules [Campioni *et al*., 2010], showing that chaperones are able to suppress toxicity at greatly sub-stoichiometric concentrations, that is with far less than one chaperone molecule per oligomer.

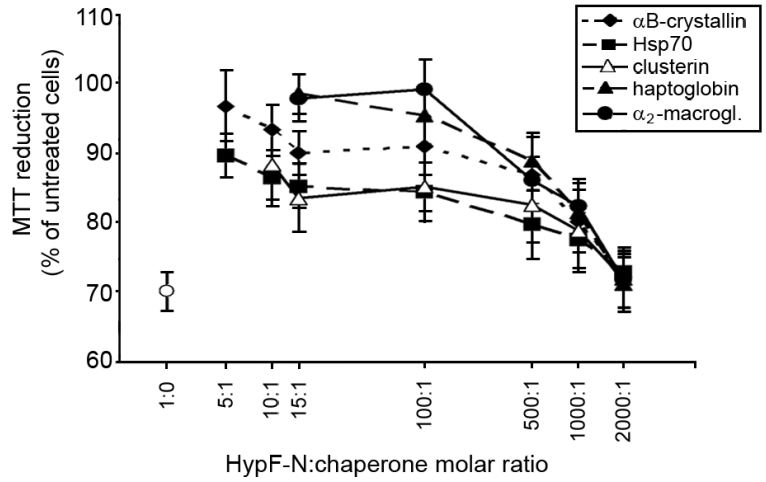

Figure 2.2. Suppression of HypF-N oligomer toxicity by chaperones at different protein:chaperone molar ratios. HypF-N oligomers were incubated for 1 hour in the absence (o) or presence of the indicated chaperones and at the indicated HypF-N:chaperone molar ratio and then added to SH-SY5Y cells. The scale on the x axis is logarithmic.

2.2.3 Chaperones prevent the interaction of oligomers with cellular membranes

Type A HypF-N oligomers have been shown to impair cell membrane and cause an influx of Ca^{2+} ions from the extracellular space into the cytosol, which triggers a complex cellular cascade eventually leading to apoptosis [Zampagni *et al*., 2011]. We therefore carried out experiments to identify the cellular mechanism by which the chaperones studied here are able to suppress oligomer-mediated toxicity. Pre-incubation of type A oligomers with each of the five chaperones in the culture medium for 1 hour, prior to addition to the cells, was found to inhibit the increase of intracellular Ca^{2+} levels caused by the oligomers, with the degree of inhibition increasing with time of pre-incubation (Figure 2.3).

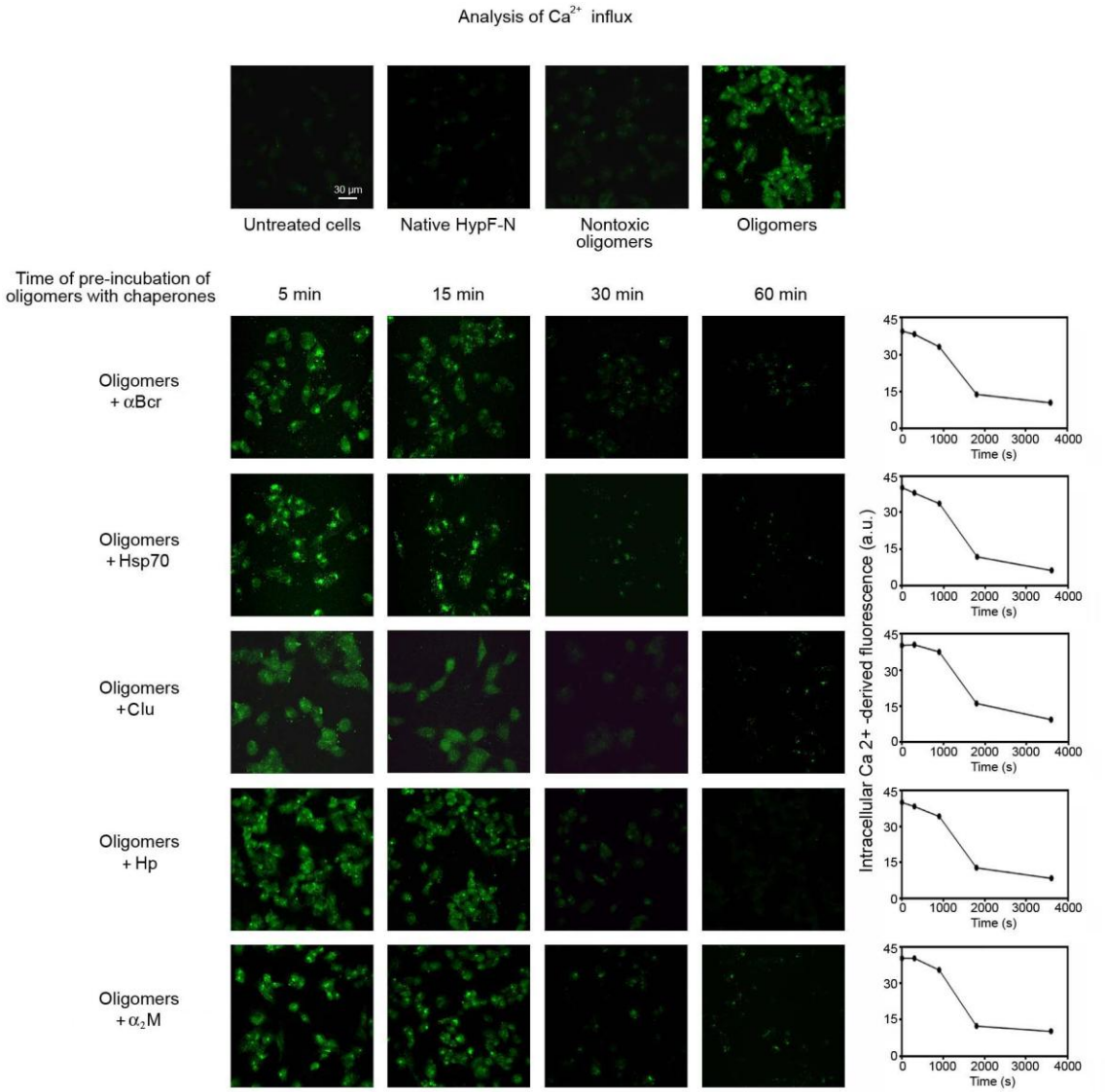

Figure 2.3. Representative confocal scanning microscope images showing intracellular Ca^{2+} levels in SH-SY5Y cells. Preformed oligomers of HypF-N were resuspended in the cell culture medium, incubated in the absence or presence of the indicated chaperones for the indicated time lengths and then added to SH-SY5Y cells for 1 hour. The figure also shows top panel images obtained with untreated cells, cells exposed for 1 hour to the native protein, nontoxic HypF-N oligomers and toxic oligomers. The kinetic plots show the mean fluorescence per cell associated with intracellular Ca^{2+} versus time elapsed after oligomer pre-incubation with each chaperone. In all images the green fluorescence arises from the intracellular Fluo3 probe bound to Ca^{2+}. Ca^{2+} influx from the extracellular medium to the cytosol mediated by the oligomers was inhibited by the 5 chaperones with an effect dependent on the time of pre-incubation of the oligomers with the chaperones.

The cellular dysfunction generated by the toxic oligomers is also manifested as increases in the levels of intracellular ROS and in caspase-3 activity, and as a release of intracellular calcein from cells, with all these events following the Ca^{2+} influx [Zampagni *et al*., 2011]. Pre-incubation of preformed type A oligomers in the culture medium for 1 hour with each of the five chaperones, prior to addition to the cells, was able to abolish to a very substantial degree all the effects generated by the oligomers, again with the extent of inhibition again being dependent on the time of pre-incubation (data not shown).

It is therefore evident that all five chaperones examined here can inhibit the initial biochemical events induced by toxic type A HypF-N oligomers, namely the influx of Ca^{2+}, thus eliminating the occurrence of later effects, manifested as oxidative stress, membrane leakage and apoptosis. In addition, the observed dependence of the degree of protection on the time of pre-incubation indicates that the chaperones generically reduce toxicity by interacting with the oligomers, rather than through a separate protective pathway mediated by direct interaction of the chaperones with the cells.

Overall, therefore, these findings reveal that the deleterious effects of adding toxic HypF-N oligomers to the extracellular medium of the cells can be abolished by chaperones only if the chaperone-oligomer interactions occur at the early stages of incubation, before the oligomers are able to interact with the cell membranes.

2.2.4 Evaluation of chaperone-promoted oligomer endocytosis

It is well known that extracellular chaperones interact with misfolded proteins and favour their clearance via endocytosis mediated by the lipoprotein receptor-related proteins 1 and 2 (LRP-1 and LRP-2) or CD163 [Hammad *et al*., 1997; Fabrizi *et al*.,

2001; Kristiansen *et al*., 2001]. In principle, therefore, it is possible that extracellular chaperones suppress the toxicity of the HypF-N oligomers via interaction with them, endocytosis and degradation. This possibility was however excluded in our system, as shown by confocal microscopy and anti-HypF-N antibodies to monitor the transfer of HypF-N from the extracellular space to the cytosol (Figure 2.4). Indeed, we have found that preformed toxic oligomers of HypF-N, unlike the native protein and nontoxic oligomers, are internalised following pre-incubation for 1 hour in the absence of chaperones. The images show that the green fluorescence arising from anti-HypF-N antibodies appears inside the cells (coloured red) only upon treatment with the toxic oligomers (Figure 2.4A). Analysis of the confocal images at median planes indicated that many of the aggregates are present inside the cells, rather than outside or attached to the membrane (Figure 2.4B).

When the experiment was repeated by pre-incubating the type A oligomers in the presence of each chaperone under the same conditions, little or no HypF-N entry was observed. The oligomers are predominantly detected, similarly to images obtained using nontoxic oligomers in the absence of chaperones, outside the cells or attached to the membrane but not within the cells (Figure 2.4A), as confirmed by analysing the confocal images at median planes parallel to the coverslip (Figure 2.4B). These observations show that the chaperones inhibit oligomer internalisation, at least under the conditions used here, rather than stimulating their intracellular degradation following endocytosis.

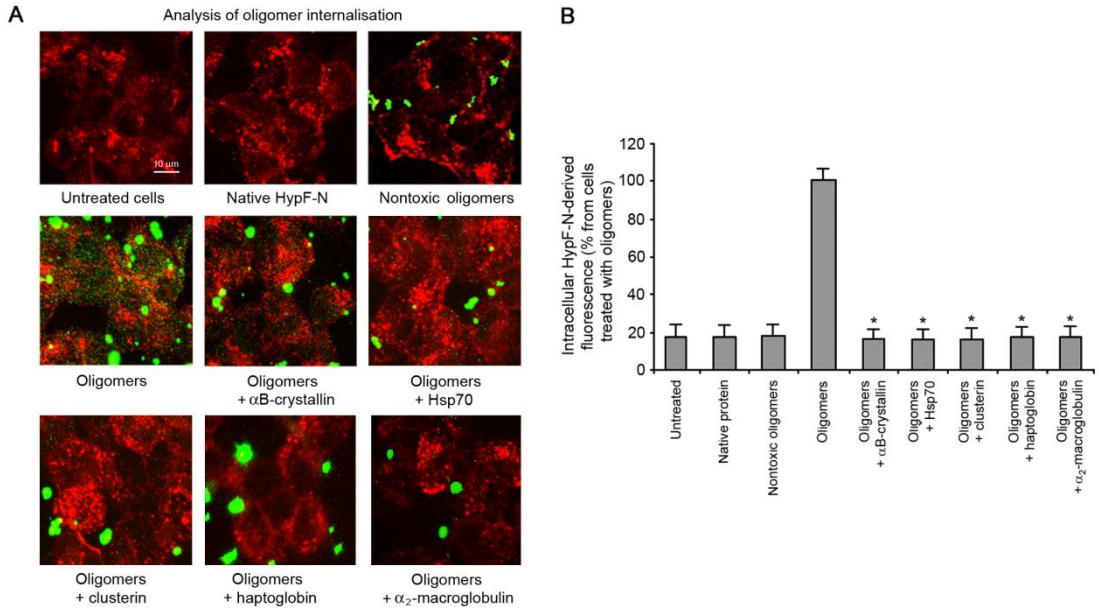

Figure 2.4. Representative confocal microscopy images showing the internalisation of HypF-N oligomers within SH-SY5Y cells. Preformed oligomers of HypF-N were resuspended in the cell culture medium, incubated for 1 hour in the absence or presence of αB-crystallin, Hsp70, clusterin, haptoglobin or α_2-macroglobulin and then added to SH-SY5Y cells. After plasma membrane permeabilisation with a 3% glycerol solution, counterstaining was performed with Alexa Fluor 633-conjugated wheat germ agglutinin to detect the plasma membranes (red) and with 1:1000 diluted rabbit polyclonal anti-HypF-N antibodies and 1:1000 diluted Alexa Fluor 488-conjugated anti-rabbit secondary antibodies (green) to detect the oligomers. (B) Quantification of the green fluorescence arising from HypF-N oligomers inside the cells (median planes). The values reported are means ± S.D. of three independent experiments. An asterisk indicates a significant difference ($p \leq 0.01$) relative to the experiment with oligomer and without chaperones.

2.2.5 Chaperones do not dissolve preformed oligomers

Three possible non-exclusive molecular mechanisms can be hypothesised to explain how chaperones suppress the toxicity of the oligomers: (i) the chaperones disassemble preformed oligomers; (ii) they bind to oligomers and promote their assembly into larger and innocuous aggregates, (iii) they catalyse a structural reorganisation of the toxic oligomers into nontoxic forms.

To investigate whether chaperones disaggregate oligomers, we took advantage of the ability of the HypF-N oligomers to bind to ThT and increase its fluorescence [Campioni *et al.*, 2010]. The presence of native HypF-N or free chaperones causes at

most only negligible increases in ThT fluorescence (Figure 2.5). By contrast, HypF-N oligomers incubated for 1 hour in a phosphate buffer at neutral pH, cause a 6/7-fold increase of ThT fluorescence, and pre-incubation of the oligomers in the same buffer for 1 hour with each of the chaperones did not change the observed ThT fluorescence emission intensity (Figure 2.5). These results indicates that the chaperones do not suppress the toxicity of the oligomers by promoting their disaggregation.

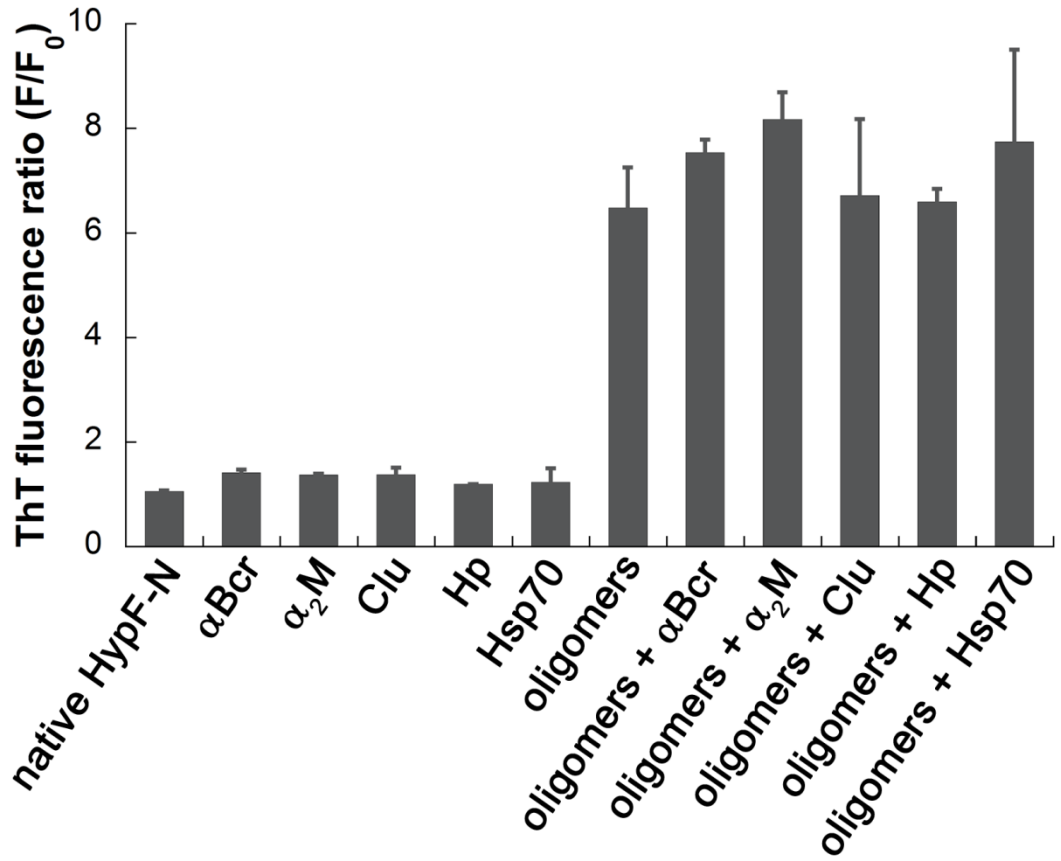

Figure 2.5. Chaperones do not disaggregate HypF-N oligomers. ThT fluorescence at 485nm (excitation 440nm) in the presence of native HypF-N, αB-crystallin, α_2-macroglobulin, clusterin, haptoglobin, Hsp70, HypF-N oligomers after 1 hour incubation in phosphate buffer in the absence or in the presence of each chaperone. The ratio between the ThT fluorescence in the presence (F) and absence (F_0) of proteins is reported; data are means ± SD of three independent experiments.

2.2.6 Chaperones bind to and assemble the oligomers into larger species

To investigate whether chaperones bind to the oligomers and promote their further assembly, we first used AFM. Discrete oligomers with a height of 2–6 nm were observed by AFM in the absence of chaperones (Figure 2.6A), but significantly larger aggregates are evident with αB-crystallin (Figure 2.6B) or α_2-macroglobulin (Figure 2.6C), used here as representative chaperones. On higher magnification of these images, the aggregates appear as clusters of oligomers (Figure 2.6D). In some cases, more complex structures are observed, consisting of very large aggregates of irregular shape with typical heights of a few tens of nanometers, often surrounded by clusters of more distinct oligomers. Large assemblies are not observed in samples containing only chaperones (Figure 2.6E,F).

The AFM data show that chaperones promote the assembly of the oligomers into larger species, but do not provide information on whether or not the chaperones remain bound to them. The oligomers can also be observed with confocal microscopy as, unlike free chaperones, they adhere to the glass coverslips (Figure 2.6G). Images obtained using oligomers pre-incubated for 1 hour with αB-crystallin or α_2-macroglobulin show larger aggregates and co-localisation of the chaperones with the large oligomer clusters (Figure 2.6H,I). Although this technique has a resolution that enables only visualisation of clusters of oligomers or areas enriched with oligomers (not individual oligomers), it shows that the chaperones are bound to the large clusters of oligomers.

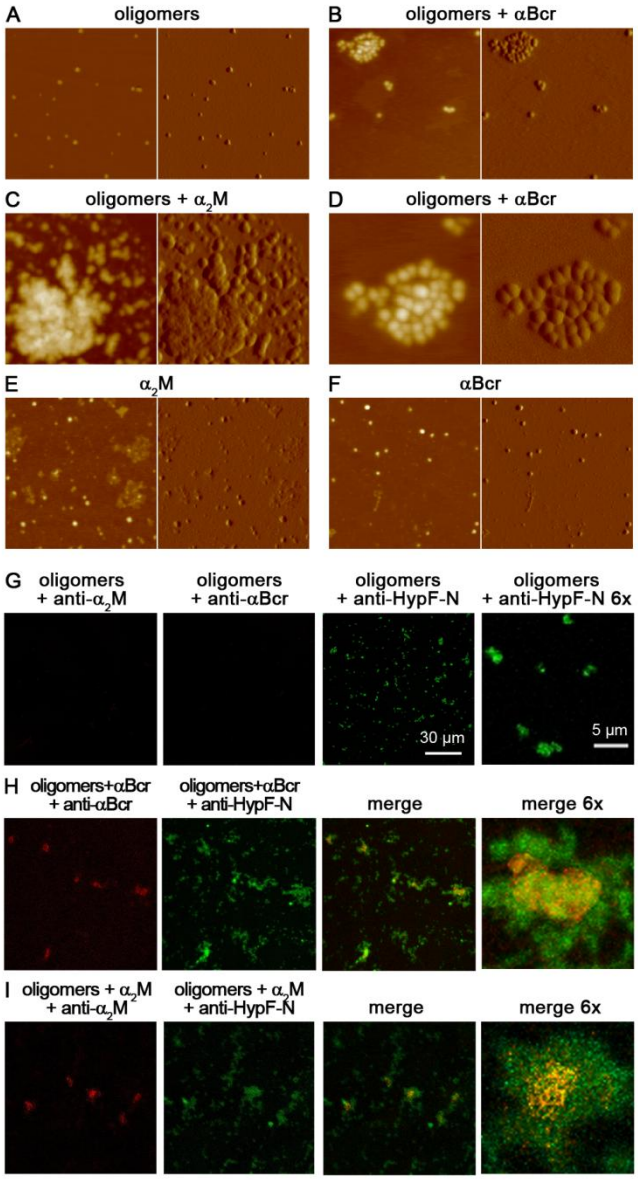

Figure 2.6. Assembly of oligomers induced by chaperones. (A-C) AFM images (left, height data; right, amplitude data) showing HypF-N oligomers pre-incubated for 1h in phosphate buffer without (A) or with αB-crystallin (B) or α_2-macroglobulin (C); control images of α_2-macroglobulin (E) and αB-crystallin (F) alone; scan size, 630 nm. (D) Enlargement of a 250x250 nm portion of (B). Z range: 10 nm (A), 13 nm (B, D), 25 nm (C), 6 nm (E), 10 nm (F). (G) Representative confocal microscope images showing HypF-N oligomers without chaperones and treated with anti- α_2-macroglobulin (red), anti-αB-crystallin (red) or anti-HypF-N (green) antibodies, as indicated. The absence of red fluorescence indicates the absence of cross-reaction. (H,I) Images showing HypF-N oligomers incubated with αB-crystallin (H) or α_2-macroglobulin (I) and treated with the same three antibodies, as indicated. The co-localization of oligomers and chaperones is shown in the merge images (yellow).

The binding between oligomers and the chaperones αB-crystallin or α_2-macroglobulin was also investigated through immuno-dot blot assays. Different quantities of αB-crystallin, α_2-macroglobulin, native HypF-N, or lysozyme were bound to nitrocellulose membranes; the membranes were then saturated with milk, treated with preformed type A oligomers and then with rabbit polyclonal anti-HypF-N antibodies and anti-rabbit secondary antibodies conjugated with horseradish peroxidase. Dose-dependent binding of oligomers was detected to immobilized chaperones but not to immobilized lysozyme (Figure 2.7A). As expected, strong binding of anti-HypF-N antibodies to immobilized native HypF-N treated with HypF-N oligomers was detected. Dot blots of membranes treated with PBS, rather than preformed oligomers, were not detected, confirming that antibody binding is specific for HypF-N (Figure 2.7B).

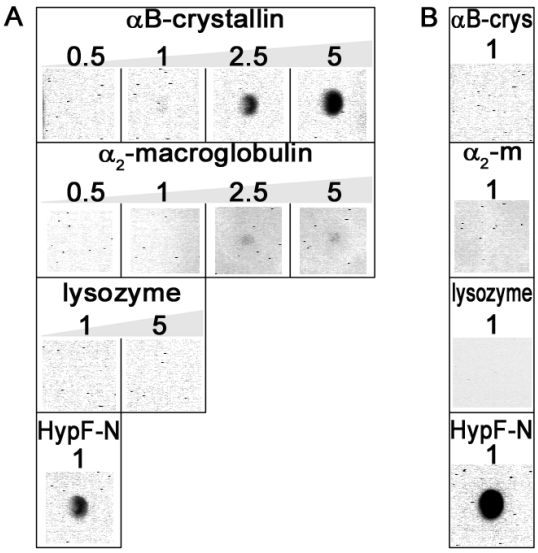

Figure 2.7. Binding of chaperones to HypF-N oligomers detected by immuno-dot blot assay. Membranes with different quantities of immobilized αB-crystallin or α_2-macroglobulin (0.5, 1, 2.5, 5 μg), lysozyme (1, 5 μg) and HypF-N (1 μg) were treated with 50 μg/ml preformed HypF-N oligomers (A) or PBS (B). Anti-HypF-N antibody treatment reveals the presence of the oligomers bound to the chaperones.

In another experiment, type A HypF-N oligomers were incubated in the presence of each chaperone for 1 hour and the resulting mixture was centrifuged to separate the soluble (supernatant, SN) and insoluble (pellet, P) fractions. These fractions were then analysed separately by SDS-PAGE. In the control samples containing oligomers or αB-crystallin alone, the HypF-N monomer (MW ~10.5 kDa) and the αB-crystallin monomer (MW ~20 kDa) were found only in the P and SN fractions, respectively (Figure 2.8A). In the sample containing both species, the HypF-N band was found only in the P fraction, whereas αB-crystallin was found to partition between the P and SN fractions (Figure 2.8A). This finding indicates that a fraction of αB-crystallin is bound to the oligomers. Moreover, the αB-crystallin found in the P fraction remains tightly associated with the oligomers after re-suspension of the pellet and further incubation (Figure 2.9). Similar results were obtained using α_2-macroglobulin (Figure 2.8B). The results, therefore, confirm that binding occurs between the oligomers and all five chaperones studied here, making it possible to pellet the otherwise soluble chaperones through centrifugation.

Fluorescence spectra of the SN fractions collected in each experiment were also acquired (Figure 2.8C,D). The SNs obtained from the samples where both oligomers and chaperones were present yielded fluorescence spectra that were less intense than the corresponding samples in which only the chaperone was present, confirming that a fraction of the chaperone population had been separated through centrifugation.

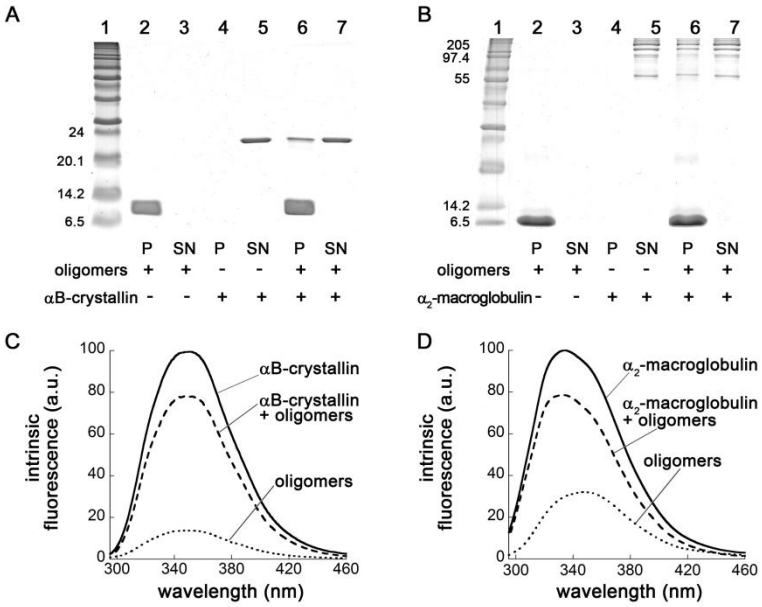

Figure 2.8. Binding of chaperones to HypF-N oligomers. (A) SDS-PAGE analysis of the P and SN fractions of samples containing HypF-N oligomers (lanes 2,3), αB-crystallin (lanes 4,5) and oligomers with αB-crystallin (lanes 6,7). The bands at ~10 and 20 kDa indicate monomeric HypF-N and αB-crystallin, respectively. The HypF-N concentration was 48 μM. (B) SDS-PAGE analysis for α_2-macroglobulin; conditions and lanes as in (A). The α_2-macroglobulin bands range from ~ 60 kDa to ~ 160 kDa. (C) Intrinsic fluorescence spectra of the SN fractions of samples containing HypF-N oligomers (dotted line), αB-crystallin (solid line) and oligomers with αB-crystallin (dashed line). The spectrum of HypF-N oligomers has been subtracted from that of chaperone plus oligomers to clear the contribution of the former. All spectra are the means of three experiments. (D) Intrinsic fluorescence analysis of α_2-macroglobulin. Conditions and spectra as in (C).

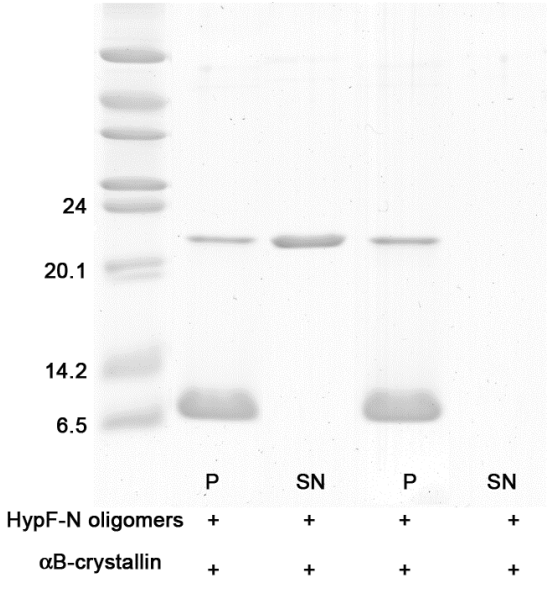

Figure 2.9. The binding between αB-crystallin and HypF-N oligomers is stable. Preformed HypF-N oligomers were incubated for 1 hour with αB-crystallin. The resulting mixture was then centrifuged and the SN and P fractions analysed with SDS-PAGE (lanes 2,3). A fraction of αB-crystallin remains in the SN, whereas a fraction is in P (lanes 2,3), due to the binding to the HypF-N oligomers. A P fraction of a similarly prepared sample was resuspended in phosphate buffer (pH 7.0) as before, incubated for 1 hour, centrifuged and then analysed with SDS-PAGE (lanes 4,5). All the chaperone is found in the P fraction, while the SN fraction is empty. This result indicated that the binding between αB-crystallin and HypF-N oligomers was stable because of the same amount of chaperone in the P fraction after washing it. The bands at ~ 10 and 22 kDa indicate HypF-N and αB-crystallin monomers, respectively.

Similar experiments of SDS-PAGE (Figure 2.10A,B,C) and intrinsic fluorescence measurements (Figure 2.10D,E,F) were acquired by treating the oligomers with Hsp70 (Figure 2.10A,D), clusterin (Figure 2.10B,E) and haptoglobin (Figure 2.10C,F). The results obtained indicate that a binding occurs also between these chaperones and HypF-N oligomers.

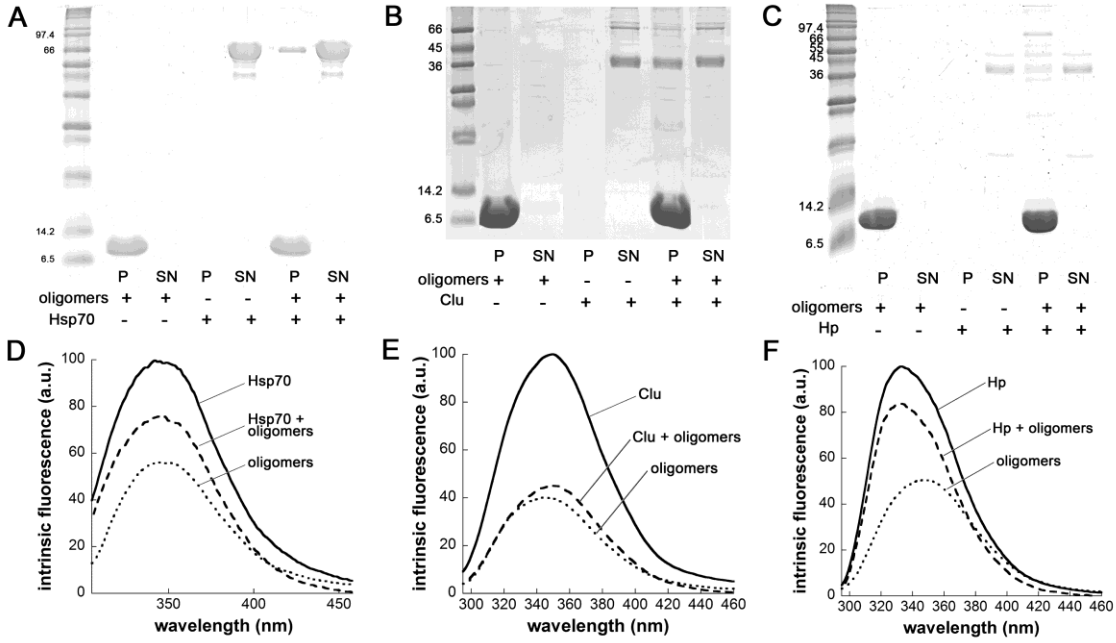

Figure 2.10. Binding of Hsp70 (A,D), clusterin (B,E) and haptoglobin (C,F) to HypF-N oligomers. (A) SDS-PAGE of the insoluble (P) and soluble (SN) fractions obtained from samples containing preformed HypF-N type A oligomers (lanes 2, 3), Hsp70 (lanes 4, 5) and preformed type A oligomers treated for 1 hour with Hsp70 (lanes 6, 7). HypF-N concentration was 48 μM (monomer concentration). The bands at ~ 10 and 70 kDa indicate HypF-N and Hsp70 respectively. (B) SDS-PAGE analysis for clusterin; conditions and lanes as in (A). The bands at ~ 10 kDa and bands ranging from 36 to 66 kDa indicate HypF-N and clusterin, respectively. Under reducing conditions, the α and β subunits of Clu co-migrate to about 36 kDa and lesser amounts of unprocessed (single chain) and variably glycosylated clusterin are also visible at higher molecular weights. (C) SDS-PAGE analysis for haptoglobin; conditions and lanes as in (A). The bands at ~ 10 kDa and bands ranging from 14 to 70 kDa indicate HypF-N and haptoglobin, respectively. Haptoglobin generates a wide range of bands due to its varied polymeric structure [Hooper and Peacock, (1976)]. (D) Intrinsic fluorescence spectra of the SN fractions obtained after centrifugation of samples containing preformed HypF-N type A oligomers (dotted line), Hsp70 (solid line) and HypF-N type A oligomers + Hsp70 (dashed line). The spectrum of HypF-N oligomers has been subtracted from that of Hsp70 + HypF-N oligomers to eliminate its contribution. All spectra are the means of three independent experiments. (E) Intrinsic fluorescence analysis of clusterin. Conditions and spectra as in (D). (F) Intrinsic fluorescence analysis of haptoglobin. Conditions and spectra as in (D).

Overall, the AFM data indicate that chaperones promote the assembly of the oligomers into larger species, whereas the other analyses indicate that the chaperones are bound to the assembled oligomers. The finding prompted by SDS-PAGE and intrinsic fluorescence that a small fraction of chaperones is bound to the oligomers, suggests that chaperones act as nucleation sites for the assembly of oligomers into larger species and explains why they are effective in suppressing their toxicity even at highly sub-stoichiometric concentrations.

2.2.7 The molecular structure of the oligomers is preserved in the large complexes with chaperones

As a next step we set out to assess if chaperones promote a structural reorganisation of the oligomers at the molecular level, in addition to inducing an assembly of the oligomers. First, examination with Fourier transform infra-red (FTIR) spectroscopy

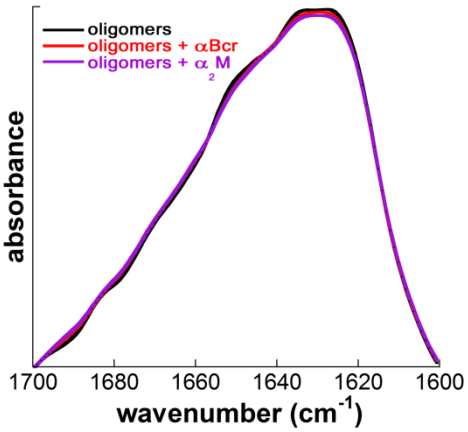

	peak (cm^{-1})	area (%)	structure
oligomers	1625.4	43.3	β-sheet
	1648.2	33.9	random coil
	1669.4	18.4	β-turn
	1683.2	4.4	β-sheet
oligomers + α_2-macroglobulin	1625.8	43.8	β-sheet
	1648.9	33.2	random coil
	1668.2	18.1	β-turn
	1682.3	4.8	β-sheet
oligomers + αB-crystallin	1626.5	46.5	β-sheet
	1649.3	29.8	random coil
	1668.1	19.4	β-turn
	1682.7	4.3	β-sheet

Figure 2.11. Lack of secondary structure reorganization of HypF-N oligomers following treatment with chaperones. FTIR amide I spectra of HypF-N oligomers after incubation without (black) and with αB-crystallin (red) or α_2-macroglobulin (purple). In the table on the right the results of the curve fitting are reported.

indicates that no secondary changes appear to have occurred following the incubation for 1 hour of the oligomers with either αB-crystallin or α_2-macroglobulin, excluding significant changes of secondary structure (Figure 2.11).

To address possible changes in the packing of the hydrophobic groups, we took advantage of the ability to discriminate between toxic and nontoxic HypF-N oligomers through the measurement of the fluorescence properties of oligomers labelled with PM at different positions in the sequence. This method consists in creating HypF-N variants containing a single cysteine at different positions along the sequence, label them with PM and allow the labelled mutants to aggregate. When two pyrene molecules are close to each other (within 10 Å of distance), excited state dimers called excimers form and can be detected because they give rise to the appearance of a peak in the emission spectrum of pyrene centred at 440-470 [Birks *et al*., 1967; Hammarström *et al*., 1999; Krishnan and Lindquist, 2005]. Monitoring the intensity of the excimer band can be used to obtain information on the spatial distance between labelled positions in the oligomers. It has been shown that toxic and non toxic HypF-N oligomers can be discriminated through the measurement of their PM emission spectra [Campioni *et al*., 2010]. In particular, the fluorescence spectra of nontoxic oligomers labelled with PM at certain positions within the hydrophobic regions of the HypF-N sequence show a strong excimer band that is, conversely, very weak in the corresponding spectra obtained with PM-labelled toxic oligomers [Campioni *et al*., 2010].

The three mutants containing a single cysteine residue at positions 25, 55 and 87, all located in the major hydrophobic regions, were therefore labelled with PM, allowed to aggregate to form type A or type B oligomers under their respective conditions, and then transferred to phosphate buffer at pH 7.0 for 1 hour in either the presence or the

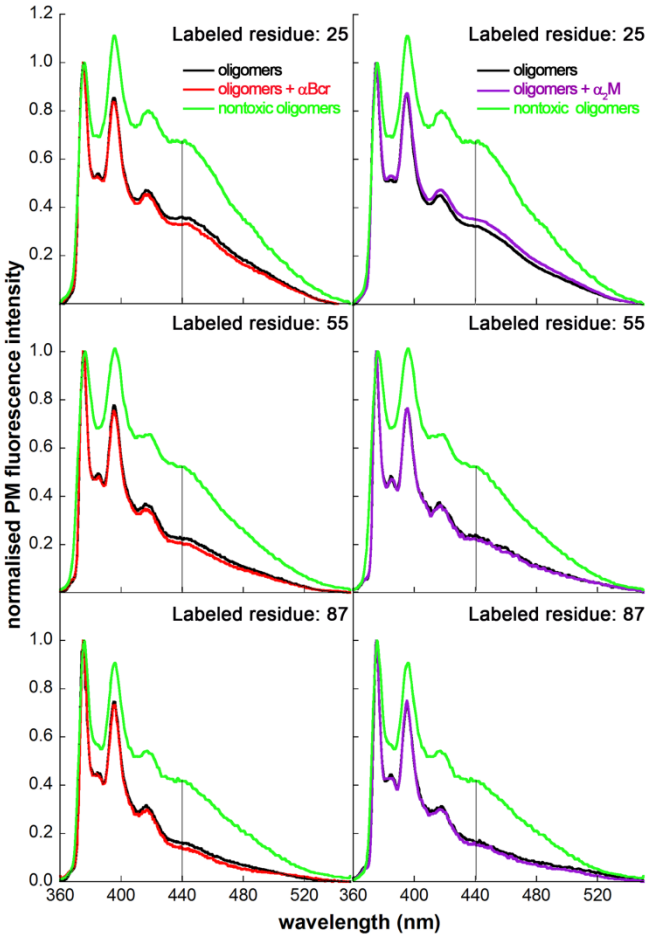

Figure 2.12. Lack of structural reorganization of HypF-N oligomers following treatment with chaperones. Fluorescence emission spectra of HypF-N oligomers labelled with PM at positions 25 (top graphs), 55 (middle graphs) and 87 (bottom graphs). The HypF-N concentration was 12 μM. The spectra refer to oligomers incubated in 20 mM phosphate buffer, pH 7.0 without (black) and with αB-crystallin (red) or α_2-macroglobulin (purple). For comparison, the corresponding spectra of nontoxic oligomers are reported in each graph (green). The spectra are normalized to the intensity of the peak centred at 375 nm. The vertical lines at 440 nm indicate the position of the excimer band.

absence of chaperones. The fluorescence spectra obtained for the type A oligomers labelled at each position after such incubation with or without αB-crystallin or α_2-macroglobulin are very similar and all show the absence of an excimer band (Figure 2.12). By contrast, the spectra obtained for type B oligomers labelled at each position after incubation in the absence of chaperones all show the presence of an excimer band

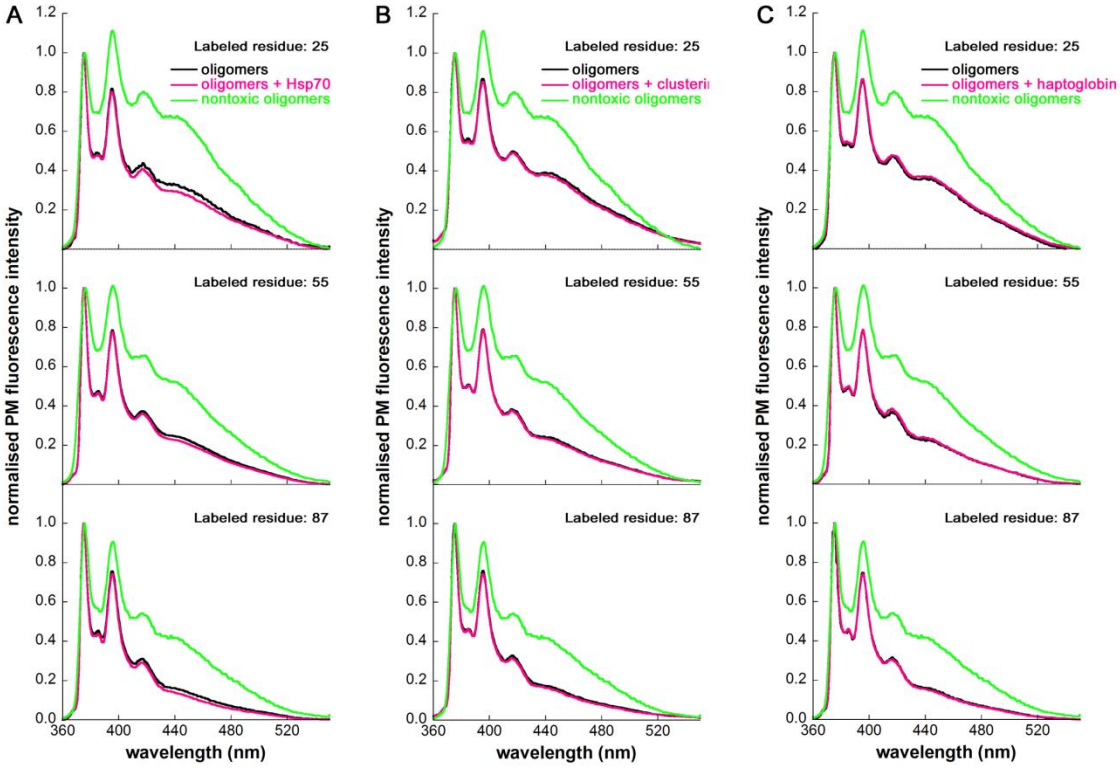

Figure 2.13. Lack of structural reorganization of HypF-N oligomers following treatment with chaperones. (A) Fluorescence emission spectra of samples containing HypF-N oligomers labeled with PM at positions 25 (top), 55 (middle) and 87 (bottom). Mutants of HypF-N containing a single cysteine at either position 25, 55 or 87 were labeled with PM, incubated to form the toxic oligomers and then 4-fold diluted, to a corresponding monomer concentration of 12 μM, into 20 mM phosphate buffer, pH 7.0, 25 °C. The spectra refer to a 1 hour incubation under these latter condition in the absence (black) and in the presence of Hsp70 (A), clusterin (B) or haptoglobin (C) (pink). The spectra have been normalized to the intensity of the peak centered at 375 nm. Spectra of nontoxic oligomers (green) labelled at the same positions are also reported [Campioni *et al.*, 2010].

(Figure 2.12), indicating a tighter packing of the polypeptide chain at these sites within the nontoxic oligomers [Campioni *et al*., 2010]. Similar data were obtained with Hsp70, clusterin and haptoglobin (Figure 2.13A,B,C).

These results reveal that lack of toxicity resulting from exposure to chaperones cannot be attributed to the conversion of type A oligomers into type B oligomers. They do not, however, rule out the possibility that the toxic type A oligomers convert into a different type of nontoxic oligomers and thus, to address this possibility, we extended our analysis to oligomers formed from 1:1 mixtures of HypF-N monomers labelled with PM at different positions. Indeed, the pattern of excimer ratio values obtained from a well defined oligomer type, after uniform PM labelling at various positions and in 1:1 mixtures of differently labeled positions, is unique and represents a molecular signature of the oligomer type, as the intensity of the excimer band reflects in each case the spatial distance between labeled positions [Birks, 1967; Hammarström *et al*. (1999); Krishnan and Lindquist, (2005)]. We have labelled 5 positions in the HypF-N sequence

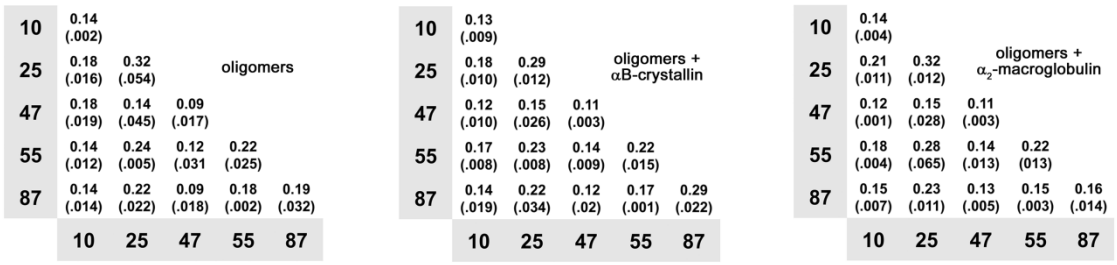

Figure 2.14. Lack of structural reorganization of HypF-N oligomers following treatment with chaperones. Ratios between the PM fluorescence intensities measured at 440 nm (excimer peak) and 375 nm (PM monomer peak) for HypF-N oligomers prepared with 1:1 mixtures of HypF-N chains PM-labelled at positions 10, 25, 47, 55 and 87 and incubated without (left panel) and with αB-crystallin (middle panel) or α_2-macroglobulin (right panel). The total HypF-N concentration was 12 μM. The SD of at least two independent experiments are reported in brackets.

(residues 10, 25, 47, 55, 87) and made all possible 1:1 mixtures, therefore obtaining excimer ratios for a total of 15 differently labelled HypF-N type A oligomers. The patterns of 15 excimer ratio values obtained in the presence of αB-crystallin or α_2-macroglobulin are essentially identical to the pattern obtained in the absence of chaperones (Figure 2.14), indicating that the spatial distribution of residues in the oligomers is preserved following interaction with the chaperones.

2.3 Discussion

The data presented here show that a representative set of chaperones can inhibit extremely efficiently the toxicity of protein oligomers formed by very different peptides and proteins. This behaviour results from the ability of the chaperones to bind to oligomers and promote their further assembly into larger species, in the absence of any significant reorganisation of their internal molecular structure. This mechanism of action is extremely effective as it allows the chaperones to suppress toxicity at highly substoichiometric levels, and remain protective even at molar ratios of client protein:chaperone as high as 500:1.

These data also suggest that the size of extracellular protein aggregates correlates inversely with their toxicity. The binding and sequestration of the misfolded proteins within larger clusters is very likely to cause both a reduction of the exposure of the hydrophobic surfaces of the oligomers and a of their diffusional mobility, both of which are expected to lead to the inhibition of their toxicity. In addition, this behaviour is reminiscent of the formation of large aggresomes and inclusion bodies in eukaryotic and bacterial cells, respectively [Kopito, 2000; Sabate *et al*., 2010], indicating such processes as an effective strategy to handle protein aggregates and ultimately facilitate their clearance.

The ability of molecular chaperones to suppress the toxicity of preformed protein oligomers in the generic manner detected in this study adds to the well established functions of molecular chaperones to facilitate folding of proteins, to inhibit their aggregation and to disaggregate or promote clearance of protein aggregates. In all the experiments performed in this work the oligomers are formed before addition of the chaperones showing that the protective action of the latter can also include the neutralisation of toxic oligomers after they are formed. This effect represents an additional protective mechanism to add to our current understanding of the concept of protein homeostasis.

Proteins are soluble mainly because a number of sequence and structural characteristics have evolved to achieve this requirement [Dobson, 2003; Monsellier and Chiti, 2007]. Chaperones act to counteract the inevitable failure of proteins to remain soluble and their protective actions occur at multiple levels, including facilitating protein folding and the degradation of protein aggregates, and inhibiting both protein aggregation and the toxicity of protein aggregates. The levels of misfolded proteins and toxic aggregates are usually low enough to permit these protective mechanisms to neutralise their potential effects. However, once this system is overwhelmed, e.g. by mutation, aging and other causes, these toxic effects can lead to malfunction and disease. Chaperones can buffer the formation of protein aggregates and their deleterious effects in living systems, explaining why, for example, the accumulation of fibrillar aggregates and associated smaller oligomers does not lead to manifest clinical signs of disease until the amyloid burden becomes unsustainable [Lachmann and Hawkins, 2006; Petersen, 2010]. The generic ability of chaperones to suppress the toxicity of protein aggregates formed by very different peptides and proteins, and to do so at very

low concentrations, indicate that they can act as efficient guardians against a multiplicity of protein aggregates, rather than a single species, when the protein homeostasis system is close to being overwhelmed.

These data also suggest that Nature may well be instructing us how to fight against protein misfolding diseases: the structure, function and mechanism of action of molecular chaperones may serve to guide the design of therapeutic interventions against diseases originating from the failure of protein homeostasis. Indeed, the finding that natural molecular chaperones can inhibit the toxicity of aberrant protein aggregates, after they are formed, with broad specificity and at very low concentrations, suggests that therapeutics based on the same type of intervention could be effective against such diseases, even at stages of the disease when the populations of toxic misfolded species have reached significant levels.

2.4 Materials and Methods

2.4.1 Cloning of the HypF-N gene, protein expression and purification

The gene for HypF-N was cloned by Dr. Giulia Calloni in a modified pQE30-Xa plasmid (Qiagen S.p.A., Milano, Italy), in which the DNA stretch coding for the factor Xa cleavage site was substituted by a sequence coding for the thrombin cleavage site (pQE30-Th). As a result of this changing, the purified protein has the N-terminal Met residue substituted by a Gly-Ser dipeptide attributed to positions 0 and 1, respectively.

Cultures of *E. coli* XL1 Blue cells harbouring the pQE30-Th/HypF-N plasmid were grown overnight at 37 °C in LB medium with 100 μg/ml ampicillin (Sigma-Aldrich) under shaking. The cells were then diluted 1:10 in fresh medium and grown at 25°C until the optical density at 600 nm (OD_{600}) reached ~ 0.6. Protein expression was

induced overnight at 25°C by means of 1 mM isopropyl β-Dthiogalactoside (IPTG) from Inalco (Milano, Italy). Cells were harvested by centrifugation, resuspended in 40 ml of lysis buffer (50 mM sodium phosphate, 300 mM NaCl, 10 mM imidazole at pH 8.0) and then lysed by 1 hour incubation with 1 mg/ml lysozyme in ice, followed by sonication at 40 kHz (five cycles of 30s each spaced by 30s in ice). The cell lysate was applied at 4 °C to an affinity chromatography column packed with the HIS-Select Nickel Affinity Gel (Sigma-Aldrich) previously equilibrated with lysis buffer at 4 °C. The column was washed with 50 mM phosphate buffer, 300 mM NaCl, 20 mM imidazole, pH 8.0, 4 °C, equilibrated in 50 mM phosphate buffer, 50 mM NaCl, pH 8.0 and then incubated overnight at 4 °C with 50 units of human thrombin (Sigma-Aldrich). Fractions containing pure HypF-N separated from the His-tag were eluted at 4 °C with 50 mM phosphate buffer, 50 mM NaCl, 10 mM imidazole, pH 8.0 and checked by SDS-PAGE. The purest fractions were buffer-exchanged (5 mM acetate buffer, 2 mM dithiothreitol (DTT), pH 5.5) and concentrated at 4 °C using an ultrafiltration cell with a 3000 Da cut-off cellulose membrane (Millipore, Billerica, MA). Protein concentration was assessed by optical absorption (ε_{280} = 12,490 M cm^{-1}) and stock solutions were stored at -20 °C in 5 mM acetate buffer, 2 mM DTT, pH 5.5.

2.4.2 Chaperones

Human Hsp70 was purified as described [Roodveldt *et al*., (2009)]. The vector pET24d(+) (Novagen, Madison, USA) containing the αB-crystallin gene was a gift from J. A. Carver (University of Adelaide, Australia). Human αB-crystallin was expressed and purified as described previously [Waudby *et al*., 2010]. Human clusterin, α_2-macroglobulin and haptoglobin were purified as described [Wilson and Easterbrook-Smith, 1992; French *et al*., 2008; Yerbury *et al*., 2005].

2.4.3 Formation of protein oligomers

Oligomeric aggregates of HypF-N were prepared by incubating the protein for 4 hour at 25 °C and at a concentration of 48 μM in 50 mM acetate buffer, 12% (v/v) TFE, 2 mM DTT, pH 5.5 (condition A). Nontoxic oligomers used as controls were prepared by incubating the protein for 4 hour at 25 °C and at a concentration of 48 μM in 20 mM TFA, 330 mM NaCl, pH 1.7, (condition B). Oligomers were centrifuged at 16100 rcf for 10 min, dried under N_2 and resuspended in cell culture media in the absence of cells (for cell biology tests) or in 20 mM potassium phosphate buffer at pH 7.0 (for biophysical/biochemical analysis). As reported, no significant dissolution of the oligomers or change in morphology/structure could be detected after this procedure [Campioni *et al*., 2010]. Native HypF-N was diluted to a final concentration of 12 μM into the same media. $A\beta_{42}$ and IAPP were obtained from Sigma-Aldrich (St. Louis, MO). Oligomers formed by $A\beta_{42}$ and IAPP were prepared as previously described [Lambert *et al*., 2001; Cecchi *et al*., 2008] and resuspended in cell culture media to obtain a final peptide concentration of 12 μM. Native $A\beta_{42}$ and IAPP were diluted to 12 μM into the same cell culture media. All oligomers were then incubated in the appropriate media for 1 hour at 37°C while shaking, in the absence or presence of chaperones, and then added to cultured cells or subjected to biophysical/biochemical analysis. The HypF-N($A\beta_{42}$/IAPP):chaperone molar ratio was 5:1 (αB-crystallin), 5:1 (Hsp70), 10:1 (clusterin), 15:1 (haptoglobin) and 100:1 (α_2-macroglobulin), unless stated otherwise (HypF-N, $A\beta_{42}$, IAPP, αB-crystallin, Hsp70 are considered as monomers, clusterin and haptoglobin as αβ dimers and α_2-macroglobulin as a tetramer, according to the functional oligomeric state).

2.4.4 Cell cultures

Human SH-SY5Y neuroblastoma cells (A.T.C.C., Manassas, VA, USA) were cultured in Dulbecco's Modified Eagle's Medium (DMEM) F-12 Ham with 25 mM N-2-hydroxyethylpiperazine-N-2-ethanesulfonic acid (HEPES) and $NaHCO_3$ (1:1) supplemented with 10% fetal bovine serum (FBS), 1.0 % glutamine and antibiotics. The cell culture was maintained in a 5.0% CO_2 humidified atmosphere at 37 °C and grown until 80% confluence for a maximum of 20 passages.

2.4.5 MTT reduction assay

The effect of protein oligomers incubated in the absence or presence of the chaperones on cell viability was assessed using SH-SY5Y cells. Preformed oligomers of HypF-N, $A\beta_{1-42}$ and IAPP (12 μM monomer concentration) were incubated for 1 hour in the absence or presence of αB-crystallin, Hsp70, clusterin, haptoglobin, α_2-macroglobulin, HEWL or BSA (HypF-N:chaperone molar ratios as described in section 2.4.3, HypF-N:HEWL and HypF-N:BSA molar ratios were 5:1), and then added to SH-SY5Y cells. The cells, seeded in 96-well plates, were treated for 24 hours at 37°C with the aggregates. The cell cultures were then incubated with 0.5 mg/ml MTT solution at 37°C for 4 hours and subsequently with cell lysis buffer (20% SDS, 50% N,N-dimethylformamide, pH 4.7) at 37°C for 3 hours. Absorbance values of blue formazan were determined at 590 nm and cell viability was expressed as percent of MTT reduction in treated cells as compared to untreated cells (assumed as 100%).

2.4.6 Measurement of intracellular Ca^{2+}

Preformed HypF-N oligomers (12 μM monomer concentration) were incubated for 1 hour in the cell culture medium without or with αB-crystallin, Hsp70, clusterin, haptoglobin or α_2-macroglobulin (HypF-N:chaperone molar ratios were 5:1, 5:1, 10:1, 15:1 and 100:1, respectively) and then added to SH-SY5Y cells seeded on glass coverslips for 60 min at 37°C. To detect intracellular Ca^{2+}, cells were then loaded with 10 μM fluo3-AM (Molecular Probes, Milan , Italy) , as described previously [Campioni *et al*., 2010; Zampagni *et al*., 2011]. Cells were also treated with nontoxic HypF-N oligomers or the native protein (12 μM monomer concentration). Cell fluorescence was analysed by confocal Leica TCS SP5 scanning microscope (Mannheim, Germany) equipped with an argon laser source for fluorescence measurements at 488 nm and 633 nm and a Leica Plan Apo 63X oil immersion objective. A series of optical sections (1024X1024 pixels), 1.0 μm in thickness, were taken through the cell depth for each examined sample. The confocal microscope was set at optimal acquisition conditions, e.g. pinhole diameters, detector gain and laser powers. Settings were maintained constant for each analysis.

2.4.7 Cell internalisation of HypF-N aggregates

Preformed HypF-N oligomers (12 μM monomer concentration) were incubated for 1 hour in the cell culture medium with no cells in the absence or presence of each chaperone (HypF-N:chaperone molar ratios as above) and then added to SH-SY5Y cells seeded on glass coverslips for 60 min at 37°C. Cells were also treated with nontoxic HypF-N oligomers or the native protein (12 μM monomer concentration). Confocal scanning microscope images were acquired as described [Campioni *et al*., 2010]. To

quantify the green fluorescence intensity arising from HypF-N oligomers inside the cells, the images were analysed at median planes parallel to the coverslip for 10-22 cells using ImageJ software (NIH, Bethesda, MD, USA). The intracellular fluorescence intensity was expressed as $(F_{obs}/F_A)\bullet 100$, where F_{obs} and F_A represent the fluorescence values of cells treated with the analysed sample and type A oligomers, respectively, in both cases after subtraction of the baseline value determined for untreated cells.

2.4.8 Thioflavin T assay

Pre-formed oligomers of HypF-N (48 μM monomer concentration) were incubated in the absence or presence of each chaperone for 1 hour (HypF-N:chaperone molar ratios as described above) and then added to a solution of 25 μM ThT dissolved in 25 mM phosphate buffer at pH 6.0, in order to obtain a 3.7-fold molar excess of dye. Final HypF-N protein concentration was 6 μM. The steady-state intensity of fluorescence emission at 485 nm (excitation at 440 nm) was recorded at 37 °C. Samples containing only native HypF-N or only chaperone, both at the corresponding concentrations, were also tested.

2.4.9 Atomic force microscopy

HypF-N oligomers were formed and then incubated without or with chaperones in the conditions detailed above. Samples were diluted from 5 to 100 times; 10 μl aliquots of the diluted samples were deposited on freshly cleaved mica and dried under mild vacuum. Tapping mode AFM images were acquired in air using a Multimode SPM, equipped with "E" scanning head (maximum scan size 10 μm) and driven by a Nanoscope IV controller, and a Dimension 3100 SPM, equipped with a 'G' scanning

head (maximum scan size 100 μm) and driven by a Nanoscope IIIa controller (Digital Instruments, Bruker AXS GmbH, Karlsruhe, Germany). Single beam uncoated silicon cantilevers (type OMCL-AC160TS, Olympus, Tokyo, Japan) were used. The drive frequency was between 290 and 310 kHz, the scan rate was between 0.4 and 0.8 Hz. Aggregate sizes were measured from the height in cross section of the topographic AFM images. The heights reported in the results result from the obtained values being multiplied by a shrinking factor of 2.2, which was evaluated comparing the heights of native HypF-N under liquid and after drying.

2.4.10 Confocal microscopy analysis for binding of HypF-N oligomers with chaperones

Preformed oligomers of HypF-N (48 μM monomer concentration) were incubated in the absence or presence of αB-crystallin or α2-macroglobulin (HypF-N:chaperone molar ratios were 5:1 and 100:1, respectively) for 1 hour in 20 mM potassium phosphate buffer at pH 7.0 and then centrifuged for 10 min at 16100 rcf. The pellet (P) was resuspended in a solution containing 1:4000 rabbit polyclonal anti-HypF-N (Primm, Milan, Italy), goat polyclonal anti-αB-crystallin or goat polyclonal anti-α_2-macroglobulin antibodies (Santa Cruz Biotechnology, Santa Cruz, CA) for 30min at 37°C. After centrifugation for 10min at 16100 rcf, samples were washed in PBS, centrifuged again and incubated with 1:1000 diluted Alexa Fluor 488-conjugated anti-rabbit secondary antibody (Molecular Probes, Milan, Italy) for 30min at 37°C. Samples were than washed in PBS and incubated with 1:4000 Texas red-conjugated anti-goat secondary antibody (Santa Cruz Biotechnology, Santa Cruz, CA) for 30 min at 37°C. After centrifugation, samples were washed in PBS and the P was resuspended in 20 μl

PBS and spotted on glass coverslips. In another series of experiments oligomers were incubated with 1:4000 goat polyclonal anti-αB-crystallin or anti-α2-macroglobulin antibodies (Santa Cruz Biotechnology, Santa Cruz, CA) for 30min at 37°C, centrifuged, washed in PBS and re-incubated with 1:4000 Texas red-conjugated anti-goat secondary antibody (Santa Cruz Biotechnology, Santa Cruz, CA). Confocal microscope images were acquired as described [Campioni *et al*., 2010].

2.4.11 Immuno-dot blot assay

Samples of chaperones (0.5, 1, 2.5, 5 µg), lysozyme (1, 5 µg) and HypF-N (1 µg) were spotted onto nitrocellulose membrane (Bio-Rad, Hercules, CA) and allowed to dry. After blocking with a 5% (w/v) skim milk powder solution in PBS, the membranes were incubated for 2 h at 37°C in PBS with or without 50 µg/ml of HypF-N preformed oligomers, washed three times (5 min each) in PBS and incubated with rabbit polyclonal anti-HypF-N antibodies (Primm, Milan, Italy). The membranes were then incubated with secondary anti-rabbit antibodies conjugated with horseradish peroxidase, followed by enhanced chemiluminescence with the Immun-Star HRP Chemiluminescence kit (Bio-Rad, Hercules, CA). After the treatments with primary and secondary antibodies, the membranes were washed three times (5 min each) in PBS containing 0.1 % (v/v) Tween 20.

2.4.12 SDS-PAGE

Preformed HypF-N oligomers, αB-crystallin and α_2-macroglobulin were incubated for 1 hour in 20 mM potassium phosphate buffer at pH 7.0 in isolation and in combination (48 µM HypF-N, HypF-N:chaperone molar ratios was 5:1 for αB-crystallin and 100:1

for α_2-macroglobulin). Samples were then centrifuged for 10 min at 16100 rcf. Aliquots of the P and SN fractions were subjected to SDS-PAGE analysis as described [Laemmli, 1970] using 15% polyacrylamide gels.

2.4.13 Intrinsic fluorescence

Intrinsic fluorescence spectra of the SN fractions collected for SDS-PAGE were acquired at 37°C using a Perkin-Elmer LS 55 spectrofluorimeter (Wellesley, MA) and a 2X10 mm quartz cell, an excitation wavelength of 280 nm. The spectrum of HypF-N oligomers was subtracted from that of the chaperone in the presence of HypF-N oligomers and all the spectra were normalized to the maximum fluorescence intensity of the chaperone spectrum.

2.4.14 FTIR spectroscopy

Preformed HypF-N oligomers were incubated for 1 hour in 20 mM potassium phosphate buffer at pH 7.0 with or without αB-crystallin or α_2-macroglobulin (48 μM HypF-N, HypF-N:chaperone molar ratios was 5:1 and 100:1 respectively) and then centrifuged and resuspended in D_2O twice to achieve a final volume of 20 μL and a final protein concentration of ~15 mg mL^{-1}. The 20 μL sample was deposited on a KBr window in a semipermanent liquid cell and the FTIR spectra were recorded at room temperature using an FT/IR 4200 spectrophotometer (Jasco, Tokyo, Japan). The system was purged with N_2 starting from 15 min before spectra recording. The background spectra were subtracted and the resulting spectra were baseline corrected and smoothed. Curve fitting on the spectra was performed using the Spectra Manager software (Jasco, Tokyo, Japan).

2.4.15 Pyrene fluorescence

HypF-N variants carrying a single cysteine residue were labelled with PM as previously described [Campioni *et al*., 2010], incubated under conditions A and B in homogeneous or 1:1 mixtures and then diluted 4-fold into 20 mM potassium phosphate buffer at pH 7.0. Fluorescence emission spectra of these samples were acquired and analyzed as previously described [Campioni *et al*., 2010] before and after 1 hour incubation in the absence or presence of chaperones. HypF-N concentration was 12 μM (monomer concentration). HypF-N:chaperone molar ratios was 5:1 for αB-crystallin and 100:1 for α_2-macroglobulin.

2.4.16 Statistical analysis

All data were expressed as mean ± standard deviation (SD). Comparisons between different groups were performed using ANOVA followed by Bonferroni's post-comparison test. A p value lower than 0.05 was considered statistically significant.

Chapter 3

TWO SIDES OF THE SAME COIN: HYDROPHOBICITY AND SIZE AS STRUCTURAL DETERMINANTS OF MISFOLDED OLIGOMER TOXICITY

3.1 Introduction

As described in section 1.2, it is increasingly recognized that the pathogenic species in protein deposition diseases are not the mature fibrils, but the early oligomeric species that precede their formation [Chiti and Dobson, 2006]. Oligomers formed by HypF-N are a widely studied system in this regard. Indeed, a number of characteristics render this protein domain particularly useful for the characterization of its protein misfolded oligomers. First, monomeric HypF-N is readily able to form spherical oligomers and amyloid-like fibrils *in vitro*, under conditions that destabilize its native state or promote its cooperative unfolding into partially structured species [Chiti *et al*., 2001; Relini *et al*., 2004; Marcon *et al*., 2005; Campioni *et al*., 2008] Second, the oligomers that form in the early stages of the aggregation process have the same morphological, structural and tinctorial features as those formed by disease-related peptides and proteins [Marcon *et al*., 2005; Campioni *et al*., 2008] and impair cell viability when added to the extracellular medium of cultured cells [Bucciantini *et al*., 2002; Bucciantini *et al*., 2004; Cecchi *et al*., 2005; Campioni *et al*., 2010; Zampagni *et al*., 2011; Evangelisti *et al*., 2012] and when injected into rat brains [Baglioni *et al*., 2006; Zampagni *et al*., 2011]. Finally, perhaps most importantly, HypF-N oligomers are sufficiently stable to maintain their morphological and structural properties when transferred to conditions that are very different from those that promote their formation, allowing a detailed biophysical and biological characterisation of their structural properties and toxicity, respectively [Campioni *et al*., 2010].

As reported in section 1.5.5, two protocols have been established to convert native HypF-N into stable oligomers, which were named type A and type B, respectively [Campioni *et al*., 2010; Zampagni *et al*., 2011; Evangelisti *et al*., 2012; Tatini *et al*., unpublished]. The two oligomeric forms share a similar morphology and size, as detected with AFM, consisting of small spherical species with a 2-6 nm diameter; they also bind the amyloid diagnostic dye ThT to a similar extent, albeit such binding is weaker than that commonly observed for amyloid fibrils [Campioni *et al*., 2010]. In spite of the similar size, morphology and ThT binding, only type A oligomers were found to be toxic to cells. When added to the extracellular medium of cultured neuronal and endothelial cells, type A oligomers, unlike type B, were found to decrease the mitochondrial MTT reduction activity, to cause an influx of extracellular calcium to the cytosol and to induce apoptosis [Campioni *et al*., 2010; Zampagni *et al*., 2011]. They were also cause cognitive impairment in animal models, with type B oligomers producing no effect [Tatini *et al*., unpublished].

In an attempt to elucidate the structural origin of the different toxicities of type A and B oligomers, it has been shown, using site directed pyrene labeling, that the three main hydrophobic regions of the HypF-N sequence spanning approximately residues 22-34, 55-59 and 75-87 are structured and buried in type B oligomers, whereas the same regions are more flexible and solvent-exposed in type A oligomers [Campioni *et al*., 2010]. In a following study, it was found that the further assembly of type A oligomers into large aggregates mediated by molecular chaperones can suppress their toxic activity [results reported in Chapter 2]. These two reports indicated that the flexibility and solvent exposure of hydrophobic moieties and the small size are important structural determinants of HypF-N oligomer toxicity.

Here we have increased, using site-directed mutagenesis, the hydrophobicity of the three main hydrophobic regions of HypF-N found to have a different solvent exposure in the two oligomer types, with an aim of investigating the effect of such mutations on the superficial hydrophobicity of the oligomers, on their size and on the toxicity of the resulting oligomeric species. We will show that the single or multiple substitutions of a charged amino acid with an apolar one affect both the solvent-exposure hydrophobicity of the HypF-N oligomers and their size, producing counteracting effects on the toxicity of the resulting species.

3.2 Results

3.2.1 Effect of hydrophobic mutations on HypF-N structure

The following five variants have been designed replacing glutamate or arginine residues with leucine within the three main hydrophobic regions of the HypF-N sequence: R23L, E55L, E87L, R23L/E55L and R23L/E87L. These mutants contain basically the same

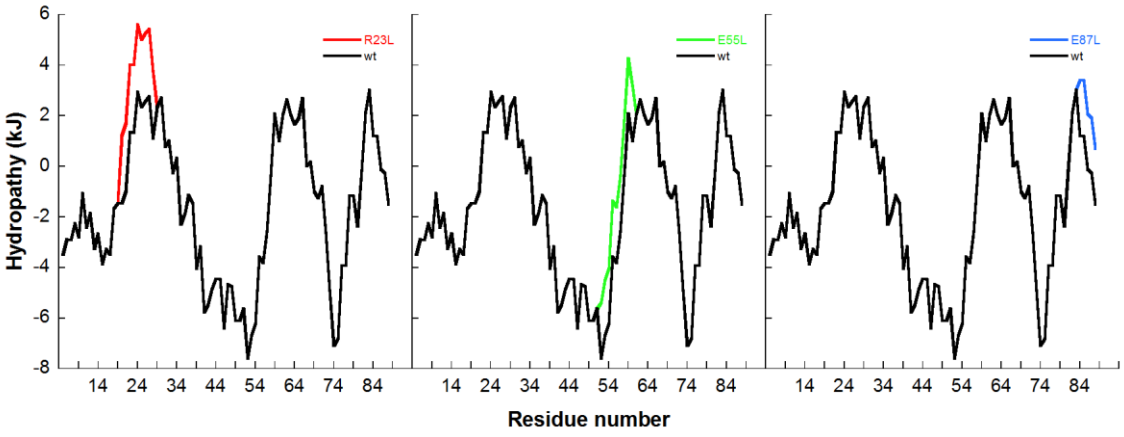

Figure 3.1. Hydropathy profile of the wt and mutant HypF-N sequences. The graphs show the comparison between the hydropathy profile of three variants carrying a single mutation and the wt protein. The hydropathy profiles were calculated using the Roseman hydrophobicity scale [Roseman, 1988].

three mutations, in isolation or in combination, which are individually able to increase the level of hydropathy of each single region involved (Figure 3.1). We decided to substitute charged residues with apolar residues rather than opposite replacements, because it has been shown that the introduction of mutations within the hydrophobic core of HypF-N alters drastically the protein stability and causes protein aggregation into the inclusion bodies following the expression in *E. coli* [Calloni *et al*., 2005]. In an attempt to avoid this phenomenon, we chose variants whose conformational stability was preliminary estimated using FoldX, an algorithm based on an empirical formula derived from the experimentally determined values of free energy change of the unfolding transition in the absence of denaturant ($\Delta G_{U\text{-}F}^{H_2O}$) of over 1000 single mutants from different proteins [Guerois *et al*., 2002].

The native structure of the variants was studied using far-UV circular dichroism (CD). Figure 3.2 reports the native structure of wt HypF-N with the mutated residues

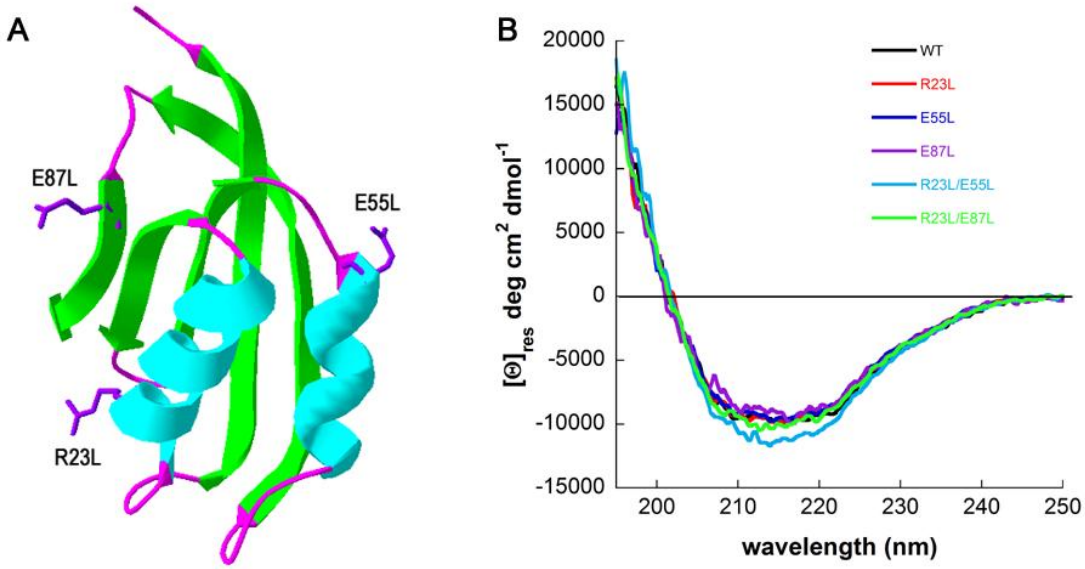

Figure 3.2. (A) Structure of wt HypF-N with the residues involved in the mutations highlighted: Arg23, Glu55 and Glu87 all substituted with leucine. (B) Far-UV CD spectra of wt and mutants of HypF-N acquired under native conditions.

highlighted (Figure 3.2A) and the CD spectra of mutant and wt proteins (Figure 3.2 B). All the variants are characterized by a spectrum typical of a folded α/β protein, with a broad negative minimum in the region between 210 and 220 nm, and similar to the spectrum obtained for the wt protein and previously reported [Calloni *et al*., 2008; Campioni *et al*., 2008]. Hence, the introduction of the hydrophobic mutations does not alter significantly the native structure of the protein variants.

3.2.2 Effect of the hydrophobic mutations on the aggregation kinetics of HypF-N

Type A and type B oligomers of wt and mutant HypF-N were obtained by incubating HypF-N at a protein concentration of 48 μM in (i) 50 mM acetate buffer, 12% (v/v) TFE, 2 mM DTT, pH 5.5 (condition A) and in (ii) 20 mM TFA, 330 mM NaCl, pH 1.7 (condition B) for 4 hours at 25 °C. Under these two conditions, the aggregation kinetics of every variant was measured by using ThT, a fluorescent probe able to bind the cross-β structure typical of amyloid aggregates and to increase its fluorescence emission intensity upon binding [Krebs *et al*., 2005]. At regular time intervals, aliquots of the samples were mixed with a ThT solution and time-course measurements of the fluorescence intensity were obtained (Figure 3.3) and fitted with a single exponential function (equation 3.2, section 3.4.4).

Apparent aggregation rate constants (k_{agg}) were calculated for all aggregation kinetic traces and are reported in Figure 3.4 for the proteins incubated in condition A (left) and B (right).

In condition A, the k_{agg} values measured for both the wt protein and the variants are similar, with the exception of E87L, which presents a higher k_{agg} value with respect to the wt protein. In condition B, all mutants do not have significantly different k_{agg} values from that of the wt protein in the same condition. These results show that the aggregates

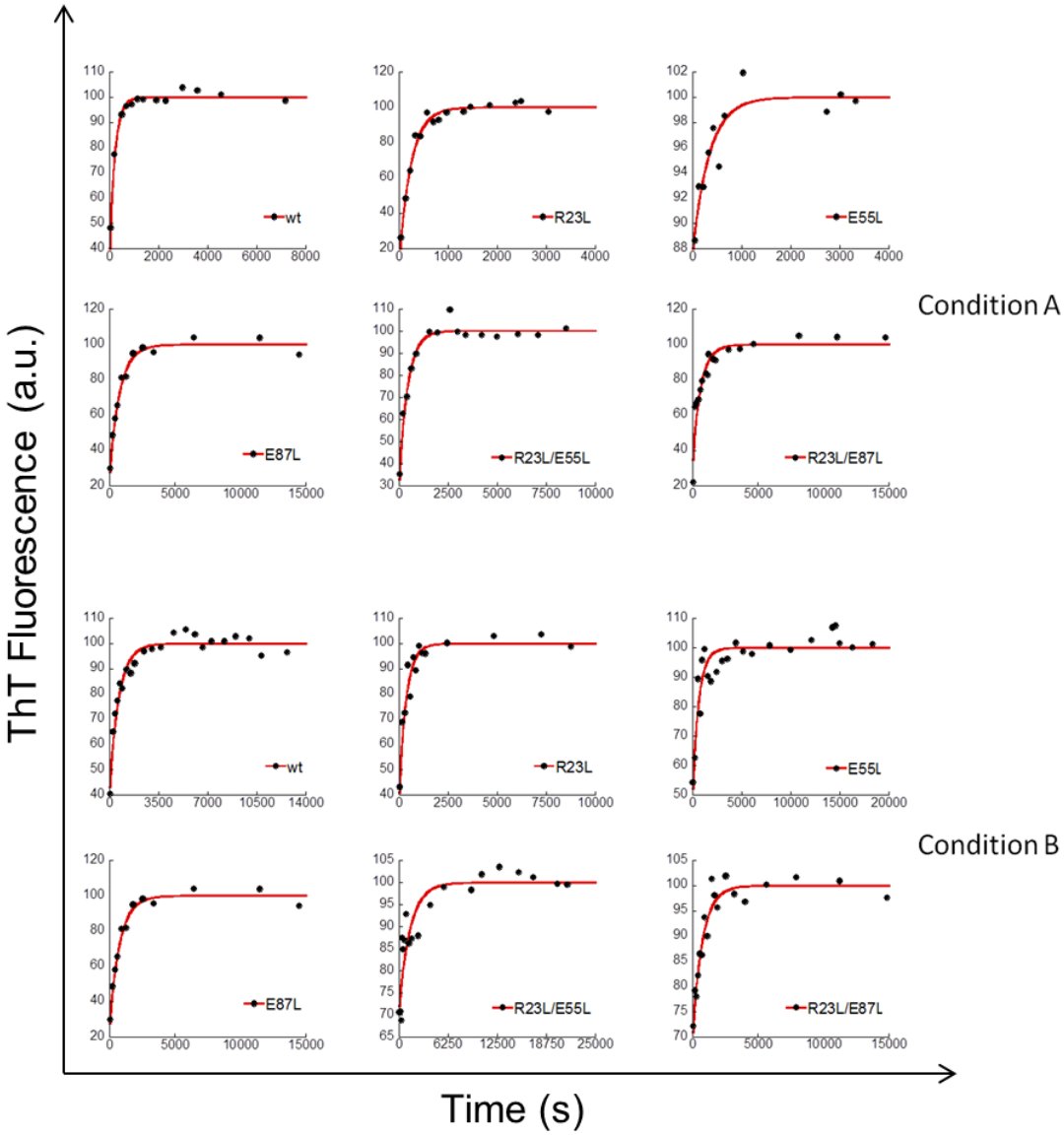

Figure 3.3. Representative aggregation time-courses of wt and variants of HypF-N measured by ThT fluorescence under conditions A (top panels) and B (bottom panels). All data points were blank-subtracted and normalized to the maximum fluorescence intensity observed at the apparent plateau. Red lines represent the best fit to a single-exponential function (equation 3.2).

formed by the hydrophobic mutants bind the amyloid specific dye ThT indicating the presence of intermolecular β-sheet structure typical of amyloids. Moreover, the development of amyloid structure follows apparent mono-exponential kinetics in the absence of a lag phase, typical of the oligomers that precede fibril formation. Finally,

the rate of the aggregation process does not appear to be affected by the introduction of the hydrophobic mutations, which the exception of the E87L variant in condition A.

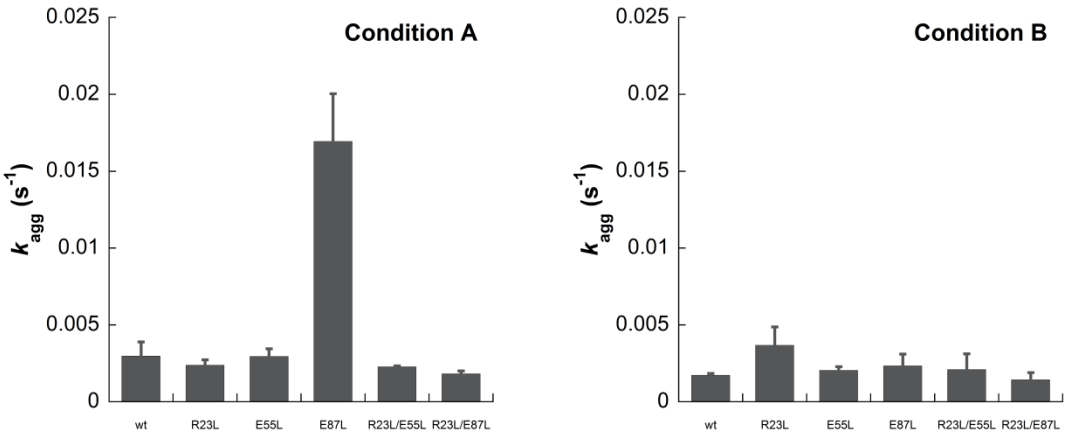

Figure 3.4. Apparent rate constants of aggregation (k_{agg}) of wt and variants in condition A (left) and B (right). Aggregation time courses were fitted with a single exponential function and the k_{agg} values for all experiments were determined. Data are means of, at least, 4 independent experiments. Error bars correspond to the standard errors of the means.

3.2.3 Biological activity of the oligomers formed by the hydrophobic variants

The biological activity of the oligomeric aggregates formed by the hydrophobic variants under condition A and B was assessed on human neuroblastoma SH-SY5Y cell cultures. For this purpose, the aggregates were transferred from the aggregation mixtures to a physiological medium through centrifugation and then added to the cell culture media. The viability of the cells treated with these aggregates was monitored by performing the MTT reduction inhibition assay, a generic biochemical test used to estimate the level of the cellular physiological stress [Mosmann, 1983]. Control experiments with the cells exposed to the native proteins were also carried out. Figure 3.5 shows the results obtained and expressed as a percentage of the value measured for the untreated cells.

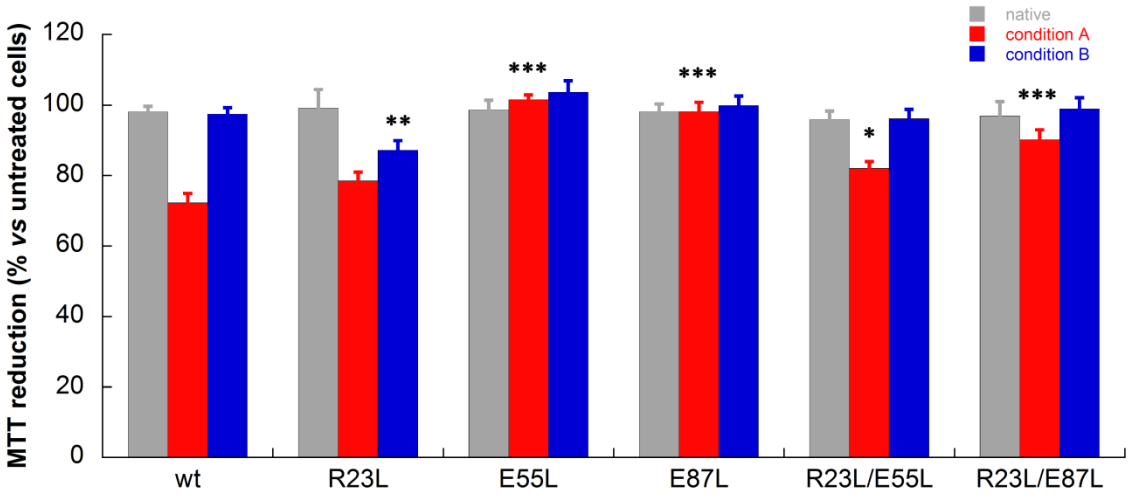

Figure 3.5. MTT reduction assay on SH-SY5Y cells treated with wt and mutant proteins in their native state (grey bars), after aggregation in condition A (red bars) and B (blue bars). Error bars correspond to standard errors of the means of 10 independent experiments. Single, double and triple asterisks refer to p values lower than 0.05, 0.01 and 0.001, respectively, with respect to wt oligomers formed under corresponding conditions.

As previously reported, type A and B oligomers generated by wt HypF-N cause a 30% reduction and no reduction in the viability of SH-SY5Y cells, respectively [Campioni *et al.*, 2010]. Interestingly, the cells treated with oligomers formed under condition A by hydrophobic variants of HypF-N show higher viability levels than the cells treated with oligomers formed in the same condition by the wt protein. However, it is important to note that the introduction of a single mutation in position 55 or 87 (E55L and E87L) and of a double mutation in positions 23 and 87 (R23L/E87L) seems to revert completely, or almost completely in the latter case, the toxic effect of the wt oligomers; by contrast, the R23L and R23L/E55L variants keep the ability to reduce the cellular viability, albeit to a lower extent with respect to the wt oligomers.

The oligomers formed by the variants in condition B maintained the MTT reduction unaltered, with the exception of the R23L mutant, which slightly affects the cellular viability. Generally, in condition B the introduction of the hydrophobic mutations taken

here in consideration does not alter significantly the biological activity of the aggregates. Similar experiments performed by treating the cells with native proteins show in all cases the inability of these proteins in their native structure to cause cellular dysfunction.

3.2.4 Staining of the nuclei with Hoeschst

Experiments with the apoptotic marker Hoechst 33342 were also carried out on SH-SY5Y cells following the exposure to the various oligomeric variants and appeared to be in agreement with the MTT test data. This marker binds to the highly condensed chromatin present in the nuclei of apoptotic cells giving rise to a strong fluorescent signal and allowing the visualization of fragmented nuclei. After the treatment with the native proteins and with type A and B aggregates, the cells were stained with the dye and visualized by fluorescence microscopy. The images obtained are shown in Figure 3.6. The nuclei of the cells treated with wt type A oligomers appear condensed and give rise to a high florescence signal, whereas such signal is generally reduced, to different extents, in cells treated with the mutant type A oligomers, with the R23L and the R23/E55L oligomers being the most effective in causing apoptosis. By contrast, the cells treated with the mutated type B oligomers, as well as with the wt type B oligomers appear to have a morphology and fluorescence intensity similar to those of untreated cells, with the exception of the cells treated with R23L type B oligomers. In all the experiments performed by exposing the cells to the native proteins no significant change in the morphology and in the fluorescence intensity of the treated cells is observed compared to the untreated ones.

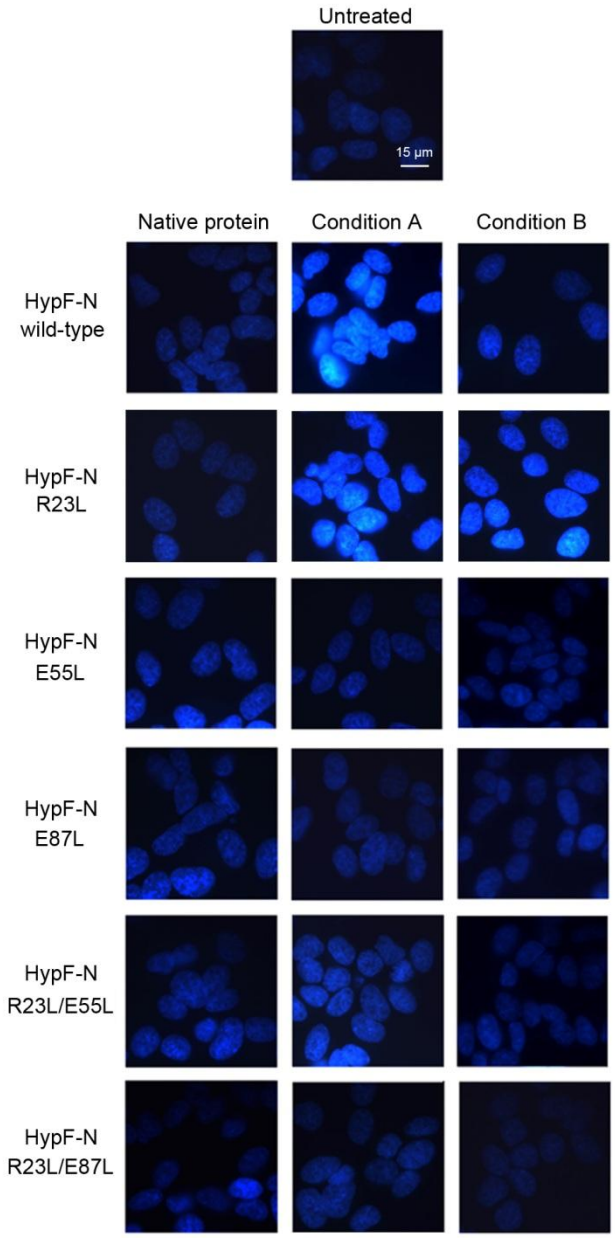

Figure 3.6. Hoechst 33342 staining of SH-SY5Y cells treated with monomeric native proteins, aggregates formed by wt and hydrophobic mutants of HypF-N under conditions A and B. The upper image show the untreated cells.

3.2.5 Measurement of level of intracellular Ca^{2+}

We also monitored the alteration of the membrane permeability by measuring the levels of intracellular Ca^{2+} ions following the exposure of the cells to the various oligomeric variants. Indeed, the influx of Ca^{2+} ions from the extracellular space into the cytosol across the membrane has been recognized to be an early damage in cells exposed to harmful protein oligomers [Orrenius *et al*., 2003; Demuro *et al*., 2005; Bojarski *et al*., 2008], including HypF-N wt type A oligomers [Canale *et al*., 2006; Zampagni *et al*., 2011]. Taking advantage of the ability of the fluorescent probe fluo3-acetoxymethyl-ester (Fluo3-AM) to bind Ca^{2+} ions and consequently give rise to a green fluorescence signal, we evaluated the level of intracellular Ca^{2+} in SH-SY5Y cells after 1 hour of incubation in presence of native proteins or oligomers formed by the variants under conditions A and B. Confocal microscopy images were acquired (Figure 3.7A) and the intensity of the fluorescence signal was expressed as a fractional change with respect to the fluorescence measured in cells treated with wt type A aggregates (Figure 3.7B). Oligomers formed in condition A by all the mutants, with the exception of the R23L and R23L/E55L mutants, do not induce an increase in cytosolic free Ca^{2+}, unlike oligomers formed by the wt protein. In condition B, both the wt and mutated oligomers do not cause any change in the intracellular Ca^{2+} levels, again with the exception of the R23L variant oligomers, whose effect is, however, lower than the one provoked by the wt type A oligomers. In similar experiments performed treating the cells with the native proteins no increase in intracellular Ca^{2+} ions was detected.

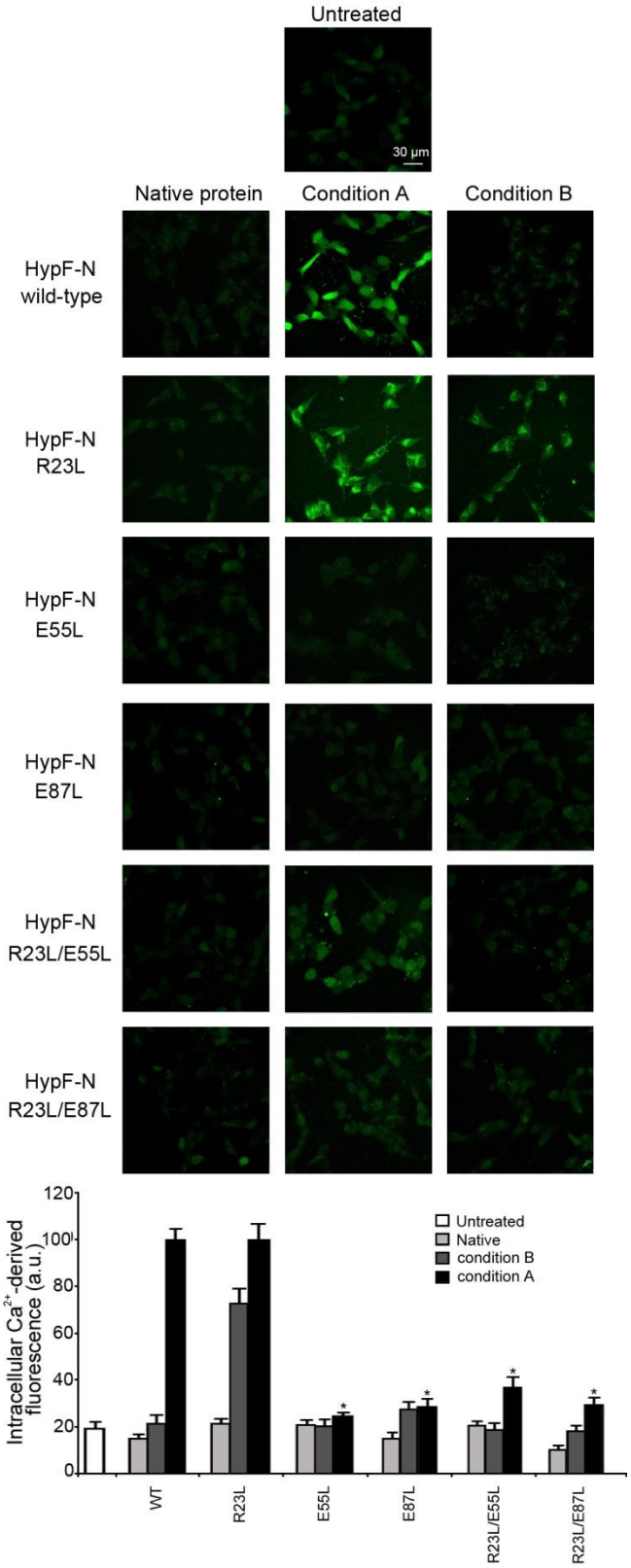

Figure 3.7. (A) Dysregulation of cytosolic Ca^{2+} analysis on SH-SY5Y cells treated with aggregates formed by wt and hydrophobic mutants of HypF-N. Confocal microscopy images of the intracellular free Ca^{2+} levels after 1 hour of treatment with monomeric native proteins, aggregates formed by wt and hydrophobic mutants of HypF-N in conditions A and B. The upper image show the untreated cells. The green fluorescence arises from the intracellular Fluo3 probe bound to Ca^{2+}. (B) Quantification of fluorescence arising from intracellular Ca^{2+} levels with respect to the fluorescence observed in cells treated with type A wt oligomers. Error bars correspond to standard errors of the means of 3 independent experiments The asterisks refer to p values lower than 0.05 with respect to wt oligomers formed under corresponding conditions.

3.2.6 Effect of the mutations on the superficial hydrophobicity of the oligomers

To the purpose of shedding light on the link between the biological activity and the structure of the oligomeric HypF-N aggregates, we focused on structural parameters, such as the hydrophobic surface exposure and the size.

The exposure to the solvent of hydrophobic surfaces of the wt and mutated oligomers formed in conditions A and B was tested by evaluating their ability to bind to the fluorescent probe 8-anilinonaphthalene-1-sulphonate (ANS). ANS binds to solvent-exposed hydrophobic clusters, and, following this binding, a strong increase of its fluorescence emission intensity and a blue shift of its maximum emission wavelength (λ_{max}) are observed [Semisotov *et al*., 1991; Cardamone and Puri, 1992]. The fluorescence emission spectra of ANS acquired in the presence of aggregates obtained in conditions A and B and their λ_{max} values are shown in Figure 3.8. All the variant oligomers formed in condition A are able to bind to ANS because for all of them it was possible to register an increase of ANS emission intensity, even though to different extents. However, with respect to the wt type A oligomers, the aggregates formed by E55L and R23L/E55L HypF-N show an increase in the intensity of the emission spectrum, whereas the oligomers generated by the E87L and R23L/E87L variants give origin to ANS spectra characterized by a lower, but still comparable to the wt oligomer spectrum, intensity. A peculiar behavior is observed for the R23L variant oligomers, whose spectrum is markedly reduced compared to that of the wt oligomers (Figure 3.8A). A notable blue shift of the λ_{max} value is observed for the oligomers formed by all mutants compared to the wt oligomers, again with the exception of the R23L variant, which is characterized by a less blue-shifted λ_{max} value (Figure 3.8C).

Type B oligomers formed by all the variants are able to bind to ANS, and the spectra recorded for the single and double variants show a very weak and more

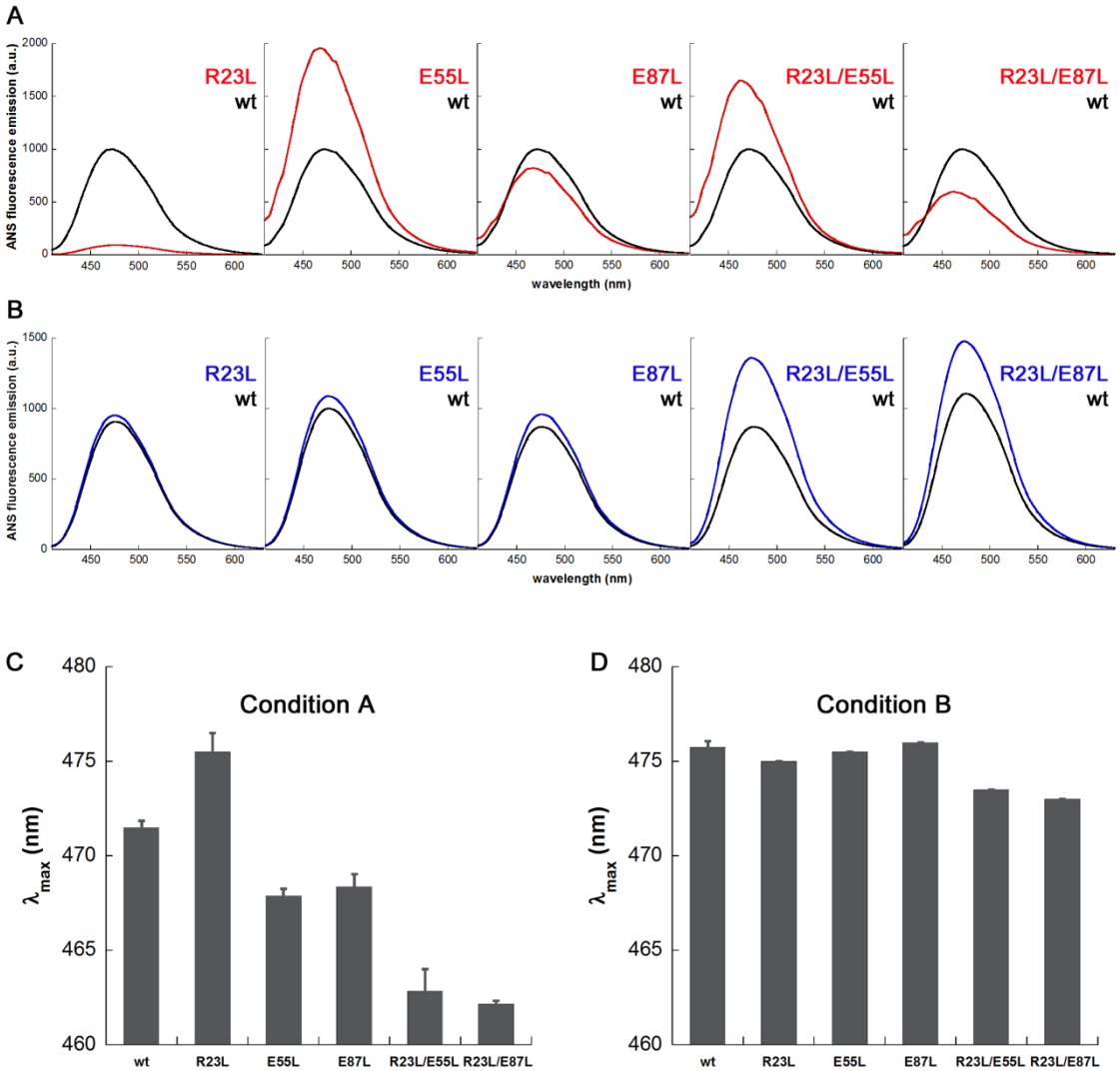

Figure 3.8. ANS binding to wt and hydrophobic variant type A and B oligomers (A,B). Fluorescence emission spectra of ANS in the presence of the aggregates of the wt protein (black) and hydrophobic variants formed in condition A (red) (A) and B (blue) (B). Wavelength of maximum emission fluorescence (λ_{max})registered for wt and hydrophobic oligomers of HypF-N in condition A (C) and B (D). Error bars correspond to standard errors from values of three different experiments.

prominent increase of the fluorescence intensity compared to the wt type B oligomers, respectively (Figure 3.8B). These results are in agreement with the λ_{max} values observed: the oligomers formed by the single mutants have λ_{max} values comparable to that ones of the wt oligomers, whereas the aggregates formed by the double mutants show more blue-shifted λ_{max} values with respect to the wt type B oligomers (Figure 3.8D).

These data show that the introduction of the hydrophobic mutations generates a strong increase in the exposure to the solvent of the hydrophobic surfaces of the oligomers aggregated in condition A, with the exception of the R23L mutation. An increase of this magnitude is not observed in the case of the mutant oligomers formed in condition B.

3.2.7 Effect of the mutations on the size of the oligomers

In order to qualitatively estimate the size of the type A and B mutated aggregates, turbidimetry and static light scattering (SLS) measurements were performed. Turbidimetry measures the loss of intensity of the light in the direction of propagation of the incident beam following the passage through a solution, and this phenomenon is due to light scattering caused by particles suspended in solution. Through the determination of the turbidity it is possible to estimate qualitatitevely the size of the particles in solution. Therefore, the turbidimetry at 500 nm was recorded for all the oligomers formed in conditions A and B, as shown in Figure 3.9A and 3.9B, respectively. The type A oligomers formed by the mutants are characterized by a similar, in the case of the E87L mutant, or higher light scattering than the wt type A aggregates. The only exception to this trend is represented by the R23L oligomers which show a lower intensity of the light scattered with respect to the wt oligomers (Figure 3.9A). By contrast, type B mutated oligomers are generally able to scatter the light to a similar extent of the wt aggregates formed under the same conditions, again with the exception of the R23L mutant, whose oligomers present a lower ability in scattering the light.

These results were confirmed by SLS measurements, as reported in Figure 3.9C and 3.9D, for the conditions A and B, respectively. In this technique the total amount of

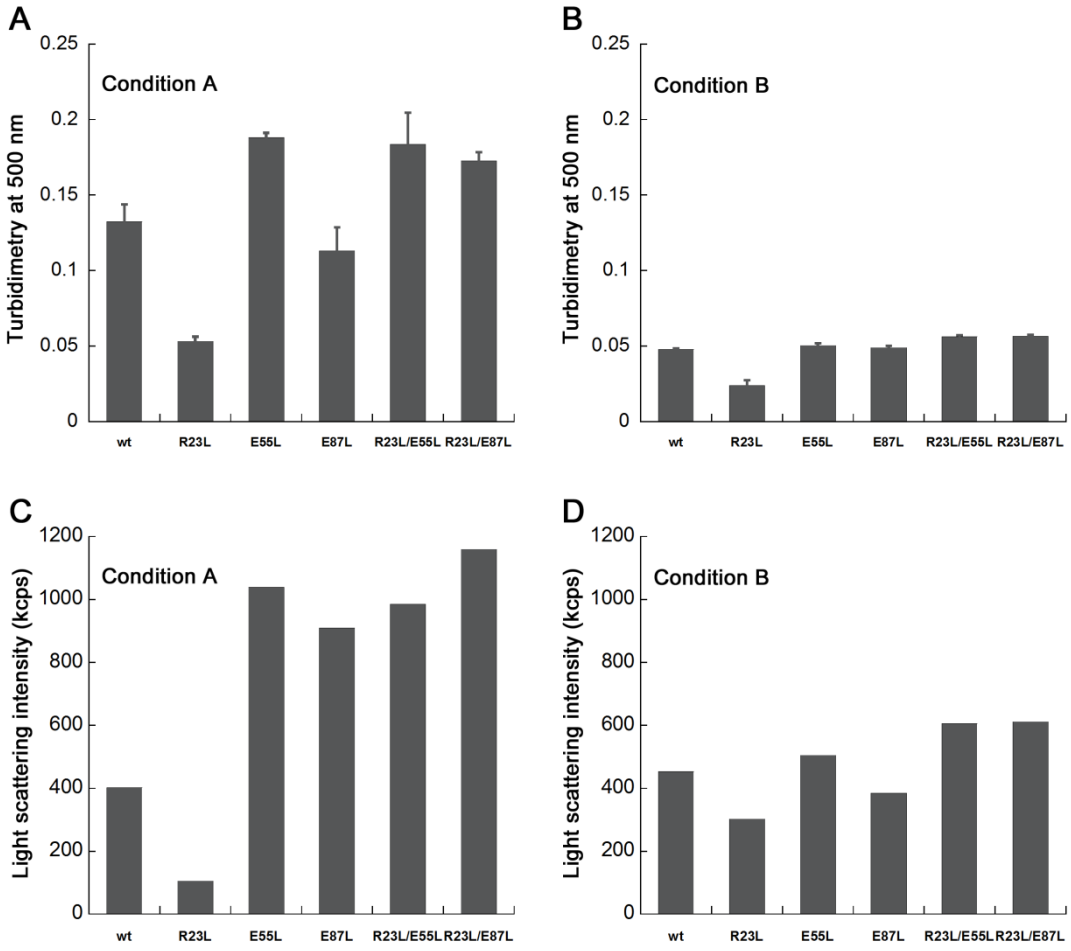

Figure 3.9. Measurements of turbidometry and SLS of HypF-N oligomers. The values of turbidimetry at 500 nm for the wt and variant oligomers formed in condition A (A) and B (B); error bars correspond to standard error values of three different experiments. Mean count rate expressed in kilocounts per second (kcps) of the type A (C) and type B (D) oligomers formed by wt and variants.

light scattered by the sample is measured by a detector at an angle different from 0 or 180°with respect to the incident light; hence, unlike turbidimetry, it is a direct measurement of the deviated light. The variants oligomerized in condition A, with the exception of the R23L mutant, are able to scatter the light to a greater extent with respect to the wt type A oligomers, whereas the values registered for the type B aggregates formed by the mutants are similar to those of the wt type B oligomers, with

the R23L oligomers having the lowest values. Taken together these results suggest that the oligomers formed in condition A by the hydrophobic mutants are bigger in size than the wt aggregates, with the exception of the R23L oligomers, which shows smaller dimensions than those of the wt oligomers. Conversely, the introduction of the hydrophobic mutations seems to maintain generally unaltered the dimensions of the aggregates generated in condition B.

3.2.8 Correlation between superficial hydrophobicity, size and toxicity

Interestingly, the surface hydrophobicity of all the studied oligomers determined by the ANS λ_{max} value significantly correlates with the size of the oligomers, as indicated by the SLS intensity. In Figure 3.10A the λ_{max} value and the intensity of scattered light of the twelve oligomeric species studied here, i.e. wt and five mutant of type A oligomers (shown in red) and wt and five mutant of type B oligomers (shown in blue), were plotted and fitted to a linear equation of the form:

$$y = q + mx \qquad \text{(Eq. 3.1)}$$

where q and m represent the intercept and the slope of the straight line, respectively. The linear correlation coefficient (R) is 0.88842, corresponding to a p value lower than 0.001, therefore indicating that the correlation is statistically significant. This point out that an increase in the of exposure of hydrophobic surfaces causes an increase of the size of the oligomers. Since these two factors increase and decrease, respectively, the oligomer toxicity, no correlation is observed between either parameter and toxicity.

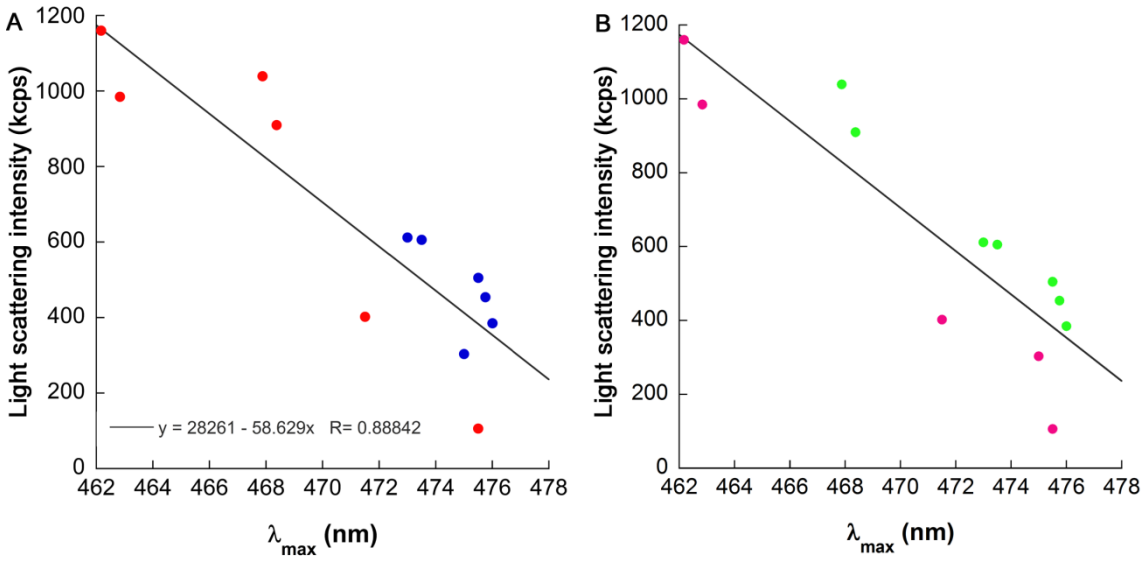

Figure 3.10. (A) Light scattering intensity expressed in kilocounts per second (kcps) *versus* the wavelength of the ANS maximum emission fluorescence (λ_{max}) of the type A (red) and type B (blue) oligomers formed by wt and mutants. All the values were analysed with a procedure of best fitting and the solid line represents the best fit to equation 3.1. (B) Same plot as in (A): the green dots correspond to aggregates characterized by MTT reduction values > 97%; the pink dots correspond to oligomers showing values of MTT reduction ranging from 70% to 90%.

In Figure 3.10B the same plot was reported highlighting the oligomeric species that do not cause cellular damage (in green) and those affecting the cell viability to different extents (in pink), as determined by the MTT test results. It is worthy to note that the nontoxic oligomers are located above the straight line representing the best fit to equation 3.1, whereas the toxic aggregates are below this line. This partitioning of the data points in the two regions of the graph indicates that a combination of high hydrophobicity and small size contributes to a high toxicity, whereas a combination of low hydrophobicity and high size determined no toxicity. This result shows that the toxicity of the oligomers is influenced by both their superficial hydrophobicity and their size and, most importantly, is finely modulated according to specific levels of these two

structural determinants, which cooperate simultaneously in determining the biological activity of the aggregates.

3.3 Discussion

3.3.1 The introduction of hydrophobic mutations generates oligomers displaying different levels of toxicity

Increasing evidence suggests that oligomers, rather than mature amyloid fibrils, are the pathogenic species in protein deposition diseases [Chiti and Dobson, 2006; Jhan and Radford, 2008]. For this reason, it is essential to investigate at a structural level which determinants are responsible for the toxicity of such species. Efforts in this direction can help to identify new therapeutical targets for the treatment of these pathologies.

In this study the importance of hydrophobic surface exposure and size as structural determinants of the biological activity of the aggregates has been taken into account through the study of a set of HypF-N variants characterized by mutations replacing hydrophilic residues with hydrophobic ones. We found that the introduction of the hydrophobic mutations studied here in the sequence of HypF-N alters neither the native structure of the proteins, as reported by far-UV CD measurements, nor the aggregation process promoting the oligomer formation under conditions A and B as shown by ThT fluorescence kinetics. By contrast, the biological activity is significantly affected by the insertion of the hydrophobic mutations. It seems, therefore, that the introduction of the mutations originates a pool of oligomeric variants characterized by different degrees of toxicity and these functional differences have to be related to differences in the structures and/or morphology of the aggregates.

3.3.2 Structural determinants of the oligomer toxicity: the double role of the superficial hydrophobicity

The structural analysis of the oligomers was based on two parameters, both recognized to play important roles as determinants of aggregate toxicity: the surface hydrophobic exposure and the size. An increase in the exposure of hydrophobic oligomeric surface is associated with a greater ability of the aggregates to cause cellular dysfunction [Kremer *et al*., 2000, Oma *et al*., 2005, Bolognesi *et al*., 2010, Olzscha *et al*., 2011; Krishnan *et al*., 2012] and this phenomenon is also observed in the case of the wt type A and B HypF-N oligomers, as described previously [Campioni *et al*., 2010]. By contrast, it is recognized that there is an inverse correlation between toxicity and oligomer size [Cizas *et al*., 2010; Ladiwala *et al*., 2011; Ojha *et al*., 2011; Bemporad and Chiti, 2012; Chapter 2] and, again, this is also observed for wt type A oligomers [Chapter 2].

According to the condition of aggregation and to the site of the mutation, the introduction of hydrophobic mutations affects, to various extents, the superficial hydrophobicity, causing consequently changes in the size of the type A and B aggregates. The explanation to these data can be found considering that the increase of hydrophobicity is accompanied by the increase in the dimensions of the aggregates. The increase in the exposure of hydrophobic surface seems to make the oligomers more sticky, facilitating their interaction and giving rise to the formation of bigger species unable to exert their toxic effects. Hence, it is reasonable to hypothesize that the increase of the solvent-exposed hydrophobic surface of a misfolded protein oligomer can have, according to its extension, a double counteracting effect on the oligomeric ability to cause cellular dysfunction, being responsible for toxicity or benignity.

3.3.3 Structural determinants of the oligomer toxicity: the importance of the size

The reduction in the ability of causing cellular dysfunction mediated by the increase in the dimensions observed in the cases of type A E55L, E87L, R23L/E55L and R23L/E87L oligomers confirms that the size is a pivotal determinant of the oligomer toxicity. It has long been known that the fibrils, bigger in dimensions than the oligomers preceding their formation, have, unlike the latter, a lower, if any, toxicity [Chiti and Dobson, 2006]. Moreover, recent studies show that oligomer size plays a key role in causing oligomer toxicity. The ability of $A\beta_{40}$ and $A\beta_{42}$ oligomers to decrease the MTT reduction in cultured cells was found to correlate inversely with the molecular weight of the oligomers, with the small species having the highest toxicity [Bemporad and Chiti, 2012]. It was also found that $A\beta_{42}$ oligomers of different sizes give rise to an inverse correlation between oligomer size and neuronal toxicity, again with the smallest species exhibiting the highest ability in causing cell damage [Cizas *et al*., 2010]. In addition, agents able to cause the further assembly of toxic oligomers into larger species, such as aromatic small molecules [Ladiwala *et al*., 2011] or molecular chaperones [Chapter 2; Ojha *et al*., 2011], suppress the toxicity of these aggregates. Larger assemblies are harmless because they have a lower diffusional mobility, which prevent them from interacting and disrupting cell membranes, and because they have a lower surface/volume ratio.

3.3.4 Cooperation of structural oligomeric characteristics in determining the ability to cause cell dysfunction

Although this study recognizes the importance of the superficial hydrophobicity and of the size as determinants of oligomer toxicity, the data on the biological effects presented here cannot be explained solely on the basis of either parameter considered individually.

To make an example, the increase in the size observed in type A E55L and R23L/E55L oligomers is similar, but their ability in affecting the cell viability is different, even if in both cases it is lower than that of wt type A oligomers. Type A E55L oligomers are not toxic at all, whereas type A R23L/E55L aggregates are able to cause a 20% reduction of the viability. In order to explain these differences in toxic behaviour, both size and hydrophobicity have to be taken into account. Indeed, type A R23L/E55L oligomers maintain a higher degree of superficial hydrophobicity with respect to type A E55L oligomers, which can be responsible of its higher degree of toxicity.

In Figure 3.10B, all the twelve oligomeric species studied here were reported in a graph plotting their light scattering against their ANS λ_{max} value, indicating the size and the superficial hydrophobicity, respectively, and highlighted according to their ability to reduce the cellular viability. It is interesting to note that specific combinations of the values of these two parameters determine the biological activity of the aggregates. They indeed seem to cooperate and contribute with their extent to the resulting biological activity of the oligomers. In aggregates having similar sizes, differences in toxicity are due to differences in the hydrophobic surface exposure, and this is the case for type A E55L and type A R23L /E55L oligomers described above, but also the case for wt type A and wt type B oligomers [Campioni *et al*., 2010]. Conversely, in aggregates having the same level of hydrophobicity, the ability to provoke cell damage is associated with a reduction in the dimension, and this is the case for wt type B and type A R23L oligomers.

In conclusion, the biological activity of the oligomeric species studied here is not explainable on the basis of the superficial hydrophobicity or the size if these two parameters are considered separately. Oligomer toxicity results from the combination of several structural and morphological determinants. Understanding the contribution of

each of these determinants can help to clarify the pathogenesis of protein deposition diseases and the molecular mechanism by which oligomers are harmful to cells.

3.4 Materials and methods

3.4.1 Site-directed mutagenesis

Mutations in the HypF-N gene were generated by using the QuikChange site-directed mutagenesis kit (Stratagene, La Jolla, CA). The three single variants R23L, E55L and E87L were created and then used as templates to obtain the double variants R23L/E55L and R23L/E87L. The entire genes were sequenced to ensure the presence of the desired mutation.

3.4.2 Preparation of HypF-N oligomers

HypF-N was expressed and purified as described in section 2.4.1. The expression and purification protocol of the mutants was similar to the one described for the wt protein. After purification, these mutants were buffer-exchanged by ultrafiltration in 20 mM phosphate buffer, 2 mM DTT at pH 8.0 and stored at -20°C.

Oligomeric aggregates of HypF-N were prepared by incubating the protein, wt or mutated, for 4 hour at 25 °C and at a concentration of 48 µM in two different experimental conditions: (i) 50 mM acetate buffer, 12% (v/v) TFE, 2 mM DTT, pH 5.5 (condition A) and (ii) 20 mM TFA, 330 mM NaCl, pH 1.7, (condition B). For cellular biology experiments, the oligomers were centrifuged at 16100 rcf for 10 min, dried under N_2 and resuspended in cell culture media to a final concentration equal to the initial one. In order to check the concentration, aliquots of these samples were taken and diluted 1:5 in a solution of 8 M guanidine chloride and incubated under vigorous shaking for 1 hour at 37 °C. Protein concentration was then assessed by optical

absorption. The remaining samples were diluted in DMEM to a final protein concentration of 12 μM concentration.

3.4.3 Far-UV CD measurements

Far-UV CD measurements were performed using a Jasco J-810 spectropolarimeter (Tokyo, Japan) equipped with a thermostated cell holder attached to a Thermo Haake C25P water bath (Karlsruhe, Germany). In all cases a 1 mm path length quartz cell was used. The spectra were acquired at 19 μM final protein concentration, 25 °C in the following conditions: (i) 5 mM acetate, 2 mM DTT, pH 5.5 for wt, (ii) 20 mM phosphate buffer, 2 mM DTT, pH 8.0 for the variants. In all cases, the spectra were blank-subtracted and converted to molar ellipticity per residue units.

3.4.4 Thioflavin T kinetics assay

Samples of wt HypF-N or mutated were incubated at a protein concentration of 48 μM in condition A and B. At different time points, aliquots of each sample were added to a solution of 25 μM ThT (Sigma-Aldrich) dissolved in 25 mM phosphate buffer at pH 6.0, in order to keep a 3.7-fold molar excess of dye. The final protein concentration was 6 μM. The steady-state intensity of fluorescence emission at 485 nm (excitation at 440 nm) was recorded at 25 °C using 2x10 mm path-length cell and a Pelkin-Elmer LS 55 spectrofluorimeter (Wellesley, MA, USA), equipped with a thermostated cell holder attached to a Thermo Haake C25P water bath (Karlsruhe, Germany). The ratio between the ThT emission in the presence (F) and absence (F_0) of HypF-N is reported as a function of time and fitted to the following monoexponential function:

$$F/F_0(t) = a + b \cdot e^{-k_{agg} \cdot t} \qquad \text{(Eq. 3.2)}$$

where *a* is the plateau value, *b* is the amplitude of the exponential phase and k_{agg} is the apparent rate of the protein aggregation process. For comparison, the data reported in the Figure 3.3 were normalised to their plateau values and fitted again to Eq. 3.2.

3.4.5 Cell cultures

Human SH-SY5Y neuroblastoma cells (A.T.C.C., Manassas, VA, USA) were cultured as described in section 2.4.4.

3.4.6 MTT assay

The toxic effect of the aggregates formed in conditions A and B by hydrophobic mutants and wt HypF-N was assessed by the MTT assay. SH-SY5Y cells were plated in a 96-well plate and treated for 24 hours at 37°C with 12 μM of the aggregates or native proteins either wt or variants of HypF-N. The cell cultures were then incubated with 0.5 mg/ml MTT solution at 37°C for 4 hours and subsequently with cell lysis buffer (20% SDS, 50% N,N-dimethylformamide, pH 4.7) at 37°C for 3 hours. Absorbance values of blue formazan were determined at 590 nm and cell viability was expressed as percent of MTT reduction in treated cells as compared to untreated cells (assumed as 100%). Native HypF-N and its hydrophobic variants was tested as describe above. Data are expressed as mean ± standard error of the mean (SEM). Comparisons between the different groups were performed by ANOVA followed by Bonferroni's t-test. P values < 0.05, 0.01 and 0.001 are indicated by single, double and triple asterisks, respectively.

3.4.7 Hoeschst staining test

The apoptotic effect of aggregate treatments on SH-SY5Y cells was evaluated using 2'-[4-ethoxyphenyl]-5-[4-methyl-1-piperazinyl]-2,5'-bi-1H-benzimidazole trihydrochloride trihydrate (Hoeschst 33342) dye staining assay.

Briefly, SH-SY5Y cells were plated on glass cover slips and treated for 24 hours with 12 µM of the aggregates formed by either wt protein of HypF-N or its hydrophobic variants. Subsequently, the cells were incubated with 20 µg/ml Hoechst 33342 dye for 15 minutes at 37 °C and then were fixed in 2.0% buffered paraformaldehyde for 10 min at room temperature. Blue fluorescence micrographs of cells were obtained under UV illumination in an epifluorescence inverted microscope (Nikon, Diaphot TMD-EF) with an appropriate filter set. Furthermore, native HypF-N and its native hydrophobic variants was tested as described above.

3.4.8 Analysis of cytosolic Ca^{2+} dyshomeostasis

Ca^{2+} dyshomeostasis was evaluated on SH-SY5Y cells cultured on glass cover slip using Fluo3-AM (Molecular Probes, Eugene, OR). The cell cultures were exposed to 12 µM of HypF-N aggregates prepared as described above for 60 minutes at 37°C. The cells were then treated for 30 minutes at 37 °C with 10 µM Fluo3-AM, 0.01% (w/v) pluronic acid F-127 (Sigma-Aldrich). The fluorescence was detected with an excitation of 488 nm by collecting the emitted fluorescence with the confocal scanning system (confocal Leica TCS SP5 scanning microscope, Mannheim, Germany).

To quantify the signal intensity of each fluorescent probe, a variable number of cells (10 to 22) were analyzed in each experiment using the ImageJ software (NIH, Bethesda, MD, USA), and the fluorescence intensities expressed as fractional changes above the resting baseline, $\Delta F/F$, where F is the average baseline fluorescence in control cells

(assumed as 100%) and ΔF represents the fluorescence changes over the baseline in cells exposed to different treatments. Comparisons between the different groups were performed by ANOVA followed by Bonferroni's t-test. A p value < 0.05 was considered statistically significant.

3.4.9 ANS fluorescence

Oligomeric aggregates of wt and mutated HypF-N were prepared by incubating the proteins for 4 hours at 25 °C at a concentration of 48 μM in conditions A and B. Aliquots of ANS (Sigma-Aldrich) dissolved in 50 mM acetate, 12% (v/v) TFE, pH 5.5 or in 20 mM TFA, 330 mM NaCl, pH 1.7 were added to type A and type B aggregates, respectively, in order to obtain a final 3:1 molar excess of dye. Fluorescence spectra were acquired at 25 °C, immediately after addition of ANS, using a 10 x 2 mm quartz cell and the equipment described in section 3.4.4, with an excitation wavelength of 380 nm. Optical absorption spectra were acquired for all the samples using a Jasco V630 spectrophotometer (Tokyo, Japan) and a 1 mm quartz cell and the fluorescence intensities of the spectra were corrected for inner filter effects with the formula reported by Lakowicz:

$$F = F_{exp} \cdot 10^{(Abs_{ex} + Abs_{em})/2} \qquad \text{(Eq. 3.3)}$$

where F is the corrected fluorescence, F_{exp} is the experimentally observed fluorescence, Abs_{ex} corresponds to the value of absorbance at the ANS excitation wavelength and Abs_{em} are the values of absorbance recorded at the same wavelengths of the fluorescence emission spectrum [Lakowicz, 1999].

3.4.10 Turbidimetry

Oligomers of wt and mutated HypF-N were prepared by incubating the proteins in conditions A and B. Subsequently, the absorbance of the samples at 500 nm was measured using a Jasco V-630 spectrophotometer (Tokyo, Japan) and a cell path of 1 mm. All the values were blank-subtracted.

3.4.11 Static light scattering

Oligomeric aggregates of wt and mutated HypF-N were prepared by incubating the proteins for 4 hours at 25 °C at a concentration of 48 μM in conditions A and B. SLS measurements were performed at 25 °C using the Malvern Zetasizer Nano S instrument (Malvern, Worcestershire, UK) with fixed parameters, equipped with a Peltier temperature controller. Disposable polystyrene cells having a 1 cm path length were used.

Chapter 4

TRANSTHYRETIN SUPPRESSES THE TOXICITY OF PROTEIN MISFOLDED OLIGOMERS

4.1 Introduction

Transthyretin (TTR) is a homotetrameric protein with a total molecular mass of 55 kDa, that is synthesized in the liver, choroid plexus of the brain, and retina of the eye [Soprano *et al*., 1985; Stauder *et al*., 1986]. In the plasma TTR transports thyroxine (T4) and the retinol binding protein (RBP), whereas in the cerebrospinal fluid TTR is the primary transporter of T4 [Reixach *et al*., 2008; Buxbaum and Reixach, 2009]. TTR is also one of 30 human proteins associated with amyloidosis [Westermark *et al*., 2007]. Amiloidogenesis of wild-type TTR occurs in the heart of 10-25% of human older than 80 years, resulting in senile systemic amyloidosis (SSA), often leading to congestive heart failure [Tanskanen *et al*. 2008; Lie *et al*., 1988]. TTR fibrillogenesis is accelerated by the presence of any of the approximately 100 different amyloidogenic mutations responsible for early-onset TTR amyloidoses [Sekijima *et al*., 2005; Connors *et al*., 2003; Jacobson *et al*., 1997a; Jacobson *et al*., 1997b]. These mutations are responsible for the impairment of thermodynamic and/or kinetic stability of native tetrameric TTR [Sekijima *et al*., 2005], leading to autosomal dominant disorders, including familial amyloid neuropathy (FAP), familial amyloid cardiomyopathy (FAC) and the rare central nervous system amyloidoses [Garzuly *et al*., 1996; Connors *et al*., 2003].

In spite of its link to human pathology, an anti-amyloidogenic effect that prevents fibril formation of Aβ disease has been proposed for TTR. In 1982 it was first found that TTR is bound to Aβ plaques in Alzheimer's disease (AD) brains [Shirahama *et al*.,

1982]. This parallels TTR to all known extracellular chaperones, which are known to be associated with Aβ deposits [Powers *et al*., 1981; Bauer *et al*., 1991; Kida *et al*., 1995]. 11 years later, it was found that amyloid fibril formation of $A\beta_{40}$ is inhibited *in vitro* by the human cerebrospinal fluid (CSF) [Wisniewski *et al*., 1993]. The protein of the CSF responsible for such inhibition was found to be TTR, through the formation of stable complexes between $A\beta_{40}$ and TTR, either as a dimer of a monomer [Schwarzman *et al*., 1994]. In the same study it was also found that purified human TTR inhibited $A\beta_{28}$ fibril formation *in vitro* [Schwarzman *et al*., 1994]. Overexpression of human TTR in transgenic *C. elegans* models of AD expressing human $A\beta_{42}$ led to a lower amount of Aβ deposits positive to the amyloid-specific dye Thioflavin S in the muscle cells of the nematodes [Link, 1995]. Similarly, overexpression of human TTR or gene knockout of murine TTR in mice overexpressing human Aβ led to a decrease and increase of the Aβ deposits in the mice brains, respectively [Choi *et al*., 2007; Buxbaum *et al*., 2008]. Importantly, reduction of amyloid deposition following overepxression of human TTR also led to significant cognitive improvement of the AD mice [Buxbaum *et al*., 2008].

Analyses of the interaction between human TTR and Aβ have showed that TTR binds to all forms of Aβ: monomers, oligomers and fibrils [Buxbaum *et al*., 2008; Costa *et al*., 2008; Liu and Murphy, 2006; Du and Murphy, 2010]. The binding is highly dependent on the quaternary structure of TTR with monomeric TTR binding Aβ with higher affinity than tetrameric TTR [Du and Murphy, 2010]. Moreover, the binding occurs with higher affinity for Aβ oligomers, aggregates and fibrils with respect to Aβ monomers [Liu and Murphy, 2006; Buxbaum *et al*., 2008; Du and Murphy, 2010]. In addition to inhibiting Aβ fibril formation by monomeric Aβ, TTR was shown to bind to preformed Aβ oligomers and fibrils and reduce their toxicity to murine primary neurons and human neuroblastoma SH-SY5Y cells [Li *et al*., 2011].

In the light of the results obtained so far, one can hypothesise that TTR can act as an endogenous detoxifier of protein oligomers with potential pathological effects, in addition to inhibiting amyloid fibril formation. However, it is not clear if such an effect occurs only on Aβ oligomers or more generically on protein misfolded oligomers. In addition, previous data do not offer any insight into the mechanism by which TTR inhibit oligomer toxicity and on the TTR form responsible for such an effect. We have previously shown that the cytotoxicity of protein oligomers formed by Aβ, IAPP and HypF-N can be suppressed by molecular chaperones, with three of the five tested chaperones being extracellular [Chapter 2]. In particular, it was shown that the chaperones inhibit the toxicity of the oligomers by binding to them and promoting their clustering into large aggregates, in the absence of any disaggregation and structural reorganisation within the individual oligomers. In this study we have examined the ability of three types of TTR having different tetramer stability, i.e. human TTR (hTTR), mouse TTR (mTTR) and an engineered monomer of human TTR carrying the V30M substitution with the additional F87M and L110M mutations (M-TTR), to suppress the toxicity of extracellularly added oligomers formed by three different peptides/proteins, i.e. $A\beta_{42}$, IAPP and HypF-N. mTTR is the most stable homotetramer that cannot dissociate into partially unfolded monomers [Reixach *et al*., 2008]; hTTR also forms stable tetramers but has the ability to dissociate into monomers [Colon and Kelly, 1992], whereas M-TTR basically exists as a stable monomer [Jiang *et al*., 2001; Du and Murphy, 2010; Bourgault *et al*., 2011]. We will show that the three types of TTR display different protective effects against oligomer-induced cytotoxicity. Following this observation we have gained molecular insight into the underlying mechanism by which suppression occurs, showing that TTR-mediated protection correlates with the capability of this protein to adopt a monomeric state, to bind to the

oligomers and promote their clustering into larger aggregates in the absence of any structural reorganisation.

4.2 Results

The cellular biology experiments were acquired in collaboration with the group of Prof. Cristina Cecchi of the University of Florence. AFM measurements were performed by Bruno Tiribilli of the Consiglio Nazionale delle Ricerche (CNR) in Florence.

4.2.1 TTRs prevent oligomer-induced cytotoxicity and apoptosis in SH-SY5Y cells

We incubated oligomers formed from $A\beta_{42}$, IAPP and HypF-N in the cell culture medium in the absence or presence of hTTR, mTTR or M-TTR for 1 hour, then added the resulting samples to SH-SY5Y cells and measured the resulting cell viability using the MTT reduction assay. All three types of oligomers confirmed their toxic action (Fig. 1A-C), as previously demonstrated [Chapter 2]. The cells treated with oligomers preincubated with hTTR and M-TTR were found to reduce MTT to levels similar to untreated cells, to cells treated with the native proteins or to cells treated with oligomers preincubated with haptoglobin, a known extracellular chaperone used here as a positive control of oligomer toxicity inhibitor (Figure 4.1A-C). Conversely, mTTR only shows a small and non-significant protective effect (Figure 4.1A-C). In addition, when the three oligomer types were incubated in the cell culture medium for 1 hour with proteins that are not expected to possess chaperone properties, such as hen egg white lysozyme (HEWL) or bovine serum albumin (BSA), the oligomers were found to maintain their toxicity (Figure 4.1A-C).

These results indicate that hTTR and M-TTR can suppress or decrease markedly the toxicity of oligomers formed by three different peptides and proteins, with a suppression that is specific for TTRs with respect to other proteins.

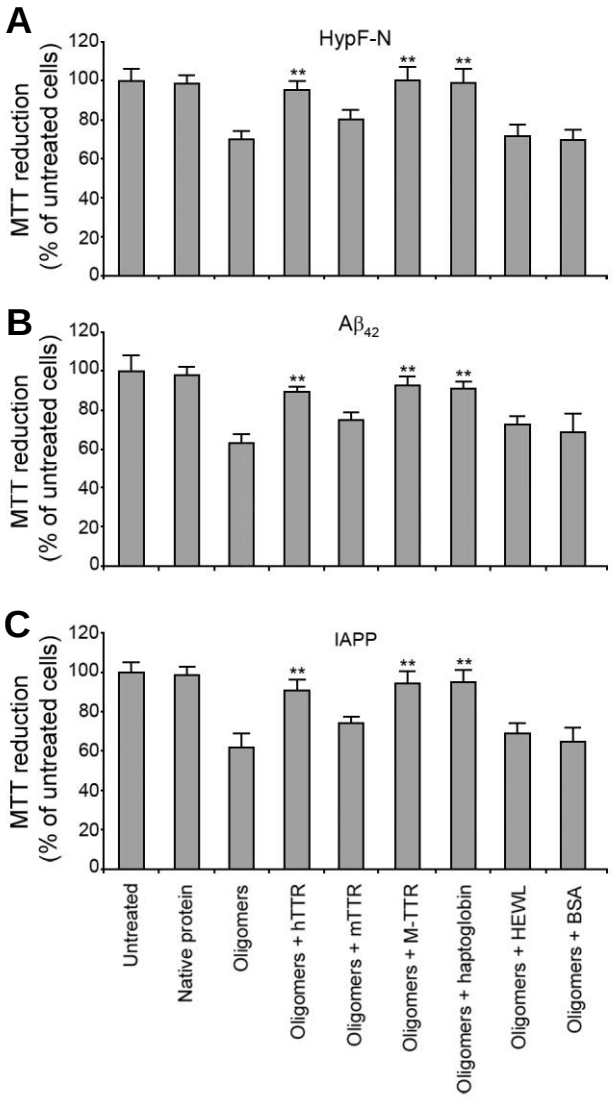

Figure. 4.1. Suppression of protein oligomer toxicity by TTRs. Preformed oligomers of HypF-N (A), Aβ42 (B) and IAPP (C) were resuspended in the cell culture medium, incubated for 1 hour at a corresponding monomer concentration of 12 μM in the absence or presence of the indicated TTRs (protein:TTR molar ratio was 10:1), human haptoglobin (protein:haptoglobin molar ratio was 15:1), HEWL (protein:HEWL molar ratio was 5:1), or BSA (protein:BSA molar ratio was 5:1) and then added to SH-SY5Y cells. Cell viability was expressed as percent of MTT reduction in treated cells with respect to untreated cells (taken as 100%). The values shown are means ± SD of three independent experiments carried out in quadruplicate. The double asterisk indicates a significant difference ($p \leq 0.01$) relative to the experiment with oligomers only.

4.2.2 Monomeric TTR reduces protein oligomer toxicity even at very low concentration

To the aim of understanding the origin of the different ability of TTRs in suppressing the toxicity of protein oligomers and the resulting effects on the cells, we have decided to concentrate our effort on the toxic oligomers of HypF-N. This protein represents a useful model system since it forms morphologically similar oligomers but distinguishable on the basis of their biological activity in toxic (type A, the same used in the present work) and non toxic (type B) and, consequently, on the basis of the their fine structure [Campioni *et al*., 2010]. Both the two types of oligomers possess their own and well characterized structural profile, as highlighted by the fluorescent probe PM [Campioni *et al*., 2010], making possible to probe structural changes experienced by the aggregates following their exposure to TTRs. Finally, HypF-N oligomers appear to be highly stable, making them easy to handle in our experiments [Campioni *et al*., 2010].

The different abilities of TTRs to prevent cell death detected by MTT tests were confirmed by the analysis of the chromatin condensation with the apoptotic marker Hoechst 33342 and by the measurements of caspase-3 activity, another indicator of apoptosis (data not shown). In addition, the MTT test was repeated by varying the concentration of each TTR in the 1 hour preincubation solution, while maintaining constant that of HypF-N. M-TTR was found to suppress the toxicity of HypF-N oligomers even at low concentration with an efficacy similar to haptoglobin and α_2-macroglobulin, two well known extracellular chaperones (Figure 4.2). M-TTR remained significantly efficient even at an HypF-N:TTR molar ratio of 400:1, becoming ineffective only at a molar ratio of 1000:1 (Figure 4.2). hTTR is also effective, but only at higher concentrations; indeed, hTTR was significantly efficient until an HypF-N:TTR

molar ratio of 40:1, becoming ineffective at molar ratios of 100:1 or higher. Conversely, mTTR did not show any protective effect, even at low molar ratios (Figure 4.2).

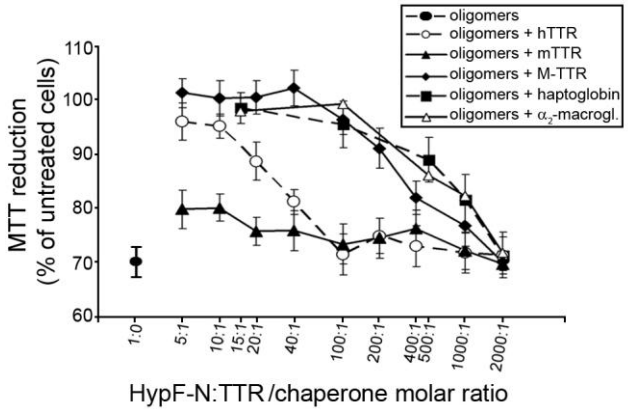

Figure 4.2. Dose-dependent suppression of HypF-N oligomer toxicity by TTRs. Preformed oligomers of HypF-N were resuspended in the cell culture medium, incubated for 1 hour in the absence (●) or presence of the indicated TTRs/chaperones and HypF-N:TTR/chaperone molar ratios and then added to SH-SY5Y cells. TTRs were always considered as tetramers in all HypF-N:TTR molar ratio values. The scale on the x axis is logarithmic. Cell viability was expressed as percent of MTT reduction in treated cells with respect to untreated cells (taken as 100%). The values shown are means ± SD of three independent experiments carried out in triplicate.

4.2.3 The molecular structure of HypF-N oligomers is preserved in the complexes with TTRs

To shed light on the different behaviour of the TTRs and on the molecular mechanism by which they exert their protection against HypF-N oligomers we investigated the oligomeric state and the molecular structure of HypF-N oligomers after the preincubation with TTRs. To assess whether the oligomers can be dissolved by the different types of TTR, we exploited the ability of the HypF-N oligomers, unlike native HypF-N, to bind to ThT and increase its fluorescence [Campioni *et al*., 2010] (Figure 4.3). HypF-N oligomers incubated for 1 hour in a phosphate buffer at neutral pH cause a 7/8-fold increase of ThT fluorescence, and the same increase was observed when the oligomers were preincubated in the same buffer for 1 hour with the different TTRs

(Figure 4.3). To exclude the possibility that TTRs bind ThT, we also analysed samples containing only TTRs under identical conditions, detecting no increase of ThT fluorescence in these cases (Figure 4.3). Overall, these results show that HypF-N oligomers remain stable and do not undergo disaggregation after TTR treatment.

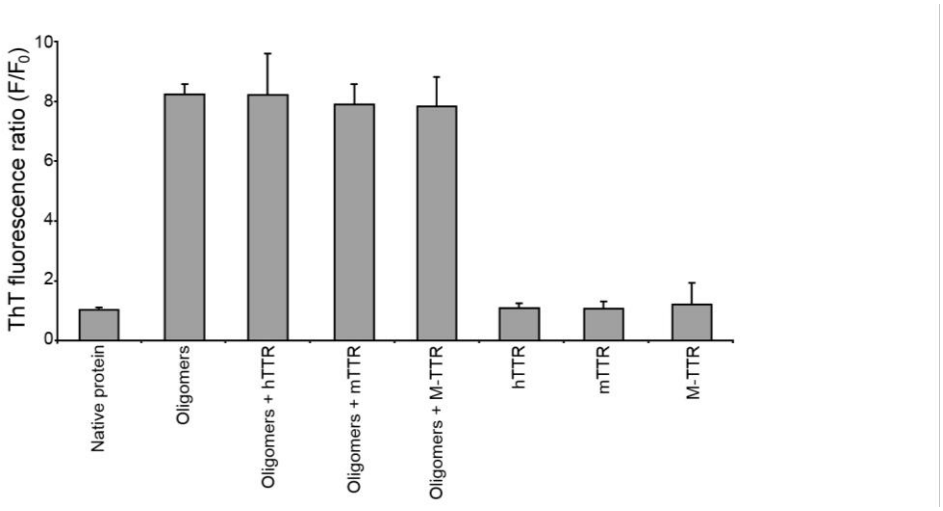

Figure 4.3. TTRs do not dissolve HypF-N oligomers. ThT fluorescence at 485 nm (excitation 440 nm) in the presence of the indicated protein components following preincubation for 1 hour in 20 mM phosphate buffer at pH 7.0 in the absence or presence of different types of TTR. The ratio between the ThT fluorescence in the presence (F) and absence (F_0) of proteins is reported; data are means ± SD of three independent experiments. The HypF-N concentration was 48 μM (in monomer units) and the HypF-N:TTR molar ratio was 10:1.

Subsequently, we verified if the oligomers are structurally re-organised at the molecular level by TTRs (Figure 4.4). To this aim we took advantage of the possibility to determine the degree of packing of the oligomers through the acquisition of fluorescence spectra of oligomers labelled with PM. In particular, the fluorescence spectra of nontoxic type B oligomers formed by HypF-N labelled with PM at position 25, 55 or 87 show an excimer band that is very weak in the corresponding spectra obtained with PM-labelled toxic type A oligomers [Campioni *et al.*, 2010]. Three variants of HypF-N containing a single cysteine residue at position 25, 55 and 87 were therefore labelled with PM, allowed to aggregate and then transferred to phosphate

buffer at neutral pH for 1 hour with or without the different types of TTR. The fluorescence spectra acquired for the oligomers in either the presence or absence of the TTRs were very similar and none of them showed an excimer band (Figure 4.4). Moreover, the ratio of the exicimer-to-monomer fluorescence intensity (FI_{440nm}/FI_{375nm}) did not change for following preincubation with any TTR, remaining lower in all cases than the corresponding value measured for the nontoxic oligomers (Figure 4.4). These results therefore reveal that none of the TTRs studied here is able to promote a structural re-organization of the toxic HypF-N oligomers.

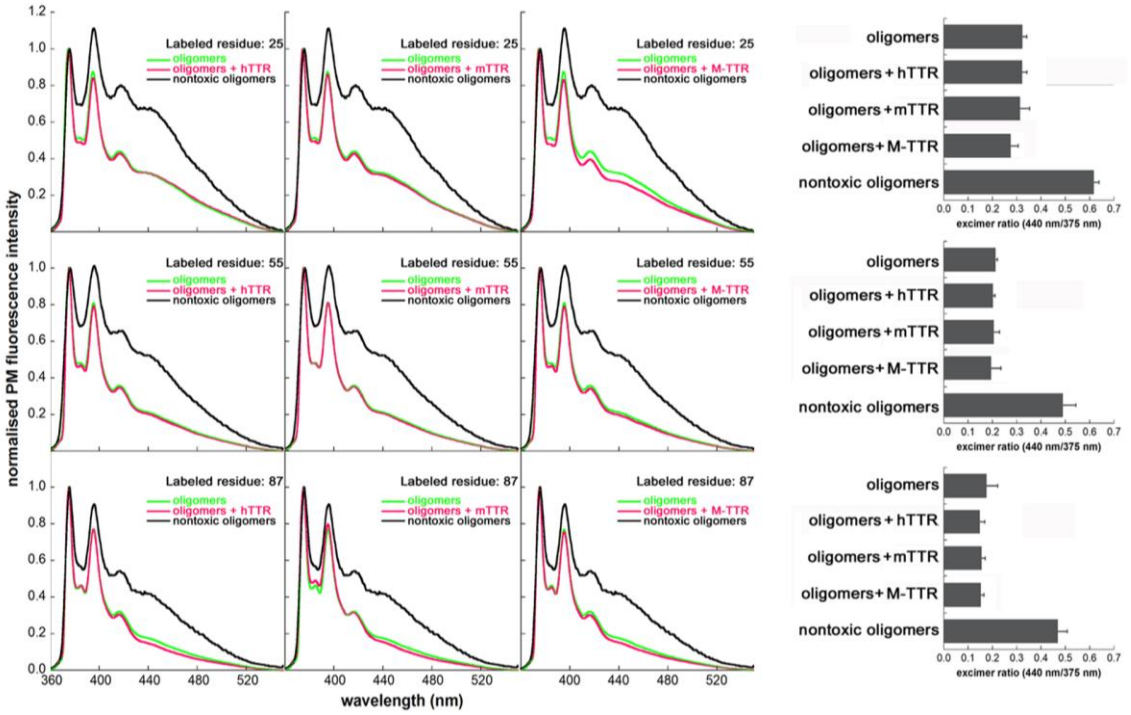

Figure 4.4. TTRs do not remodel HypF-N oligomers. Fluorescence emission spectra of samples containing HypF-N oligomers labeled with PM at positions 25 (top), 55 (middle) and 87 (bottom) were acquired at 12 μM HypF-N concentration following 1 hour of incubation in the absence (green) or in the presence (pink) of hTTR (left panels), mTTR (middle panels) or M-TTR (right panels). The molar ratio of HypF-N:TTR was 10:1. For comparison, the corresponding spectra of nontoxic oligomers are reported in each graph (black). The spectra have been normalized to the intensity of the peak centered at 375 nm. On the right, the exicimer-to-monomer fluorescence intensity (FI_{440nm}/FI_{375nm}) of each sample and of the nontoxic oligomers [Campioni *et al.*, 2010] is reported.

4.2.4 TTRs bind to the oligomers

To determine whether TTRs bind to the oligomers we used TTR-derived intrinsic fluorescence and sodium dodecylsulfate polyacrylamide gel electrophoresis (SDS-PAGE). HypF-N oligomers sediment at a relatively low centrifugal force; therefore, if the TTRs are able to bind to the oligomers and the interaction between them is stable, the concentration of the TTRs in the supernatant will decrease following centrifugation, depending on the strength of the interaction. HypF-N oligomers and TTRs were incubated in isolation or in combination for 1 hour in phosphate buffer at pH 7.0 and each resulting sample was centrifuged to separate the pellet fraction (P), which contains the TTR bound to the oligomers, from the supernatant (SN), which contains the soluble unbound TTR. The amount of TTR in the SN was measured by its intrinsic fluorescence (Figure 4.5A-C). The fluorescence spectra of the SNs collected from the samples where oligomers and hTTR or M-TTR were present were less intense than the corresponding ones in which only the TTRs were present, indicating that a fraction of hTTR, and to a greater extent M-TTR, is bound to the oligomers. In contrast, the fluorescence spectrum of the SN collected from the sample containing oligomers and mTTR was similar to the corresponding one in which only mTTR was present.

As a further evidence of the binding, the P and SN fractions collected in each experiments were also analysed by SDS-PAGE. In the samples containing oligomers or TTR alone, the HypF-N monomer (MW ~10.5 kDa) and the TTR monomer (MW ~15 kDa) were found only in the P and SN fractions, respectively (Figure 4.5D-F). In the sample containing both HypF-N oligomers and M-TTR, the HypF-N band was present only in the P fraction, whereas M-TTR was found to partition between the P and SN fractions (Figure 4.5F). This result confirms that a small fraction of M-TTR is bound to the oligomers. Similar results, but to a lower extent, were obtained with hTTR (Figure

4.5D). In contrast, we found mTTR only in the SN fraction, suggesting that mTTR did not bind to HypF-N oligomers (Figure 4.5E). These results show that TTRs have a different ability to bind to the oligomers. Interestingly, such ability correlates with the capability of TTR to adopt the monomeric state.

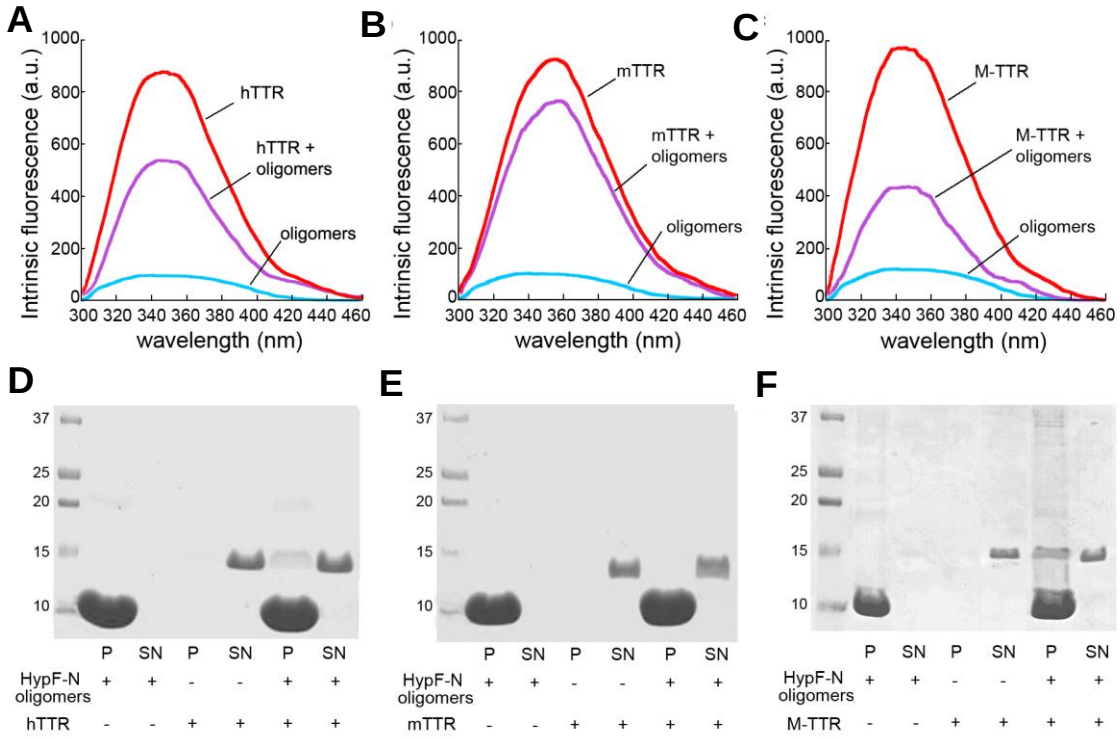

Figure 4.5. TTRs binds to HypF-N oligomers. (A-C) Intrinsic fluorescence spectra of the SN fractions obtained after centrifugation of samples containing preformed HypF-N oligomers (blue), TTR (red) and HypF-N oligomers + TTR (purple). For hTTR (A), mTTR (B) and M-TTR (C) the fluorescence emission spectra (excitation at 280 nm) were acquired at 37°C. The spectrum of HypF-N oligomers has been subtracted from that of TTR + HypF-N oligomers to eliminate its contribution. (D-F) SDS-PAGE analysis of the insoluble (P) and soluble (SN) fractions obtained from samples containing preformed HypF-N oligomers (lanes 2, 3), TTR (lanes 4, 5) and preformed oligomers treated for 1 hour with TTR (lanes 6, 7) for hTTR (D), mTTR (E) and M-TTR (F). The HypF-N concentration was 48 μM (in monomer units) and the molar ratio of HypF-N:TTR was 10:1.

4.2.5 The binding of TTRs to the oligomers promotes their assembly into larger species

To investigate whether the binding of TTRs to the oligomers promotes their further assembly, we first used AFM. Discrete HypF-N oligomers with a height of 1–4 nm were observed by AFM in the absence of TTR (Figure 4.6A), but significantly larger aggregates were evident in the presence of M-TTR and, to a lower extent, of hTTR (Figure 4.6A). More complex structures were observed in the presence of M-TTR, consisting of very large aggregates of irregular shape with typical heights of a few tens of nanometers. Large assemblies were not observed in samples containing oligomers with mTTR (Figure 4.6A), or in samples containing only TTR (data not shown).

As an additional evidence of the ability of TTRs to promote oligomer assembly, we took advantage of turbidimetry measurements at 500 nm, which revealed a similar trend. As reported in Figure 4.6B the oligomers incubated in the presence of h-TTR and to a greater extent the ones incubated in presence of M-TTR show a higher light scattering than the aggregates incubated in absence of TTR or in the presence of m-TTR.

The AFM and turbidity results show that M-TTR and hTTR promote the assembly of the HypF-N oligomers into larger species.

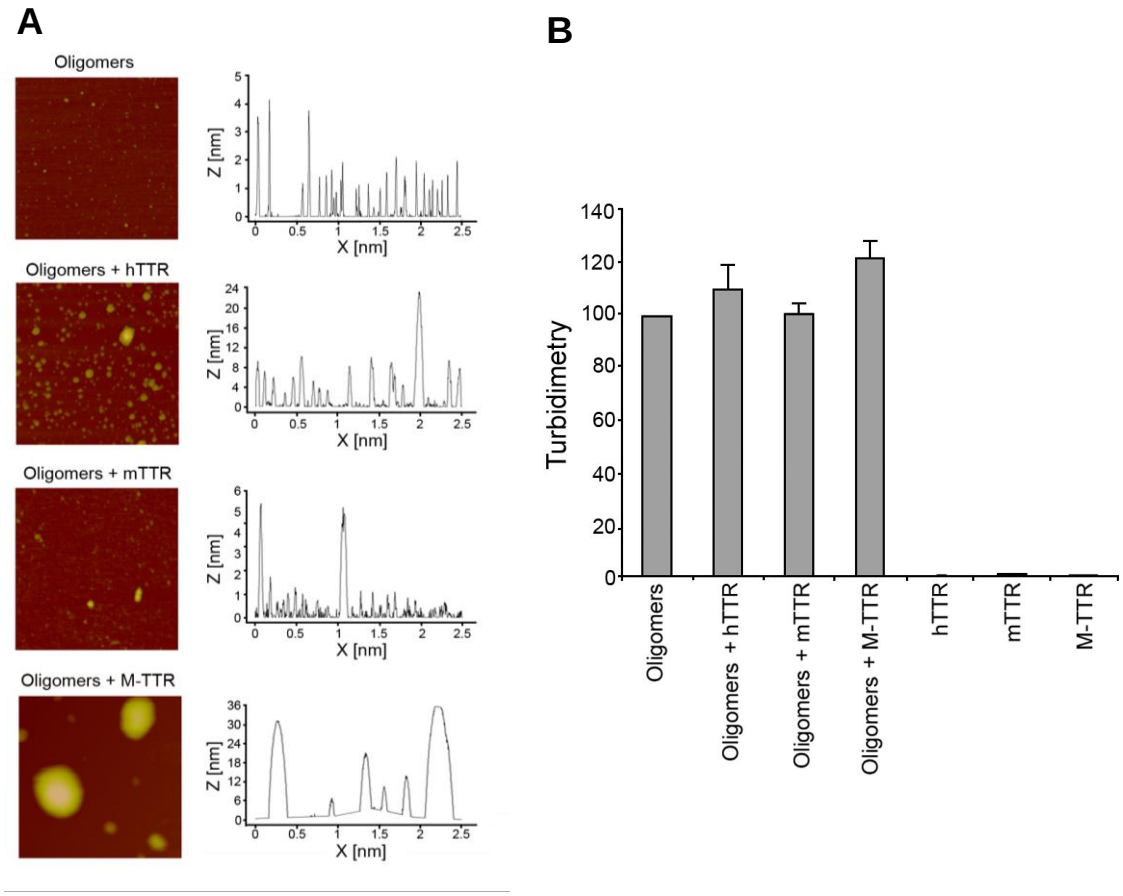

Figure 4.6. Assembly of HypF-N oligomers induced by TTRs. (A) AFM images and corresponding height analysis of HypF-N oligomers preincubated with or without TTRs. Preformed oligomers of HypF-N were resuspended in phosphate buffer pH 7.0, incubated for 1 h at a corresponding monomer concentration of 48 μM in the absence or presence of the indicated TTRs (HypF-N:TTR molar ratio was 10:1) and then deposited on mica; the scan size is 1 μm. Z range: 5 nm (oligomers), 24 nm (oligomers + hTTR), 6 nm (oligomers + mTTR), 36 nm (oligomers + M-TTR). (B) Measurements of turbidimetry at 500 nm of HypF-N oligomers incubated with or without TTRs and TTRs alone. Conditions as in (b) of HypF-N oligomers preincubated with or without TTRs and TTRs alone. Absorbance at 500 nm was measured at 48 μM HypF-N and at a HypF-N:TTR molar ratio of 10:1. Error bars correspond to standard error values of at least six indipendent experiments.

4.3 Discussion

4.3.1 TTR inhibits the cellular dysfunction caused by protein misfolded oligomers

TTR was shown to inhibit aggregation and amyloid plaque formation of Aβ, the peptide associated with AD. Such inhibition was observed *in vitro*, using SDS-PAGE, transmission electron microscopy, laser light scattering and measurements of ThT

fluorescence and Congo red birefringence under cross-polarised light [Schwarzman *et al*., 1994; Liu and Murphy, 2006; Du and Murphy, 2010]. It was also observed *in vivo*, using nematode and mouse models genetically modified to overexpress human TTR or to have the endogenous TTR gene knocked out; indeed, these transgenic animals were found to accumulate a lower and greater amount of Aβ plaques, respectively [Link, 1995; Choi *et al*., 2007; Buxbaum *et al*., 2008].

Analyses carried out *in vitro* on the interaction between TTR and Aβ have shown that TTR binds monomeric Aβ, explaining its ability to prevent aggregation of the peptide [Schwarzman *et al*., 1994; Costa *et al*., 2008; Du and Murphy, 2010]. However, TTR-Aβ binding occurs with higher affinity for aggregated Aβ, such as oligomers and fibrils, relative to monomeric Aβ, with monomeric TTR exhibiting stronger binding than tetrameric TTR [Liu and Murphy, 2006; Buxbaum *et al*., 2008; Du and Murphy, 2010]. The high affinity between monomeric TTR and aggregated Aβ suggests an important role for such an interaction. Indeed, TTR was shown to bind to preformed Aβ oligomers and reduce their toxicity to murine primary neurons and human neuroblastoma SH-SY5Y cells [Li *et al*., 2011]. In such studies, TTR-mediated toxicity suppression was not due to the ability of TTR to inhibit Aβ aggregation, but to act on preformed oligomers.

Here, we found that TTR is able to suppress the toxicity of extracellularly added oligomers formed by three different peptides/proteins, namely $A\beta_{42}$, IAPP and HypF-N, adding two proteins to the preliminary observation obtained with $A\beta_{42}$ [Li *et al*., 2011]. TTR was found to inhibit the influx of Ca^{2+} caused by the oligomers, thus eliminating the occurrence of later effects, manifested as oxidative stress, membrane leakage and apoptosis. In addition, the observed dependence of the degree of protection on the time of preincubation indicates that TTR suppresses oligomer toxicity by interacting with the

oligomers, rather than through a separate protective pathway mediated by direct interaction of TTR with the cells. Overall, therefore, these findings reveal that the interaction of misfolded protein oligomers with cell membrane and the following deleterious effects, can be abolished by the presence of TTR.

The three types of TTR examined here, namely hTTR, mTTR and M-TTR, were found to display different protective effects against oligomer-induced cytotoxicity. Indeed, monomeric M-TTR was able to protect SH-SY5Y neuroblastoma cells and rat primary neurons against oligomer-induced cytotoxicity; the highly stable tetrameric mTTR only showed a small and non significant protective effect, whereas the less stable tetrameric hTTR had intermediate rescuing effects between the two forms, or displayed a protective action slower or at higher concentrations than M-TTR. Hence, the ability of TTR to protect neuronal cells and neurons against misfolded protein oligomers correlates with the ability of the protein to adopt a monomeric state.

4.3.2 TTR promotes the formation of larger assemblies of oligomers

To shed light on the molecular mechanism by which TTR exerts its protection, we focused on HypF-N oligomers, probing their oligomeric state and molecular structure after the incubation with TTRs *in vitro*. Using ThT fluorescence we found that TTR does not disaggregate the preformed oligomers. Nor does it appear to promote a structural re-organization of the discrete oligomers, as shown by site-directed pyrene labelling. Rather, TTR was found to bind to the oligomers, as determined with SDS-PAGE and intrinsic fluorescence, and promote their further assembly into larger aggregates, as shown by AFM and turbidimetry. The ability of TTR to bind to and further assemble preformed HypF-N oligomers correlated again with its ability to adopt a monomeric state, as the efficiency of such process followed the same order as that

found for toxicity suppression, i.e. M-TTR > hTTR > mTTR. These data also suggest that the size of extracellular protein aggregates is an inverse correlate of their toxicity. The TTR-induced oligomer clusters are characterized by a reduction in their exposed hydrophobic surface and diffusional mobility, both of which are expected to reduce their toxicity to cells, in agreement with previous findings [Chapter 2; Chapter 3; Ojha *et al*., 2011; Ahmed *et al*., 2010; Cizas *et al*., 2010; Bemporad and Chiti, 2012].

Overall, the molecular mechanism through which monomeric TTR protects the cells against the deleterious effects of protein aggregation seems to involve two different levels of intervention, that is inhibition of protein aggregation and fibril formation, as previously demonstrated [Schwarzman *et al*., 1994; Liu and Murphy, 2006; Du and Murphy, 2010; Link, 1995; Choi *et al*., 2007; Buxbaum *et al*., 2008], and neutralisation of protein oligomer toxicity once the oligomers are formed, as shown here. Such a dual protective behaviour has also been demonstrated for a number of proteins that have been widely recognised as molecular chaperones, such as αB-crystallin, Hsp70 (both with and without ATP), clusterin, α_2-macroglobulin and haptoglobin [Chapter 2], suggesting that TTR can also act as an ATP-independent, extracellular chaperone. The early observation that TTR is tightly bound to Aβ plaques in AD patients, which remained without significant follow-up for years, [Shirahama *et al*., 1982], is also reminiscent of the behaviour of extracellular chaperones, as they all have been found associated with extracellular Aβ deposits in such patients [Powers *et al*., 1981; Bauer *et al*., 1991; Kida *et al*., 1995].

4.4 Materials and methods

4.4.1 Formation of protein oligomers

HypF-N was expressed and purified as described in section 2.4.1. Toxic HypF-N oligomers were generated by incubating the protein for 4 hour at 25 °C and at a concentration of 48 μM in 50 mM acetate buffer, 12% (v/v) TFE, 2 mM DTT, pH 5.5. $A\beta_{42}$ and IAPP oligomers were produced as reported [Lambert *et al*., 2001; Cecchi *et al*., 2008] and resuspended in the cell culture medium to 12 μM. HypF-N oligomers were centrifuged at 16100 rcf for 10 min, dried under N_2 and resuspended in cell culture media in the absence of cells (for cell biology tests) or in 20 mM potassium phosphate buffer at pH 7.0 (for biophysical/biochemical analysis). Native proteins were diluted to a final concentration of 12 μM into the same media. Oligomers were then incubated in the appropriate media for 1 hour at 37 °C while shaking, in the absence or presence of each TTR, and then added to cultured cells or subjected to biophysical/biochemical analysis. The protein:TTR molar ratio was 10:1, unless stated otherwise (hTTR, mTTR and M-TTR are considered as tetramers).

4.4.2 Preparation of TTRs

hTTR, mTTR and M-TTR were prepared and purified in an *Escherichia Coli* expression system as described elsewhere [White and Kelly, 2001; Jiang *et al*., 2001; Hammarstrom *et al*., 2003]. The three protein variants were purified by gel filtration on a Superdex 75 column (Amersham Biosciences) in 10 mM phosphate buffer, 100 mM KCl, 1 mM EDTA pH 7.6 before each experiment to ensure that no aggregates were present in the starting material. Liquid chromatography-electrospray ionization mass spectrometry was used to confirm the molecular weight of the proteins.

4.4.3 Cell cultures

Human SH-SY5Y neuroblastoma cells (A.T.C.C., Manassas, VA) were cultured as described in section 2.4.4.

4.4.4 MTT reduction assay

The effect of protein oligomers on cell viability was assessed using SH-SY5Y cells seeded in 96-well plates, and using the MTT assay as described in section 2.4.5. Preformed oligomers of HypF-N, $A\beta_{42}$ and IAPP (12 μM monomer concentration) were incubated for 1 hour in the absence or presence of hTTR, mTTR, M-TTR, haptoglobin, HEWL or BSA (protein:TTR molar ratio was 10:1 unless otherwise stated; protein:haptoglobin, protein:HEWL and protein:BSA molar ratio was 5:1), and then added to the cells. Each TTR (1.2 μM tetramer concentration) or 12 μM native HypF-N, $A\beta_{42}$ and IAPP were also used as controls.

4.4.5 Thioflavin T assay

Preformed HypF-N oligomers (12 μM monomer concentration) were incubated for 1 hour at 37 °C under shaking in the presence or absence of each TTR (HypF-N:TTR molar ratio as described above). Aliquots of these samples were added to a solution of 25 μM ThT dissolved in 25 mM phosphate buffer at pH 6.0, in order to obtain a 3.7-fold molar excess of dye. Final protein concentration was 6 μM. The steady-state intensity of fluorescence emission at 485 nm (excitation at 440 nm) was recorded at 37 °C using a Perkin-Elmer LS 55 spectrofluorimeter (Wellesley, MA) equipped with a thermostated cell holder attached to a Haake F8 water bath (Karlsruhe, Germany). Each TTR (1.2 μM tetramer concentration) and 12 μM native HypF-N were also used as controls.

4.4.6 Pyrene fluorescence emission spectra

HypF-N variants carrying a single cysteine residue were labeled with PM as previously described [Campioni *et al*., 2010], converted into toxic aggregates as previously reported [Campioni *et al*., 2010] and then 4-fold diluted into 20 mM potassium phosphate buffer at pH 7.0. Fluorescence emission spectra of these samples were measured after 1 h of incubation at 37 °C under shaking in the absence and presence of each TTR. The spectra were acquired at 12 μM HypF-N concentration, 37 °C, with an excitation of 344 nm using a Perkin-Elmer LS 55 spectrofluorimeter (Wellesley, MA) equipped with a thermostated cell holder attached to a Haake F8 water bath (Karlsruhe, Germany), and a 1.5 × 1.5 mm quartz cell. The spectra have then been normalized to the intensity of the peak centered at 375 nm.

4.4.7 Intrinsic fluorescence

HypF-N oligomers and each TTR incubated in isolation and in combination as described before were centrifuged for 10 min at 16100 rcf. The intrinsic fluorescence of the SNs were measured at 37 °C with excitation at 280 nm using a Perkin-Elmer LS 55 spectrofluorimeter (Wellesley, MA) equipped with a thermostated cell holder attached to a Haake F8 water bath (Karlsruhe, Germany), and a 2 × 10 mm quartz cell. The spectrum of HypF-N oligomers has been subtracted from that of TTR+HypF-N oligomers.

4.4.8 SDS-PAGE

HypF-N oligomers and each TTR incubated in isolation and in combination as described before were centrifuged for 10 min at 16100 rcf. P and SN aliquotes were collected and mixed with 4× sample buffer with 20 % 2-mercaptoethanol. SDS-PAGE

analysis was performed in accordance with Laemmli [Laemmli, 1970] using a 16% polyacrylamide gels. Proteins were visualized by Coomassie Blue staining (0.1% Coomassie Blue, 10% acetic acid, 40% methanol).

4.4.9 Atomic force microscopy

HypF-N oligomers were incubated for 1 hour at 37 °C under shaking in 20 mM potassium phosphate buffer at pH 7.0, in the presence or absence of each TTR. Samples were diluted 1000-fold and immediately deposited on a freshly cleaved mica substrate and dried under a gentle nitrogen flux. Non-contact AC mode atomic force microscopy (AFM) images were acquired in air using a PicoSPM microscope equipped with an AC-mode controller (Molecular Imaging, Phoenix, AZ). Rectangular non-contact cantilever (model NSG01, NT-MDT Moscow, Russia), with typical resonance frequency of 150 Khz, were used. Oligomer sizes were measured from the height in cross section of the topographic AFM images. The reported heights result from the obtained values multiplied by a shrinking factor of 2.2, which was evaluated comparing the heights of native HypF-N under liquid and after drying.

4.4.10 Turbidimetry

HypF-N oligomers (12 μM monomer concentration) were incubated for 1 hour at 37 °C under shaking in 20 mM potassium phosphate buffer at pH 7.0 in the absence or presence of each TTR. Samples containing TTRs were also used as controls. Subsequently, the absorbance of the samples at 500 nm was measured using a Jasco V-630 UV-Vis Spectrophotometer (Tokyo, Japan) and a cell path of 0.1 cm. All the measurements were blank-subtracted.

4.4.11 Statistical analysis

Data was expressed as mean ± standard deviation (SD). Comparisons between different groups were performed using ANOVA followed by Bonferroni's post-comparison test. A p value lower than 0.05 was considered statistically significant.

Chapter 5

GLIAL INFLAMMATORY RESPONSE TRIGGERED BY MISFOLDED PROTEIN OLIGOMERS AND THE ROLE OF HSPS AS IMMUNE MEDIATORS

5.1 Introduction

Increasing evidence suggests that the neurodegeneration associated with protein deposition diseases, such as Alzheimer's disease, Parkinson's disease, Hungtington's disease and spongiform encephalopathies, is the result of many causes. Indeed, these neurodegenerative pathologies are characterized by such a complex nature that the scientific community has begun to consider targeting single molecules or processes as ineffective for therapeutic purposes [Mangialasche *et al*., 2010]. Recently, the chronic inflammatory response, caused by a massive activation of microglial cells in the brain, has been established as a central process in the onset and progression of these pathologies. In fact, it has been observed in brains affected by Parkinson's disease [Kim and Joh, 2006], Alzheimer's disease [McGeer *et al*., 2006] and Huntington's disease [Masters and O'Neill, 2011].

It has been suggested that the trigger factor of the innate response is the exposure of hydrophobic surfaces [Seong and Matzinger, 2004]. Such an exposure is a property shared by amyloidogenic proteins/peptides and misfolded aggregates, which are strong inducers of inflammation in agreement with this hypothesis [Masters and O'Neill, 2011]. In particular, the early forming oligomers, that are thought to be the major pathogenic species in protein deposition diseases, having a high degree of superficial hydrophobicity, are believed to be highly responsible for the activation of the inflammatory process [Roodveldt *et al*., 2011; Amor *et al*., 2010].

Following these considerations, we have investigated the inflammatory response triggered by misfolded oligomers, taking advantage of the well-known property of the HypF-N aberrant oligomers to be toxic or benign according to the conditions in which they form [Campioni *et al*., 2010]. Moreover, we also investigated the role of two Hsps, αB-crystallin and Hsp70, as immune mediators in the CNS, since they are released in the extracellular space and act as signal molecules for the immune system in a cytokine- of chemokine- manner [van Noort, 2008; Chen and Cao, 2010]. This aspect is particularly interesting in the contest of the injury caused by aberrant oligomers; indeed, Hsps have also been found to interact with misfolded oligomers, clustering them and making them harmless [Ojha *et al*., 2011; Chapter 2].

The results presented in this chapter show that the toxic and the nontoxic HypF-N oligomers are able to activate microglia in a different manner, even though they both trigger a pro-inflammatory response. In addition, the nontoxic oligomers and the assemblies of the toxic oligomers neutralized by chaperones have an ability to induce inflammation without affecting cellular viability.

5.2 Results

5.2.1 The viability of microglia cells is affected by HypF-N oligomers

The ability of type A and type B oligomers to cause cell death has been assessed by means of the MTT assay on a variety of cell lines, including the neuroblastoma cells (SH-SY5Y) [Campioni *et al*., 2010; Chapter 2], mouse endothelial cells (Hend) [Campioni *et al*., 2010], chinese hamster ovarian cells (CHO) [Saridaki *et al*., 2012] and human embryonic kidney 293 cells (HEK293) [Mannini *et al*., 2012]. In all these experiments, the cells were treated with a 12 μM concentration of HypF-N aggregated

either in condition A or in condition B and the biological activity of the resulting oligomers was found to be different: whereas type B oligomers did not affect the cellular viability, type A aggregates reduced the viability by 30-40% with respect to the untreated cells.

We first checked the response of microglia cells to the administration of type A and type B oligomers, using the same MTT reduction inhibition assay. The oligomers aggregated under the two distinct conditions were centrifuged, resuspended in the cell culture medium and then added to murine N13 microglia cells. The results, displayed in Figure 5.1 as a percentage of the value measured for the untreated cells, show that at the HypF-N concentration of 12 μM, the two types of oligomers presented a difference in the biological activity, with the type A aggregates being able to cause a 40% decrease in the viability and the type B ones maintaining unaltered the mitochondrial ability to reduce MTT. This result confirms the different ability of the two oligomers to cause cell dysfunction, even in the case of murine N13 microglia cells.

In order to enable the direct comparison of the inflammatory response triggered by type A and type B oligomers, we looked for conditions in which both types of aggregates do not affect the cellular viability. Therefore, MTT tests were repeated by decreasing the concentration of the aggregates (Figure 5.1). Lower concentrations of type B oligomers did not alter the viability, whereas type A aggregates showed a dose-dependent effect, reaching very low levels of cytotoxicity and not significantly different from the ones of untreated cells at the concentration of 0.7 μM (Figure 5.1). These viability data allow to study the immunological properties of type A and B aggregates in conditions in which they display different biological activities, i.e. at concentrations

ranging from 12 to 3 μM and in conditions in which they are both unable to cause cellular damage (0.7 μM).

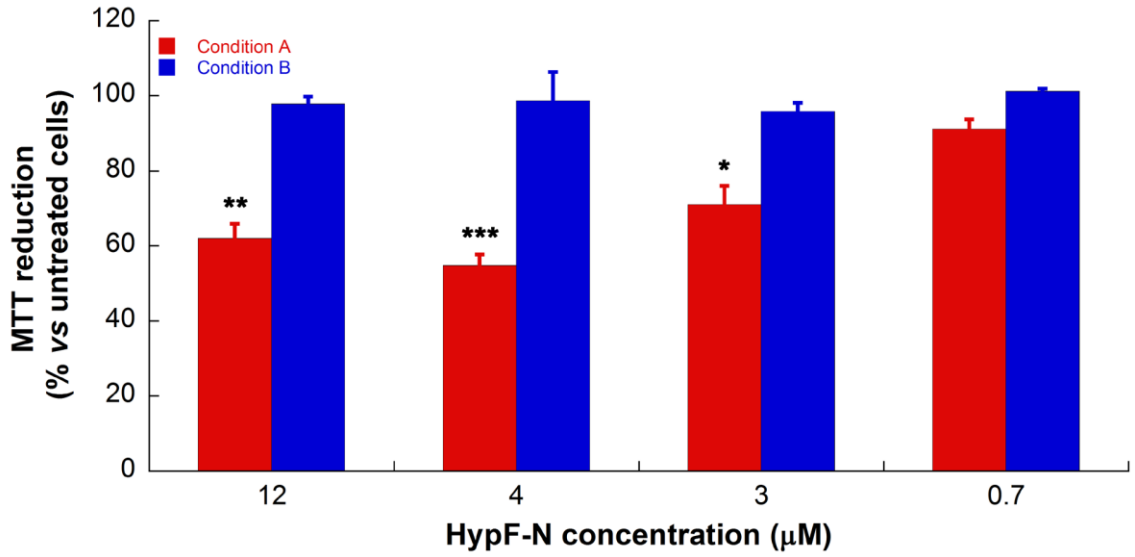

Figure 5.1. MTT reduction assay on murine N13 cells treated with different concentrations of type A (red bars) and B (blue bars) oligomers. Error bars correspond to standard errors of the means of 2 independent experiments. Single, double and triple asterisks refer to p values lower than 0.05, 0.01 and 0.001, respectively with respect to untreated cells.

5.2.2 HypF-N oligomers trigger a pro-inflammatory response

The inflammatory response to type A and B oligomers was evaluated by measuring the release of a series of key cytokines in N13 cells by means of ELISA assays. We measured the release of three pro-inflammatory cytokines, i.e. IL-6, TNF-α and IL-1β, and the release of IL-10, recognized as an anti-inflammatory cytokine. The cells were incubated with exogenously added type A and B oligomers at a concentration in which they maintain their different biological activity (3 or 4 μM, as stated). As shown in

Figure 5.2, both types of oligomers were able to induce the release of the three pro-inflammatory cytokines to a different extent.

The release of IL-6 was moderately induced by type A and B oligomers but it was substantially lower than the release stimulated by lipopolysaccharide (LPS), used here as a positive control (Figure 5.2A). Indeed, LPS is a major constituent of the outer cell membrane of Gram-negative bacteria and it is recognized to induce the secretion of pro-inflammatory cytokines in microglia [Kettermann *et al*., 2011]. In addition, type A and type B aggregates were found to trigger the release of not significantly different amounts of IL-6 (Figure 5.2A). The TNF-α response observed for HypF-N type A and type B oligomers was found to be greater than that induced by LPS (Figure 5.2B). Moreover, as observed in the case of IL-6 release measurement, type A and type B oligomers were able to induce the TNF-α release to a similar extent (Figure 5.2B). The treatment of the microglial cells with HypF-N oligomers cause a significant rise in IL-1β levels relative to the untreated cells only in the case of type A oligomers (Figure 5.2C). By contrast, the amount of this cytokine in the culture supernatants of cells treated with the medium alone was found to be not significantly different from the amount detected after type B oligomers treatment (Figure 5.2C). In addition, the release of IL-1β was found to be higher in cells stimulated by type A oligomers with respect to cells incubated with type B oligomers (p value < 0.05) (Figure 5.2C). Finally, the release of IL-10 was also tested on N13 cells, but no amount of this cytokine was detected after the incubation of the cells with both types of HypF-N aggregates (data not shown).

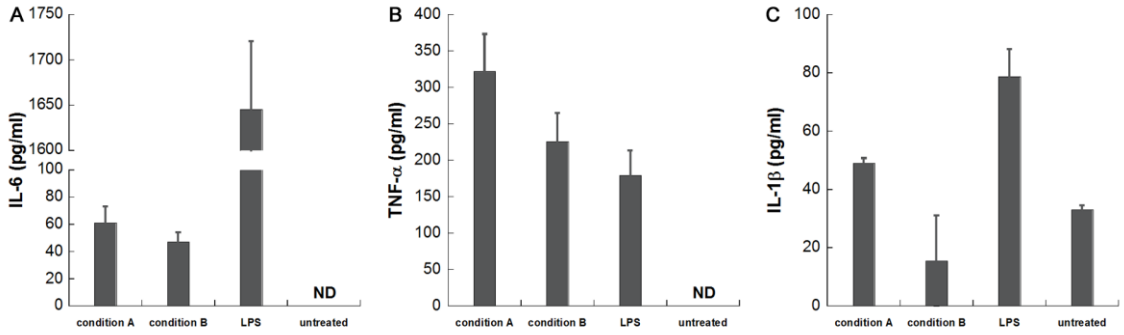

Figure 5.2. Interleukin profile of microglia cells stimulated by type A and B oligomers. IL-6 (A), TNF-α (B) and IL-1β (C) release measured by ELISA assays in culture supernatants of murine N13 cells treated with 3 μM (A and B) or 4 μM (C) type A and type B oligomers. In every experiment LPS at a concentration of 1 μg/ml and culture medium alone were used as positive and negative controls, respectively. Non detectable amounts of cytokines were indicated with ND. Error bars correspond to standard errors of the means of 6 (A), 5 (B) or 2 (C) independent experiments.

The release of pro-inflammatory mediators, such as IL-6, TNF-α and IL-1β, indicates that HypF-N oligomers trigger a pro-inflammatory response. Conversely, the lack of stimulation of the IL-10 secretion suggests that they are not able to induce the release of this anti-inflammatory signal. Moreover, at a concentration in which the oligomers have different abilities to damage the cells, type A and type B oligomers stimulate the release of IL-6 and TNF-α to a similar extent. Only in the case of IL-1β, type A oligomers were found to be stronger inducers than type B aggregates.

5.2.3 Differences between type A and type B oligomers in stimulating the inflammatory response

In order to better understand the biological mechanism of the pro-inflammatory response triggered by type A and type B oligomers, we performed ELISA tests in

conditions in which both types of aggregates do not display significant levels of cytotoxicity, as indicated by the MTT results shown in Figure 5.1. Therefore, N13 cells were treated with different concentrations of oligomers and the release of IL-6 and TNF-α was measured. The results reported in Figure 5.3 show that type A oligomers stimulated the release of IL-6 in a dose-dependent manner (Figure 5.3A), whereas such a release was found to be less affected by the different concentrations of type B oligomers (Figure 5.3A). A similar trend was also revealed in the measurement of TNF-α levels, where the release of this mediator induced by type A oligomers rose by increasing the HypF-N concentration, whereas type B aggregates triggered a secretion of TNF-α in a dose-independent manner (Figure 5.3B).

In addition, type B oligomers were able to stimulate a considerable release of both IL-6 and TNF-α even when they were added at the low concentration of 0.7 μM. By contrast, the same concentration of type A oligomers is not sufficient to induce such a release of

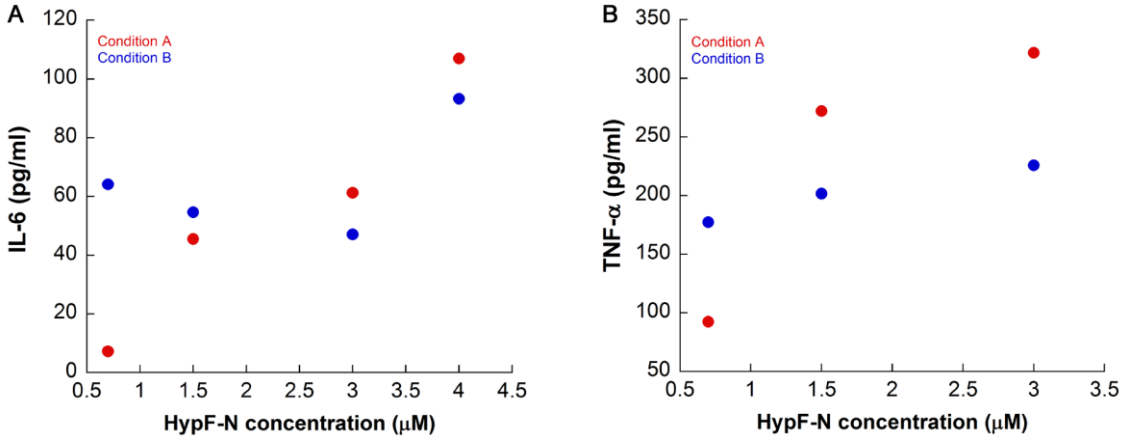

Figure 5.3. Pro-inflammatory interleukin profile of microglia cells stimulated by type A and B oligomers. IL-6 (A) and TNF-α (B) release measured by ELISA assays in culture supernatants of murine N13 cells treated with the indicated concentrations of type A (red dots) and B (blue dots) oligomers.

these mediators. Therefore, it is interesting to notice that at very low concentration of oligomeric protein, in which the two types of oligomers do not affect the cellular viability to any detectable extent, type B aggregates differ significantly with respect to type A oligomers in releasing both IL-6 (p value < 0.001) and TNF-α (p value < 0.05), with type B oligomers being stronger inducers of the inflammatory response than type A oligomers.

5.2.4 Differences in cell internalisation between type A and B oligomers

The difference in stimulating the cytokine secretion observed following a treatment with type A and B oligomers at the concentration in which they do not alter the cellular viability was further investigated.

As described in section 1.4.1, cytokine release can be triggered following the recognition of DAMPs, such as misfolded oligomers, by pattern-recognition receptors located on membranes [Glass *et al*., 2010; Amor *et al*., 2010; O'Neill, 2004].

The different ability of the extracellularly added type A and B oligomers in interacting with such receptors may be responsible of their differences in stimulating the cytokine secretion. The interaction with the receptors can be related to differences in the affinity of the two types of oligomers for the receptors, or to differences in penetrating into the cells. Since now, only the second hypothesis has been investigated.

We posited that the entrance of the oligomers in the cells could be responsible for the reduction of the ability to induce cytokine release, whereas the permanence outside the cells makes the oligomers able to maintain their stimulus.

Therefore, microglia N13 cells were incubated for 24 hours in the presence of either type A or type B oligomers. The cells were washed accurately, permeabilized and

treated with anti-HypF-N primary antibodies and then with Alexa Fluor 633-conjugated anti-rabbit secondary antibodies. Other cell samples, after the incubation with of the oligomers and the intensive washing step, were treated with the antibodies without being permeabilized. Nuclei were stained with 4',6-diamidino-2-phenylindole (DAPI). The two sets of samples were then compared through the acquisition of confocal microscopy images (Figure 5.4). In the cell samples not subjected to permeabilization, the antibodies were prevented from entering and detecting the oligomers inside the cells. Therefore, the red fluorescence signal indicating the presence of HypF-N oligomers arises from aggregates that are stuck on the membrane. By contrast, in the permeabilized samples the red fluorescence derives from both the oligomers stuck on membranes and the oligomers that are inside the cells.

The comparison of the two sets of images obtained after the treatment of the cells with type A oligomers revealed that numerous red dots are present in the permeabilized samples (Figure 5.4A and magnification in Figure 5.4E), whereas such dots are hardly detectable in the samples not permeabilized (Figure 5.4B). This result suggests that most of the type A oligomers are inside the cells and very few remain outside on the cell surfaces.

Regarding the cells incubated with type B oligomers, the amounts of oligomers in the permeabilized (Figure 5.4C and magnification in Figure 5.4F) and not permeabilized (Figure 5.4D) samples are similar, indicating that the net number of oligomers internalized into the cells is very low and the majority remains outside.

Moreover, type B oligomers seem to be more tightly bound to membranes than type A oligomers, since it is more difficult to remove them in the washing step, as indicated by the higher amount of type B oligomers in the cell samples not permeabilized (Figure

5.4D) with respect to the amount of type A aggregates detected in cell samples similarly treated (Figure 5.4B).

No red fluorescence signals were observed in the cells incubated in absence of the oligomers (Figure 5.4G)

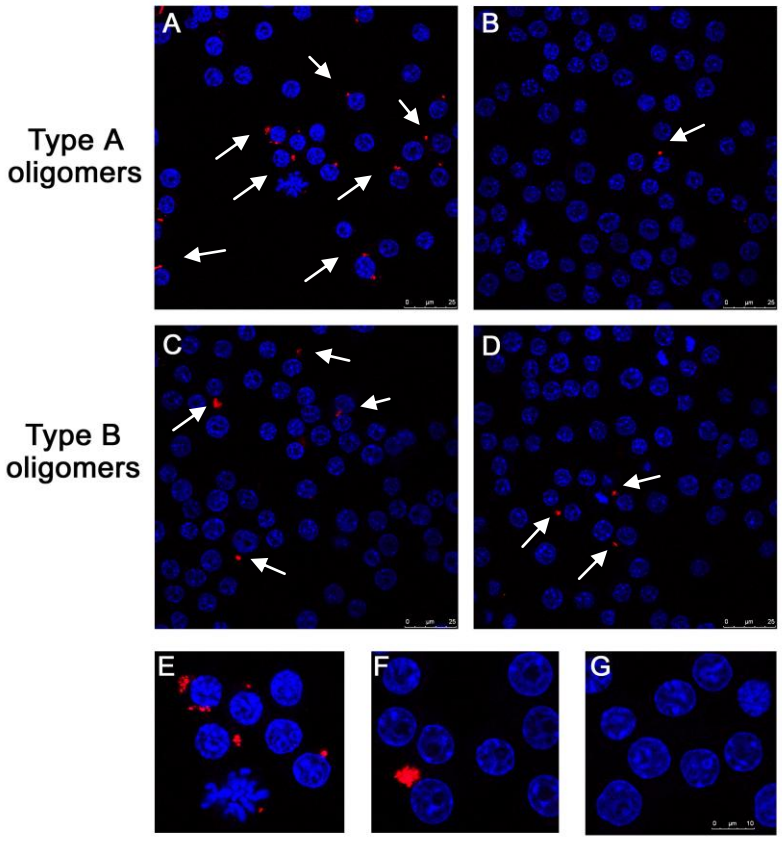

Figure 5.4. Representative confocal microscopy images showing the internalization of type A and B oligomers in N13 cells. Microglia cells were seeded on glass coverslips and incubated with preformed type A (A and B) and B (C and D) oligomers resuspended in the cell culture medium at the final concentration of 0.7 μM. After 24 hours treatment, the cells were washed with phosphate-buffered saline and fixed. Half of the coverslips were treated with a PBS solution containing 3% BSA (w/v) and 0.5% (v/v) triton in order to allow plasma membrane permeabilization (A and C); the remaining coverslips were not permeabilized and treated with a PBS solution containing 3% BSA only (B and D). The coverslips were incubated with rabbit polyclonal anti-HypF-N antibodies and then with Alexa Fluor 633-conjugated anti-rabbit secondary antibodies (red). In (E) enlarged detail of (A); in (F) enlarged detail of (D). In (G) untreated cells. The nuclei were stained with DAPI (blue). Confocal scanning microscope images of the median planes were reported in all cases.

Overall, these data suggest that in N13 cells there is a preferential internalization of type A oligomers with respect to type B aggregates, which, in addition, seem to be prone to adhere to cell membranes. Hence, the results obtained confirm the hypothesis according to which type A oligomers are internalized and consequently prevented to exert their cytokine release stimulation; whereas type B aggregates remain outside on the surface membrane where they can realize their induction.

5.2.5 Hsps protect microglia cells from toxic HypF-N oligomers

Since Hsp70 and αB-crystallin are able to protect SH-SY5Y and HEK293 cells from the damage of type A aggregates, provided the oligomers are incubated in the presence of the chaperones before they are added to the cells [Chapter 2], we performed a preliminary analysis to verify the ability of the chaperones to prevent the toxic effects caused by type A oligomers in N13 microglia cells. The final goal was to reveal the potency of Hsps as immune mediators. As a further indication in this regard, it has been demonstrated that extracellular Hsp70 can act as an autocrine or paracrine signal [Henderson and Pockley, 2010].

Hence, type A oligomers were incubated in the absence or in the presence of Hsp70 or αB-crystallin for 1 hour at 37 °C and then added to N13 cells at the corresponding monomer concentration of 3 μM. Viability measurements of untreated cells and of cells incubated in the presence of the chaperones alone were also acquired. As a control, cells were also treated with 3 μM type B oligomers incubated with or without the two chaperones. The cellular viability was assessed by means of the MTT reduction test and the results are reported in Figure 5.5. N13 microglial cells, treated with type A oligomers pre-incubated with the chaperones, were found to reduce MTT to levels

comparable to untreated cells or to cells treated with the chaperones alone or with type B oligomers, pre-incubated in isolation or in combination with the chaperones. Hence, the ability of Hsp70 and of αB-crystallin to protect SH-SY5Y and HEK293 cells from oligomer mediated damage was confirmed with N13 microglia cells.

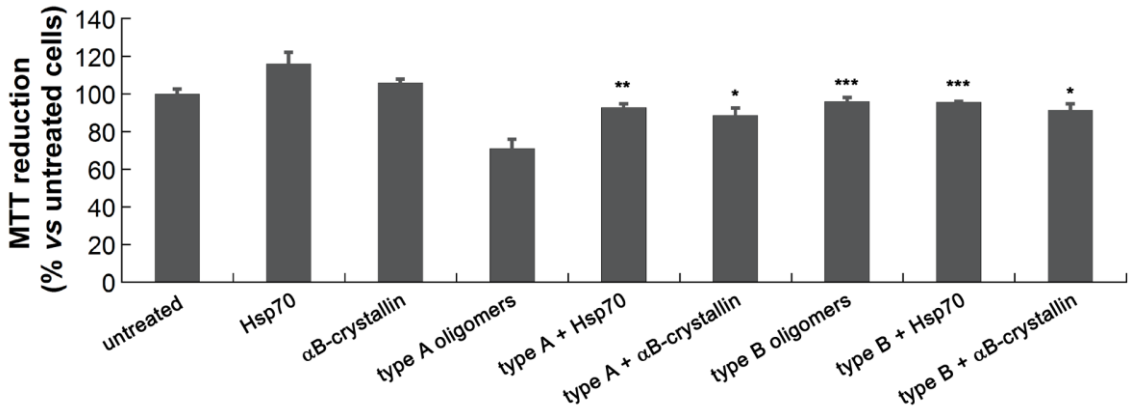

Figure 5.5. MTT reduction assay on murine N13 cells treated with Hsp70, αB-crystallin, type A oligomers incubated in isolation or in combination with Hsp70 or αB-crystallin and type B oligomers incubated with or without Hsp70 or αB-crystallin. Oligomers were added at a corresponding monomer concentration of 3 μM in the absence or presence of the indicated chaperones; protein:chaperone molar ratio was 5:1. Error bars correspond to standard errors. Single, double and triple asterisks refer to p values lower than 0.05, 0.01 and 0.001, respectively with respect to the experiment with type A oligomers.

5.2.6 Hsp70 as an immune mediator

The role of Hsp70 as an immune mediator in the extracellular space was investigated through the evaluation of the activation of the microglial cells in terms of secretion of IL-6 and TNF-α, pro-inflammatory cytokines, and IL-10, anti-inflammatory cytokine. Firstly, N13 cells were treated by adding different concentrations of Hsp70 to their extracellular medium and, after incubation, the culture supernatants were collected. Figure 5.6 shows the data obtained from ELISA assays of these samples. Hsp70 was

found to trigger the release of IL-6 (Figure 5.6A) and TNF-α (Figure 5.6B) in a dose dependent manner, in agreement with previous findings [Kakimura *et al*., 2002]; by contrast IL-10 was not detected in the samples, even in those treated with the highest concentration of Hsp70 (data not shown).

For comparison, Figure 5.7 reports, in the same graph, the release of IL-6 (Figure 5.7A) and TNF-α (Figure 5.7B) stimulated by Hsp70 and type A and B oligomers, all added to the cells at the concentration of 0.7 μM. As described in section 5.2.3, at this concentration type B oligomers are stronger inducers of both IL-6 and TNF-α than type A oligomers. Hsp70 was found to induce a higher and comparable secretion of IL-6 with respect to type A and type B aggregates, respectively (Figure 5.7A). By contrast, a similar and significantly lower amount of TNF-α was detected after the treatment with Hsp70, with respect to type A and type B oligomers, respectively (Figure 5.7B). These data suggest that different pathways of microglial activation might be used by Hsp70 and by the aggregates.

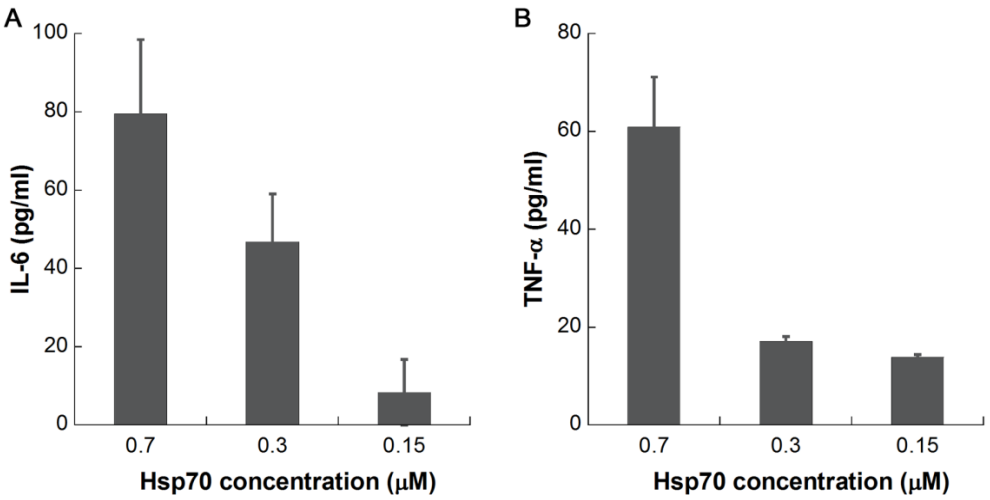

Figure 5.6. Pro-inflammatory interleukin profile of microglia cells stimulated by Hsp70. IL-6 (A) and TNF-α (B) release in culture supernatants of murine N13 cells treated with different concentrations Hsp70 measured by ELISA assays. Error bars correspond to standard errors.

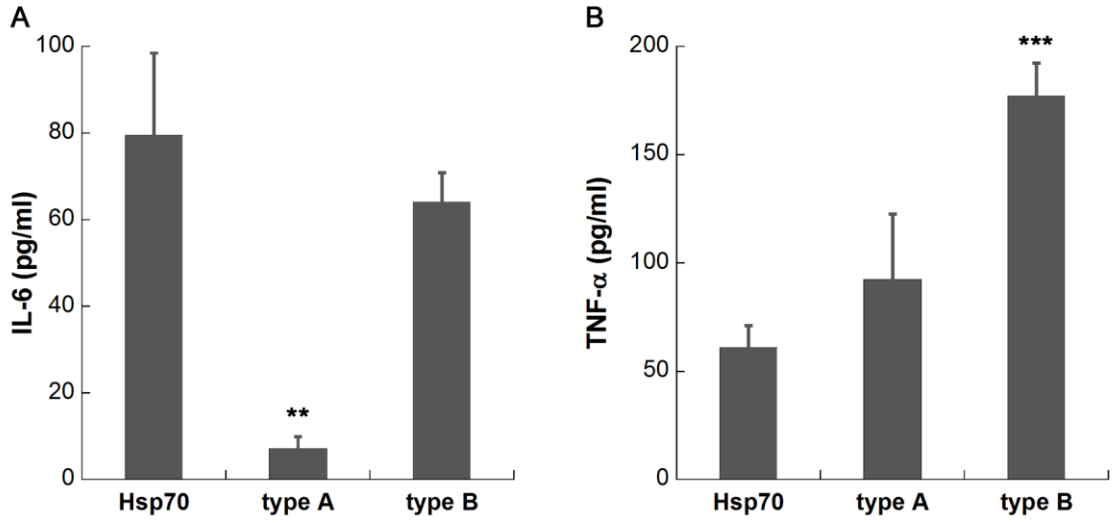

Figure 5.7. Comparison between the ability of Hsp70 and type A and B aggregates, all added to N13 cells at 0.7 μM, in stimulating the secretion of IL-6 (A) and TNF-α (B) measured by ELISA assays. Error bars correspond to standard errors. Double and triple asterisks refer to p values lower than 0.01 and 0.001, respectively with respect to the experiment with Hsp70.

In order to assess if Hsp70 affects the inflammatory response mediated by HypF-N oligomers, this chaperone was incubated in isolation or in combination with type A and B oligomers at different HypF-N:Hsp70 molar ratios, and the resulting mixtures were added to N13 cells. After proper incubation, culture supernatants were recovered and analyzed by means of ELISA tests. Since an inflammatory response is observed also in the presence of Hsp70 alone, it is necessary to consider the specific contribution of type A and B oligomers to the stimulation of IL-6 and TNF-α secretion, as opposed to that of Hsp70 itself.

In Figure 5.8, the amount of cytokine (IL-6 or TNF-α), detected in supernatants of cells treated with the oligomers (type A, indicated in red; type B, indicated in blue) pre-incubated with Hsp70, has been divided by the sum of the amounts of cytokine released after the treatment with Hsp70 and HypF-N oligomers. This ratio is indicated as

$cyt_{olig+chap}$ / (cyt_{chap} + cyt_{olig}) and it allows to point out three scenarios: (i) $cyt_{olig+chap}$ / (cyt_{chap} + cyt_{olig}) = 1, in which the amount of cytokine secretion stimulated by the mixture Hsp70+oligomers simply corresponds to the sum of the contributes of Hsp70 and oligomers; (ii) $cyt_{olig+chap}$ / (cyt_{chap} + cyt_{olig}) < 1, in which the mixture Hsp70+oligomers has a lower ability in triggering the cytokine release with respect to Hsp70 and the oligomers, both added to the cells in isolation; (iii) $cyt_{olig+chap}$ / (cyt_{chap} + cyt_{olig}) > 1, in which the mixture Hsp70+oligomers is a stronger inducer of the cytokine release with respect to Hsp70 and the oligomers both added on the cells in isolation. The HypF-N:Hsp70 molar ratios were 5:1 (Figure 5.8A), 10:1 (Figure 5.8B) and 20:1 (Figure 5.8C), while HypF-N aggregates were at a corresponding monomer concentration of 3 µM in all cases.

When Hsp70 was incubated with HypF-N oligomers at the HypF-N:Hsp70 molar

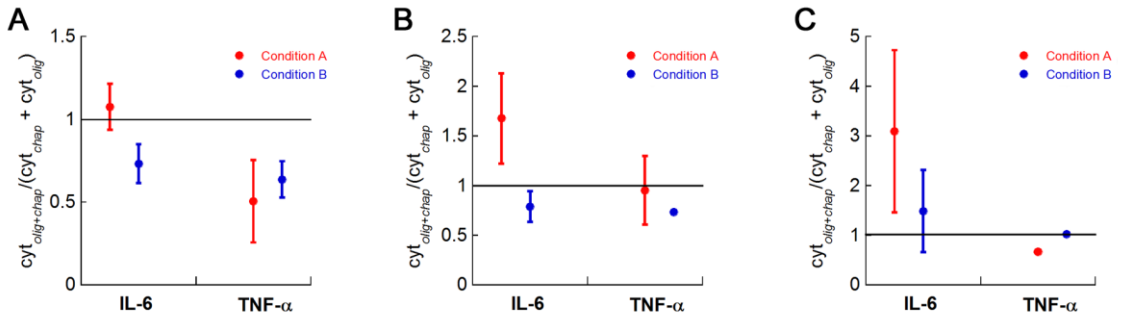

Figure 5.8. Effect of Hsp70 and type A and B oligomers in triggering the release of IL-6 or TNF-α. The ratio $cyt_{olig+chap}$ / (cyt_{chap} + cyt_{olig}) is repored, where $cyt_{olig+chap}$ corresponds to the amount of cytokine (IL-6 or TNF-α) detected in supernatants of N13 cells treated with the oligomers (type A, red dots; type B, blue dots) pre-incubated with Hsp70; cyt_{chap} is the amount of cytokine released after the treatment with Hsp70; cyt_{olig} represents the amount of cytokine secreted after the treatment with HypF-N oligomers. The HypF-N:Hsp70 molar ratios were 5:1 (A), 10:1 (B) and 20:1 (C). In all cases HypF-N aggregates were at a corresponding monomer concentration of 3 µM. Error bars correspond to standard error.

ratio of 5:1, the $cyt_{olig+chap}$ / (cyt_{chap} + cyt_{olig}) values were found to be similar or slightly lower than 1, indicating that the oligomers, after the incubation with Hsp70, maintain unaltered or slightly decrease the ability in triggering the cytokine release (Figure 5.8A). By decreasing the HypF-N:Hsp70 molar ratio to 10:1 (Figure 5.8B), the $cyt_{olig+chap}$ / (cyt_{chap} + cyt_{olig}) values were generally similar to 1. At the 20:1 HypF-N:Hsp70 molar ratio (Figure 5.8C), the $cyt_{olig+chap}$ / (cyt_{chap} + cyt_{olig}) values resulted to be similar to or higher than 1. Although this trend suggests an ability of high concentration of Hsp70 to lower the cytokine secretion induced by the type A and B oligomers, this anti-inflammatory effect of Hsp70 is not evident at HypF-N:Hsp70 molar ratio of 10:1 and 20:1, and the effect is weak even at a molar ratio of 5:1.

5.2.7 αB-crystallin an as immune mediator

In order to study the role of αB-crystallin as an immune mediator, we estimated its ability to activate microglial cells, by means of ELISA measurements of the release of IL-6, TNF-α and IL-10. To this purpose, αB-crystallin was incubated in isolation or in combination with the two types of HypF-N oligomers and then added to N13 cells. In Figure 5.9 four representative experiments are reported. When αB-crystallin was added to microglial cells, neither IL-6 (Figure 5.9A,B) nor TNF-α (Figure 5.9C,D) were detected in cell culture supernatants, indicating that this protein is not able to activate N13 microglial cells. Following the incubation of αB-crystallin with type A and B oligomers at a corresponding monomer concentration of 3 μM (Figure 5.9A,C) and 0.7 μM (Figure 5.9B,D), no significant changes in either IL-6 (Figure 5.9A,B) or TNF-α (Figure 5.9C,D) secretion were found with respect to the release stimulated by HypF-N aggregates alone. The $cyt_{olig+chap}$ / (cyt_{chap} + cyt_{olig}) values reported in Figure 5.9E,F are

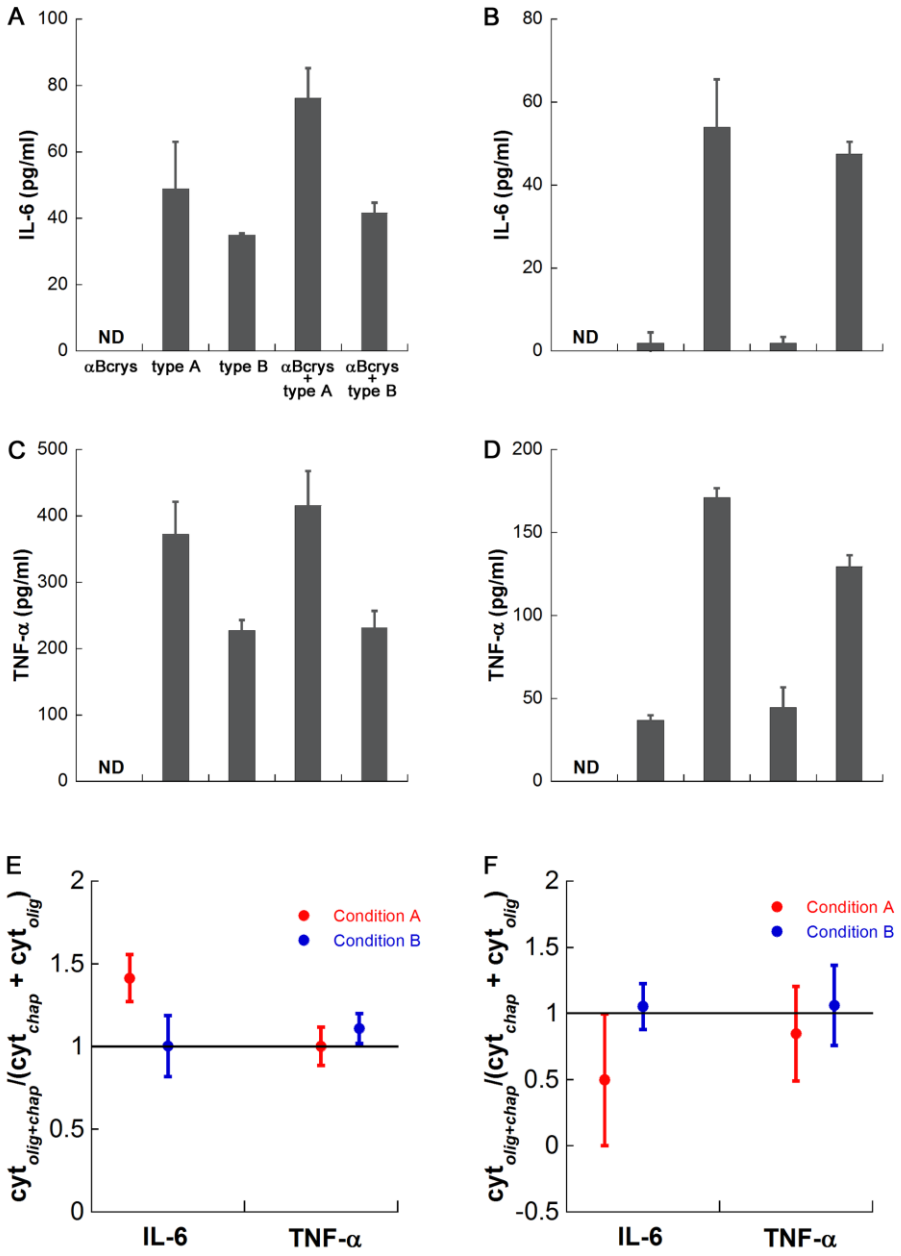

Figure 5.9. Effect of αB-crystallin and type A and B oligomers in triggering the release of IL-6 or TNF-α. IL-6 (A,B) and TNF-α (C,D) release measured by ELISA assays in culture supernatants of murine N13 cells treated with αB-crystallin and 3 μM (A,C) or 0.7 μM (B,D) type A and type B oligomers incubated in isolation or in combination. The HypF-N:αB-crystallin molar ratio was 5:1 in all cases. (E,F) The ratio $cyt_{olig+chap}$ / (cyt_{chap} + cyt_{olig}) is repored, where $cyt_{olig+chap}$ corresponds to the amount of cytokine (IL-6 or TNF-α) detected in supernatants of N13 cells treated with the oligomers (type A, red dots; type B, blue dots) pre-incubated with αB-crystallin; cyt_{chap} is the amount of cytokine released after the treatment with αB-crystallin; cyt_{olig} represents the amount of cytokine secreted after the treatment with HypF-N oligomers. HypF-N aggregates were at a corresponding monomer concentration of 3 μM (E) or 0.7 μM (F). The HypF-N:αB-crystallin molar ratio was 5:1 in all cases. Error bars correspond to standard errors of the means of two independent experiments.

close to 1 and confirm that HypF-N oligomers, after the incubation with αB-crystallin, maintain unaltered their ability to trigger the cytokine release. The cytokine IL-10 was not detected (data not shown), indicating that both αB-crystallin and the mixture αB-crystallin+HypF-N aggregates are not able to induce this anti-inflammatory signal.

5.3 Discussion

5.3.1 Type A and B oligomers: a useful tool to investigate inflammation in protein deposition disease

The study of the mechanisms of neurodegeneration has led to the evidence that a single scientific perspective might not be sufficient to understand the multifactorial nature of neuropathologies. The inflammatory process, inevitably associated with neurodegeneration, has been recognized to give an important contribution to the onset and progression of neuropathologies. For this reason, the activation of microglia has been studied following the treatment with type A and type B HypF-N oligomers.

Type A and B oligomers were found to stimulate the release of pro-inflammatory cytokines, in agreement with previous results obtained for disease-related misfolded oligomers [Masters and O'Neill, 2011]. Interestingly, when the activity of type A and B oligomers was evaluated at a concentration in which neither type is toxic, type B oligomers were found to be stronger inducers of the cytokine release. Such a release is not coupled to alterations in cellular viability and therefore represents a specific oligomer mediated-response.

An explanation to this phenomenon possibly resides in the differences of internalization of the two oligomer types into the cells. Indeed, through the analysis of confocal microscopy images and in agreement with previous analysis performed on

neuroblastoma cells [Campioni *et al*., 2010; Zampagni *et al*., 2011], type B oligomers were found to remain outside and stuck on the membranes, where they can produce a prolonged stimulation responsible for the stronger cytokine response detected in our experiments. By contrast, type A oligomers were found inside the cells and therefore not able to act on the membrane receptors. In addition, microglia cells are the resident phagocytes of the CNS [Perry and Gordon, 1988]. Hence, the entrance of the oligomers into the cells can be an active or a passive mechanism that deserves further investigation.

Most importantly, it is worthwhile to study other aspects for which type A and B oligomers can be useful tools, such as differences of affinity for pattern-recognition receptors and differences in the ability to induce the transcription of such receptors.

The similar morphology and diverse fine structure of type A and B oligomers [Campioni *et al*., 2010] could shed light on the structural determinants responsible for the immune properties of misfolded oligomers and, importantly, offer the opportunity to understand if a persistent inflammatory stimulus can damage the cells on the long timescale, to an extent similar to that by which toxic aggregates kill the cells on the short timescale.

5.3.2 Inflammation induction in the absence of toxicity and the role of Hsps

Type B oligomers and type A oligomers neutralized by Hsp70 and αB-crystallin are not toxic to N13 microglial cells, confirming previously reported data [Campioni *et al*., 2010; Zampagni *et al*., 2011; Chapter 2], but they were found to be able to trigger the inflammatory response. This could be a beneficial mechanism adopted by the cells in order to repair the insult given by the presence of exogenous material. Indeed, in the

acute phase, inflammation is targeted to the damage resolution and to the protection of the tissue from the insult.

In agreement with this hypothesis, Hsp70 itself has been found to trigger the release of IL-6 and TNF-α, as previously reported [Kakimura *et al*., 2002], suggesting that the microglia activation is a protective mechanism. Interestingly, it has been reported that the activation of microglia by Hsp70 correlates with an increase in the uptake and clearance of Aβ aggregates [Kakimura *et al*., 2002; Kakimura *et al*., 2001; Takata *et al*., 2003].

It would be of much interest to evaluate the oligomer uptake capacity in microglia following the stimulation by Hsp70, and if this ability is affected by the different type A and B oligomers. Indeed, the results obtained with neuroblastoma cells and reported in Chapter 2 indicated that neither Hsp70 nor αB-crystallin were able to promote the uptake of the HypF-N oligomers in this cell types (Figure 2.4). In addition, it is important to investigate if a detrimental effect occurs when the molecular machinery dedicated to the clearance of the extracellular material is overwhelmed and the release of inflammatory mediators is sustained for long periods.

Noteworthy, Hsps seems to have a double role in the context of neurodegenerative diseases associated with protein misfolding: the well established studied traditional function of molecular chaperones [Hartl *et al*., 2011] and the function of immune regulators [van Noort, 2008; Henderson and Pockley, 2010]. With particular regard to misfolded oligomers, Hsps were found to abolish the oligomer toxicity [Chapter 2; Ojha *et al*.,2011] and both Hsp70 and the neutralised type A oligomers+Hsps were found to trigger inflammation, indicating the participation of Hsps in different processes as

diverse as protein oligomer-induced cell dysfunction and inflammation in neurodegeneration.

Assessing the importance, the contribute and the balance of such processes could led to a multiple approach in the treatment of protein deposition diseases, examining neurodegeneration from different perspectives.

5.4 Materials and Methods

5.4.1 LAL assay and preparation of HypF-N oligomers

The content of endotoxins in HypF-N protein solution samples, purified as described in section 2.4.1 (Chapter 2), was determined by toxin sensor Limulus Amebocyte Lysate (LAL) assay kit (Genscript, Piscataway, NJ, USA) and resulted to be ~ 0.02 EU/ml.

Oligomeric aggregates of HypF-N were prepared by incubating the protein for 4 hour at 25 °C and at a concentration of 48 µM in two different experimental conditions: (i) 50 mM acetate buffer, 12% (v/v) TFE, 2 mM DTT, pH 5.5 (condition A) and (ii) 20 mM TFA, 330 mM NaCl, pH 1.7, (condition B) [Campioni *et al*., 2010]. The oligomers were centrifuged at 16100 rcf for 10 min, resuspended in cell culture media at a corresponding monomer concentration ranging from 12 µM to 0.7 µM and used for treatments of the cells. In a set of experiments the preformed oligomers, after resuspension in the cell culture media, were incubated at a corresponding monomer concentration of 12 µM in isolation or in combination with αB-crystallin or Hsp70 for 1 hour at 37 °C under shaking, then diluted to a final concentration of 3 µM or 0.7 µM and finally added to cell cultures. In these experiments, the molar ratio of HypF-N:αB-crystallin used was 5:1; whereas the molar ratios of HypF-N:Hsp70 were 5:1, 10:1 or 20:1, as stated. The molecular chaperones αB-crystallin and Hsp70 were obtained as described in section 2.4.2 (Chapter 2).

5.4.2 Cell cultures

Murine N13 microglia cells were cultured in Dulbecco's Modified Eagle's Medium (DMEM) F12 supplemented with 10% fetal bovine serum (FBS), 1.0% non-essential amino acids, glutamine and antibiotics. The cell culture was maintained in a 5.0% CO_2 humidified atmosphere at 37 °C and grown until 80% confluence for a maximum of 20 passages.

5.4.3 MTT reduction assay

The cytotoxic effect of type A and type B oligomers on N13 cell cultures was assessed performing the MTT assay by using the Cell Proliferation Kit I (MTT) (Roche, Mannheim, Germany). In a set of experiments, type A and type B oligomers and the molecular chaperones αB-crystallin or Hsp70 were incubated in isolation or combination and then added to cell culture media. Absorbance values of blue formazan were determined at 575 nm and cell viability was expressed as percent of MTT reduction in treated cells as compared to untreated cells (assumed as 100%).

5.4.4 Cytokine release measurements

Murine N13 mcroglia cell cultures were stimulated with type A and type B oligomers and, in a set of experiments, with type A and type B oligomers and the molecular chaperones αB-crystallin or Hsp70 incubated in isolation or combination. LPS at a concentration of 1 μg/ml, and culture medium alone were used as positive and negative controls, respectively. The stimulation lasted 6 hours and 24 hours for TNF-α and for IL-6, IL-1β and IL-10 release measurements, respectively. Culture supernatants were harvested and centrifuged at 400 rcf for 5 min and cell-cleared supernatants were

recovered and stored at –20 °C before cytokine measurement. IL-6, IL-1β, TNF-α and IL-10 levels were assayed through ELISA tests using Mouse IL-6/IL-1β/TNF-α/IL-10 BD OptEIA ELISA set (BD Biosciences, Madrid, Spain) according to the manufacturer's protocol.

5.4.5 Cell internalisation of HypF-N oligomers

N13 cells were seeded on glass coverslips and incubated for 24 hours by adding to the culture medium type A and type B oligomers at a corresponding monomer concentration of 0.7 μM. Cells were also treated with culture medium alone for control. The cells were washed with phosphate-buffered saline and fixed in 2% (w/v) buffered paraformaldehyde for 15 min at 4 °C. Half of the coverslips were treated for 1 hour at 4 °C with a PBS solution containing 3% BSA (w/v) and 0.5% (v/v) Triton X-100 in order to allow plasma membrane permeabilization; the remaining coverslips were not permeabilized and therefore treated with a PBS solution containing 3% BSA only for 1 hour at 4 °C. The coverslips were incubated over night with 1:1000 diluted rabbit polyclonal anti-HypF-N antibodies (Primm srl) and then for 1 hour at room temperature in the dark with 1:800 diluted Alexa Fluor 633-conjugated anti-rabbit secondary antibodies. The nuclei were stained with 1 μg/ml DAPI for 5 minutes at room temperature. Confocal scanning microscope images were acquired using a Leica TCS SP5 confocal scanning microscope (Mannheim, Germany).

5.5 Acknowledgements

This work was supported by the Federation of European Biochemical Societies (FEBS) through the short term fellowship granted to Benedetta Mannini for the project "Glial

immune response triggered by misfolded protein oligomers and the role of Hsp70 as immune mediator" in the laboratory of Prof. David Pozo Pérez in CABIMER - Andalusian Center for Molecular Biology and Regenerative Medicine (Spanish National Research Council - CSIC; University of Seville), Seville, Spain.

REFERENCES

Ahmad B, Winkelmann J, Tiribilli B, Chiti F (2010) Searching for conditions to form stable protein oligomers with amyloid-like characteristics: The unexplored basic pH. Biochim Biophys Acta 1804:223-34.

Ahmed M, Davis J, Aucoin D, Sato T, Ahuja S, Aimoto S, Elliott JI, Van Nostrand WE, Smith SO (2010) Structural conversion of neurotoxic amyloid-β_{1-42} oligomers to fibrils. Nat Struct Mol Biol 17:561-7.

Aloisi F (2001) Immune function of microglia. Glia 36:165-79.

Amaral MD (2004) CFTR and chaperones: processing and degradation. J Mol Neurosci 23:41-8

Amor S, Puentes F, Baker D, van der Valk P (2010) Inflammation in neurodegenerative diseases. Immunology 129:154-69.

Auluck PK, Chan HY, Trojanowski JQ, Lee VM, Bonini NM (2002) Chaperone suppression of α-synuclein toxicity in a Drosophila model for Parkinson's disease. Science 295:865-8.

Baglioni S, Casamenti F, Bucciantini M, Luheshi LM, Taddei N, Chiti F, Dobson CM, Stefani M (2006) Prefibrillar amyloid aggregates could be generic toxins in higher organisms. J Neurosci 26:8160-7.

Bajramovic JJ, Bsibsi M, Geutskens SB, Hassankhan RR, Verhulst K, Stege GJJ (2000) Differential expression of stress proteins in human adult astrocytes in response to cytokines. J Neuroimmunol 106:14-22.

Balbach JJ, Petkova AT, Oyler NA, Antzutkin ON, Gordon DJ, Meredith SC, Tycko R (2002) Supramolecular structure in full-length Alzheimer's β-amyloid fibrils: evidence for a parallel β-sheet organization from solid-state nuclear magnetic resonance. Biophys J 83:1205-16.

Balch WE, Morimoto RI, Dillin A, Kelly JW (2008) Adapting proteostasis for disease intervention. Science 319:916-19.

Banati RB, Daniel SE, Blunt SB (1998) Glial pathology but absence of apoptotic nigral neurons in long-standing Parkinson's disease. Mov Disord 13:221-7.

Banci L, Bertini I, D'Amelio N, Gaggelli E, Libralesso E, Matecko I, Turano P, Valentine JS (2005) Fully metallated S134N Cu, Zn-superoxide dismutase displays abnormal mobility and intermolecular contacts in solution. J Biol Chem 280:35815-21.

Barral JM, Broadley SA, Schaffar G, Hartl FU (2004) Roles of molecular chaperones in protein misfolding diseases. Semin Cell Dev Biol 15:17-29.

Bauer J, Strauss S, Schreiter-Gasser U, Ganter U, Schlegel P, Witt I, Yolk B, Berger M (1991) Interleukin-6 and alpha-2-macroglobulin indicate an acute-phase state in Alzheimer's disease cortices. FEBS Lett 285:111-4.

Bauer HH, Aebi U, Häner M, Hermann R, Müller M, Merkle HP (1995) Architecture and polymorphism of fibrillar supramolecular assemblies produced by in vitro aggregation of human calcitonin. J Struct Biol 115:1-15.

Behrends C, Langer CA, Boteva R, Böttcher UM, Stemp MJ, Schaffar G, Rao BV, Giese A, Kretzschmar H, Siegers K, Hartl FU (2006) Chaperonin TRiC promotes the assembly of polyQ expansion proteins into nontoxic oligomers. Mol Cell 23:887-97.

Bejarano E and Cuervo AM (2010) Chaperone-mediated autophagy. Proc Am Thorac Soc 7:29-39.

Bemporad F, Calloni G, Campioni S, Plakoutsi G, Taddei N, Chiti F (2006) Sequence and structural determinants of amyloid fibril formation. Acc Chem Res 39:620-7.

Bemporad F and Chiti F (2012) Protein misfolded oligomers: experimental approaches, mechanism of formation, and structure-toxicity relationships. Chem Biol 19:315-27.

Betcher-Lange SL and Lehrer SS (1978) Pyrene excimer fluorescence in rabbit skeletal alphaalphatropomyosin labeled with N-(1-pyrene)maleimide. A probe of sulfhydryl proximity and local chain separation. J Biol Chem 253:3757-60.

Bhat NR and Sharma KK (1999) Microglial activation by the small heat shock protein α-crystallin. NeuroReport 10:2869-73.

Billings LM, Oddo S, Green KN, McGaugh JL, LaFerla FM (2005) Intraneuronal Aβ causes the onset of early Alzheimer's disease-related cognitive deficits in transgenic mice. Neuron 45:675-88.

Birks JB (1967) Excimers and exciplexes. Nature 214:1187-1190.

Bitan G, Kirkitadze MD, Lomakin A, Vollers SS, Benedek GB, Teplow DB (2003) Amyloid β-protein (Aβ) assembly: Aβ40 and Aβ42 oligomerize through distinct pathways. Proc Natl Acad Sci U S A 100:330-5.

Boggs LN, Fuson KS, Baez M, Churgay L, McClure D, Becker G, May PC (1996) Clusterin (Apo J) protects against in vitro amyloid-β (1-40) neurotoxicity. J Neurochem 67:1324-7.

Bojarski L, Herms J, Kuznicki J (2008) Calcium dysregulation in Alzheimer's disease. Neurochem Int 52:621–33.

Bolognesi B, Kumita JR, Barros TP, Esbjorner EK, Luheshi LM, Crowther DC, Wilson MR, Dobson CM, Favrin G, Yerbury JJ (2010) ANS binding reveals common features of cytotoxic amyloid species. ACS Chem Biol 5:735-40.

Bouchard M, Zurdo J, Nettleton EJ, Dobson CM, Robinson CV (2000) Formation of insulin amyloid fibrils followed by FTIR simultaneously with CD and electron microscopy. Protein Sci 9:1960-7.

Bourgault S, Choi S, Buxbaum JN, Kelly JW, Price JL, Reixach N (2011) Mechanisms of transthyretin cardiomyocyte toxicity inhibition by resveratrol analogs. Biochem Biophys Res Commun 410:707-13.

Broadley SA and Hartl FU (2009) The role of molecular chaperones in human misfolding diseases. FEBS Lett 583:2647-53.

Broadley SA, Vanags D, Williams B, Johnson B, Feeney D, Griffiths L, Shakib S, Brown G, Coulthard A, Mullins P, Kneebone C (2009) Results of a phase IIa clinical trial of an anti-inflammatory molecule, chaperonin 10, in multiple sclerosis. Mult Scler 15:329-36.

Bucciantini M, Giannoni E, Chiti F, Baroni F, Formigli L, Zurdo J, Taddei N, Ramponi G, Dobson CM, Stefani M (2002) Inherent toxicity of aggregates implies a commonmechanism for protein misfolding diseases. Nature 416:507-11.

Bucciantini M, Calloni G, Chiti F, Formigli L, Nosi D, Dobson CM, Stefani M (2004) Prefibrillar amyloid protein aggregates share common features of cytotoxicity. J Biol Chem 279:31374-82.

Bucciantini M, Rigacci S, Berti A, Pieri L, Cecchi C, Nosi D, Formigli L, Chiti F, Stefani M (2005) Patterns of cell death triggered in two different cell lines by HypF-N prefibrillar aggregates. FASEB J 19:437-9.

Bukau B, Hesterkamp T, Luirink J (1996) Growing up in a dangerous environment: a network of multiple targeting and folding pathways for nascent polypeptides in the cytosol.
Trends Cell Biol 6:480-6.

Bukau B and Horwich AL (1998) The Hsp70 and Hsp60 chaperone machines. Cell 92:351-66.

Bukau B, Weissman J, Horwich A (2006) Molecular chaperones and protein quality control. Cell 125:443-51.

Buxbaum JN and Reixach N (2009) Transthyretin: the servant of many masters. Cell Mol Life Sci 66:3095-101.

Buxbaum JN, Ye Z, Reixach N, Friske L, Levy C, Das P, Golde T, Masliah E, Roberts AR, Bartfai T (2008) Transthyretin protects Alzheimer's mice from the behavioral and biochemical effects of Aβ toxicity. Proc Natl Acad Sci U S A 105:2681-6.

Calamai M, Canale C, Relini A, Stefani M, Chiti F, Dobson CM (2005) Reversal of protein aggregation provides evidence for multiple aggregated states. J Mol Biol 346:603-16.

Calderwood SK, Mambula SS, Gray PJ, Theriault JR (2007) Extracellular heat shock proteins in cell signalling. FEBS Lett 581:3689-94.

Calloni G, Lendel C, Campioni S, Giannini S, Gliozzi A, Relini A, Vendruscolo M, Dobson CM, Salvatella X, Chiti F (2008) Structure and dynamics of a partially folded protein are decoupled from its mechanism of aggregation. J Am Chem Soc 130:13040-50.

Calloni G, Zoffoli S, Stefani M, Dobson CM, Chiti F (2005) Investigating the effects of mutations on protein aggregation in the cell. J Biol Chem 280:10607-13.

Campioni S, Mossuto MF, Torrassa S, Calloni G, de Laureto PP, Relini A, Fontana A, Chiti F (2008) Conformational properties of the aggregation precursor state of HypF-N. J Mol Biol 379:554-67.

Campioni S, Mannini B, Zampagni M, Pensalfini A, Parrini C, Evangelisti E, Relini A, Stefani M, Dobson CM, Cecchi C, Chiti F (2010) A causative link between the structure of aberrant protein oligomers and their toxicity. Nat Chem Biol 6:140-7.

Campioni S, Mannini B, López-Alonso JP, Shalova IN, Penco A, Mulvihill E, Laurents DV, Relini A, Chiti F (2012) Salt anions promote the conversion of HypF-N into amyloid-like oligomers and modulate the structure of the oligomers and the monomeric precursor state. J Mol Biol 424:132-49.

Canale C, Torrassa S, Rispoli P, Relini A, Rolandi R, Bucciantini M, Stefani M, Gliozzi A (2006) Natively folded HypF-N and its early amyloid aggregates interact with phospholipid monolayers and destabilize supported phospholipid bilayers. Biophys J 91:4575–88.

Cardamone M, Puri NK (1992) Spectrofluorimetric assessment of the surface hydrophobicity of proteins. Biochem J 282:589-93.

Carson MJ, Doose JM, Melchior B, Schmid CD, Ploix CC. (2006) CNS immune privilege: hiding in plain sight. Immunol Rev 213:48-65.

Carulla N, Zhou M, Arimon M, Gairí M, Giralt E, Robinson CV, Dobson CM (2009) Experimental characterization of disordered and ordered aggregates populated during the process of amyloid fibril formation. Proc Natl Acad Sci U S A 106:7828-33.

Casalot L and Rousset M (2001) Maturation of the [NiFe] hydrogenases. Trends Microbiol 9:228-37.

Cecchi C, Baglioni S, Fiorillo C, Pensalfini A, Liguri G, Nosi D, Rigacci S, Bucciantini M, Stefani M (2005) Insights into the molecular basis of the differing susceptibility of varying cell types to the toxicity of amyloid aggregates. J Cell Sci 118:3459-70.

Cecchi C, Pensalfini A, Stefani M, Baglioni S, Fiorillo C, Cappadona S, Caporale R, Nosi D, Ruggiero M, Liguri G (2008) Replicating neuroblastoma cells in different cell cycle phases display different vulnerability to amyloid toxicity. J Mol Med 86:197-209.

Chakraborty S, Kaushik DK, Gupta M, Basu A (2010) Inflammasome signaling at the heart of central nervous system pathology. J Neurosci Res 88:1615-31.

Chen T and Cao X (2010). Stress for maintaining memory: HSP70 as a mobile messenger for innate and adaptive immunity. Eur J Immunol 40:1541-4.

Chiti F, Webster P, Taddei N, Clark A, Stefani M, Ramponi G, Dobson CM (1999) Designing conditions for in vitro formation of amyloid protofilaments and fibrils. Proc Natl Acad Sci U S A 96:3590-4.

Chiti F, Bucciantini M, Capanni C, Taddei N, Dobson CM, Stefani M (2001) Solution conditions can promote formation of either amyloid protofilaments or mature fibrils from the HypF N-terminal domain. Protein Sci 10:2541-7.

Chiti F and Dobson CM (2006) Protein misfolding, functional amyloid, and human disease. Annu Rev Biochem 75:333-66.

Choi SH, Leight SN, Lee VM, Li T, Wong PC, Johnson JA, Saraiva MJ, Sisodia SS (2007) Accelerated Aβ deposition in APPswe/PS1deltaE9 mice with hemizygous deletions of TTR (transthyretin). J Neurosci 27:7006-10.

Cizas P, Budvytyte R, Morkuniene R, Moldovan R, Broccio M, Lösche M, Niaura G, Valincius G, Borutaite V (2010) Size-dependent neurotoxicity of β-amyloid oligomers. Arch Biochem Biophys 496:84-92.

Claessen JH, Kundrat L, Ploegh HL (2012) Protein quality control in the ER: balancing the ubiquitin checkbook. Trends Cell Biol 22:22-32.

Cleary JP, Walsh DM, Hofmeister JJ, Shankar GM, Kuskowski MA, Selkoe DJ, Ashe KH (2005) Natural oligomers of the amyloid-β protein specifically disrupt cognitive function. Nat Neurosci 8:79-84.

Cohen E, Bieschke J, Perciavalle RM, Kelly JW, Dillin A (2006) Opposing activities protect against age-onset proteotoxicity. Science 313:1604-10.

Colbeau A, Elsen S, Tomiyama M, Zorin NA, Dimon B, Vignais PM (1998) Rhodobacter capsulatus HypF is involved in regulation of hydrogenase synthesis through the HupUV proteins. Eur J Biochem 251:65-71.

Colon W and Kelly JW (1992) Partial denaturation of transthyretin is sufficient for amyloid fibril formation in vitro. Biochemist 31:8654-60.

Connors LH, Lim A, Prokaeva T, Roskens VA, Costello CE (2003) Tabulation of human transthyretin (TTR) variants, 2003. Amyloid 10:160-84.

Costa R, Gonçalves A, Saraiva MJ, Cardoso I (2008) Transthyretin binding to A-beta peptide - Impact on A-beta fibrillogenesis and toxicity. FEBS Lett 582:936-42.

Courgeon AM, Maisonhaute C, Best-Belpomme M (1984) Heat shock proteins are induced by cadmium in Drosophila cells. Exp Cell Res 153:515-21.

Cowan KJ, Diamond MI, Welch WJ (2003) Polyglutamine protein aggregation and toxicity are linked to the cellular stress response. Hum Mol Genet 12:1377-91.

Danzer KM, Haasen D, Karow AR, Moussaud S, Habeck M, Giese A, Kretzschmar H, Hengerer B, Kostka M (2007) Different species of α-synuclein oligomers induce calcium influx and seeding. J Neurosci 27:9220-32.

Dedmon MM, Christodoulou J, Wilson MR, Dobson CM (2005) Heat shock protein 70 inhibits α-synuclein fibril formation via preferential binding to prefibrillar species. J Biol Chem 280:14733-40.

DeMartino GN and Slaughter CA (1999) The proteasome, a novel protease regulated by multiple mechanisms. J Biol Chem 274:22123-6.

Demuro A, Mina E, Kayed R, Milton SC, Parker I, Glabe CG (2005) Calcium dysregulation and membrane disruption as a ubiquitous neurotoxic mechanism of soluble amyloid oligomers. J Biol Chem. 280:17294-300.

Derham BK and Harding JJ (1997) Effect of aging on the chaperone-like function of human alpha-crystallin assessed by three methods. Biochem J 328:763-8.

Deshpande A, Mina E, Glabe C, Busciglio J (2006) Different conformations of amyloid β induce neurotoxicity by distinct mechanisms in human cortical neurons. J Neurosci 26:6011-8.

Dickson DW, Lee SC, Mattiace LA, Yen SH, Brosnan C (1993) Microglia and cytokines in neurological disease, with special reference to AIDS and Alzheimer's disease. Glia 7:75-83.

Dobson CM, Sali A, Karplus M (1998) Protein folding: a perspective from theory and experiment. Angew Chem Int Ed Engl 37:868-93.

Dobson CM (1999) Protein misfolding, evolution and disease. Trends Biochem Sci 24:329-32.

Dobson CM (2003) Protein folding and misfolding. Nature 426:884-890.

Dong Y and Benveniste EN (2001) Immune function of astrocytes. Glia 36:180-190.

Du J and Murphy RM (2010) Characterization of the interaction of β-amyloid with transthyretin monomers and tetramers. Biochemistry 28:8276-89.

Du Y, Bales KR, Dodel RC, Liu X, Glinn MA, Horn JW, Little SP, Paul SM (1998) α2-macroglobulin attenuates β-amyloid peptide 1-40 fibril formation and associated neurotoxicity of cultured fetal rat cortical neurons. J Neurochem 70:1182-8.

Duennwald ML and Lindquist S (2008) Impaired ERAD and ER stress are early and specific events in polyglutamine toxicity. Genes Dev 22:3308-19.

Dusa A, Kaylor J, Edridge S, Bodner N, Hong DP, Fink AL (2006) Characterization of oligomers during α-synuclein aggregation using intrinsic tryptophan fluorescence. Biochemistry 45:2752-60.

Eanes ED and Glenner GG (1968) X-ray diffraction studies on amyloid filaments. J Histochem Cytochem 16:673-7.

Ellis RJ, van der Vies SM, Hemmingsen SM (1989) The molecular chaperone concept. Biochem Soc Symp 55:145-53.

Erickson RR, Dunning LM, Holtzman JL (2006) The effect of aging on the chaperone concentrations in the hepatic, endoplasmic reticulum of male rats: the possible role of protein misfolding due to the loss of chaperones in the decline in physiological function seen with age. J Gerontol A Biol Sci Med Sci 61:435-43.

Evangelisti E, Cecchi C, Cascella R, Sgromo C, Becatti M, Dobson CM, Chiti F,Stefani M (2012) Membrane lipid composition and its physicochemical properties define cell vulnerability to aberrant protein oligomers. J Cell Sci 125:2416-27.

Fabrizi C, Businaro R, Lauro GM, Fumagalli L (2001) Role of α2-macroglobulin in regulating amyloid β-protein neurotoxicity: protective or detrimental factor? J Neurochem 78:406-12.

Fändrich M, Fletcher MA, Dobson CM (2001) Amyloid fibrils from muscle myoglobin. Nature 410:165-6.

Fersht AR (2000) Transition-state structure as a unifying basis in protein-folding mechanisms: contact order, chain topology, stability, and the extended nucleus mechanism. Proc Natl Acad Sci U S A 97:1525-9.

Förster T (1969) Excimers. Angew Chem Int Ed Engl 8:333-43.

French K, Yerbury JJ, Wilson MR (2008) Protease activation of α2-macroglobulin modulates a chaperone-like action with broad specificity. Biochemistry 47:1176-85.

Garzuly F, Vidal R, Wisniewski T, Brittig F, Budka H (1996) Familial meningocerebrovascular amyloidosis, Hungarian type, with mutant transthyretin (TTR Asp18Gly). Neurology 47:1562-7.

Gast K, Modler AJ, Damaschun H, Kröber R, Lutsch G, Zirwer D, Golbik R, Damaschun G (2003) Effect of environmental conditions on aggregation and fibril formation of barstar. Eur Biophys J 32:710-23.

Gharibyan AL, Zamotin V, Yanamandra K, Moskaleva OS, Margulis BA, Kostanyan IA, Morozova-Roche LA (2007) Lysozyme amyloid oligomers and fibrils induce cellular death via different apoptotic/necrotic pathways. J Mol Biol 365:1337-49.

Gidalevitz T, Ben-Zvi A, Ho KH, Brignull HR, Morimoto RI (2006) Progressive disruption of cellular protein folding in models of polyglutamine diseases. Science 311:1471-4.

Glass CK, Saijo K, Winner B, Marchetto MC, Gage FH (2010) Mechanisms underlying inflammation in neurodegeneration. Cell 140:918-34.

Glezer I, Simard AR, Rivest S (2007) Neuroprotective role of the innate immune system by microglia. Neuroscience 147:867–83.

Goldsbury C, Frey P, Olivieri V, Aebi U, Müller SA (2005) Multiple assembly pathways underlie amyloid-β fibril polymorphisms. J Mol Biol 352:282-98.

Gosal WS, Morten IJ, Hewitt EW, Smith DA, Thomson NH, Radford SE (2005) Competing pathways determine fibril morphology in the self-assembly of β_2-microglobulin into amyloid. J Mol Biol 351:850-64.

Griffin WS, Stanley LC, Ling C, White L, MacLeod V, Perrot LJ, White CL 3rd, Araoz C (1989) Brain interleukin 1 and S-100 immunoreactivity are elevated in Down syndrome and Alzheimer disease. Proc Natl Acad Sci U S A 86:7611–7615.

Guerois R, Nielsen JE, Serrano L (2002) Predicting changes in the stability of proteins and protein complexes: a study of more than 1000 mutations. J Mol Biol 320:369-87.

Guijarro JI, Sunde M, Jones JA, Campbell ID, Dobson CM (1998) Amyloid fibril formation by an SH3 domain. Proc Natl Acad Sci U S A 95:4224-8.

Haass C and Selkoe DJ (2007) Soluble protein oligomers in neurodegeneration: lessons from the Alzheimer's amyloid β-peptide. Nat Rev Mol Cell Biol 8:101-12.

Habich C, Kempe K, Gomez FJ, Lillicrap M, Gaston H, van der Zee R (2006) Heat shock protein 60: identification of specific epitopes for binding to primary macrophages. FEBS Lett 580:115-20.

Hammad SM, Ranganathan S, Loukinova E, Twal WO, Argraves WS (1997) Interaction of apolipoprotein J-amyloid β-peptide complex with low density lipoprotein receptor-related protein-2/megalin. A mechanism to prevent pathological accumulation of amyloid β-peptide. J Biol Chem 272:18644-9.

Hammarström P, Kalman B, Jonsson BH, Carlsson U (1997) Pyrene excimer fluorescence as a proximity probe for investigation of residual structure in the unfolded state of human carbonic anhydrase II. FEBS Lett 420:63-8.

Hammarström P, Persson M, Freskgård PO, Mårtensson LG, Andersson D, Jonsson BH, Carlsson U (1999) Structural mapping of an aggregation nucleation site in a molten globule intermediate. J Biol Chem 274:32897-903.

Hartl FU and Hayer-Hartl M (2002) Molecular chaperones in the cytosol: from nascent chain to folded protein. Science 295:1852-8.

Hartl FU, Bracher A, Hayer-Hartl M (2011) Molecular chaperones in protein folding and proteostasis. Nature 475:324-32.

Hay DG, Sathasivam K, Tobaben S, Stahl B, Marber M, Mestril R, Mahal A, Smith DL, Woodman B, Bates GP (2004) Progressive decrease in chaperone protein levels in a mouse model of Huntington's disease and induction of stress proteins as a therapeutic approach. Hum Mol Genet 13:1389-405.

Hayes GM, Woodroofe MN, Cuzner ML (1987) Microglia are the major cell type expressing MHC class II in human white matter. J Neurol Sci 80:25-37.

Heikkila JJ, Schultz GA, Iatrou K, Gedamu L (1982) Expression of a set of fish genes following heat or metal ion exposure. J Biol Chem 257:12000-5.

Henderson B and Pockley AG (2010) Molecular chaperones and protein-folding catalysts as intercellular signaling regulators in immunity and inflammation. J Leukoc Biol 88:445-462.

Hooper DC and Peacock AC (1976) Determination of the Subunit Composition of Haptoglobin 2-l Polymers Using Quantitative Densitometry of Polyacrylamide Gels. J Biol Chem. 251:5845-5851 .

Hoseki J, Ushioda R, Nagata K (2010) Mechanism and components of endoplasmic reticulum-associated degradation. J Biochem 147:19-25.

Humphreys DT, Carver JA, Easterbrook-Smith SB, Wilson MR (1999) J Biol Chem 274:6875-81.

Huurman VA, van der Meide PE, Duinkerken G, Willemen S, Cohen IR, Elias D, Roep BO (2008) Immunological efficacy of heat shock protein 60 peptide DiaPep277 therapy in clinical type I diabetes. Clin Exp Immunol 152:488-97.

Iijima K, Chiang HC, Hearn SA, Hakker I, Gatt A, Shenton C, Granger L, Leung A, Iijima-Ando K, Zhong Y (2008) Aβ42 mutants with different aggregation profiles induce distinct pathologies in Drosophila. PLoS One 3:e1703.

Irani DN (1998) Brain-derived gangliosides induce cell cycle arrest in a murine T cell line. J Neuroimmunol 87:11-16.

Jacobson DR, Pan T, Kyle RA, Buxbaum JN (1997a) Transthyretin ILE20, a new variant associated with late-onset cardiac amyloidosis. Hum Mutat 9:83-5.

Jacobson DR, Pastore RD, Yaghoubian R, Kane I, Gallo G, Buck FS, Buxbaum JN (1997b) Variant-Sequence Transthyretin (Isoleucine 122) in Late-Onset Cardiac Amyloidosis in Black Americans. N Engl J Med 336:466-73.

Jahn TR and Radford SE (2008) Folding versus aggregation: polypeptide conformations on competing pathways. Arch Biochem Biophys 469:100-17.

Jain S and Udgaonkar JB (2011) Defining the pathway of worm-like amyloid fibril formation by the mouse prion protein by delineation of the productive and unproductive oligomerization reactions. Biochemistry 50:1153-61.

Jan A, Adolfsson O, Allaman I, Buccarello AL, Magistretti PJ, Pfeifer A, Muhs A, Lashuel HA (2011) Aβ42 neurotoxicity is mediated by ongoing nucleated polymerization process rather than by discrete Aβ42 species. J Biol Chem 286:8585-96.

Jaroniec CP, MacPhee CE, Bajaj VS, McMahon MT, Dobson CM, Griffin RG (2004) High-resolution molecular structure of a peptide in an amyloid fibril determined by magic angle spinning NMR spectroscopy. Proc Natl Acad Sci U S A 101:711-6.

Jiang X, Smith CS, Petrassi HM, Hammarström P, White JT, Sacchettini JC, Kelly JW (2001) An engineered transthyretin monomer that is nonamyloidogenic, unless it is partially denatured. Biochemistry 40:11442-52.

Jones EM and Surewicz WK (2005) Fibril conformation as the basis of species- and strain-dependent seeding specificity of mammalian prion amyloids. Cell 121:63-72.

Kajava AV, Aebi U, Steven AC (2005) The parallel superpleated beta-structure as a model for amyloid fibrils of human amylin. J Mol Biol 348:247-52.

Kakimura JI, Kitamura Y, Taniguchi T, Shimohama S, Gebicke-Haerter PJ (2001) Bip/GRP78-induced production of cytokines and uptake of amyloid-β(1–42) peptide in microglia. Biochem Biophys Res Commun 281:6–10.

Kakimura JI, Kitamura Y, Takata K, Umeki M, Suzuki S, Shibagaki K (2002) Microglia activation and amyloid-β clearance induced by exogenous heat shock proteins. FASEB J 16:601-3.

Kapoor A and Sanyal AJ (2009) Endoplasmic reticulum stress and the unfolded protein response. Clin Liver Dis 13:581-90.

Kaylor J, Bodner N, Edridge S, Yamin G, Hong DP, Fink AL (2005) Characterization of oligomeric intermediates in α-synuclein fibrillation: FRET studies of 125W/Y133F/Y136F α-synuclein. J Mol Biol 353:357-72.

Keshet B, Yang IH, Good TA (2010) Can size alone explain some of the differences in toxicity between β-amyloid oligomers and fibrils? Biotechnol Bioeng 106:333-7.

Kida E, Choi-Miura NH, Wisniewski KE (1995) Deposition of apolipoproteins E and J in senile plaques is topographically determined in both Alzheimer's disease and Down's syndrome brain. Brain Res 685:211-6.

Kim YS and Joh TH (2006) Microglia, major player in the brain inflammation: their roles in the pathogenesis of Parkinson's disease. Exp Mol Med 38, 333-47.

Kitada T, Asakawa S, Hattori N, Matsumine H, Yamamura Y, Minoshima S, Yokochi M, Mizuno Y, Shimizu N (1998) Mutations in the parkin gene cause autosomal recessive juvenile parkinsonism. Nature 392:605-8.

Kitamura A, Kubota H, Pack CG, Matsumoto G, Hirayama S, Takahashi Y, Kimura H, Kinjo M, Morimoto RI, Nagata K (2006) Cytosolic chaperonin prevents polyglutamine toxicity with altering the aggregation state. Nat Cell Biol 8:1163-70.

Klunk WE, Pettegrew JW, Abraham DJ (1989) Quantitative evaluation of congo red binding to amyloid-like proteins with a beta-pleated sheet conformation. J Histochem Cytochem 37:1273-81.

Kodali R and Wetzel R. (2007) Polymorphism in the intermediates and products of amyloid assembly. Curr Opin Struct Biol 17:48-57.

Koffie RM, Meyer-Luehmann M, Hashimoto T, Adams KW, Mielke ML, Garcia-Alloza M, Micheva KD, Smith SJ, Kim ML, Lee VM, Hyman BT, Spires-Jones TL (2009) Oligomeric amyloid β associates with postsynaptic densities and correlates with excitatory synapse loss near senile plaques. Proc Natl Acad Sci U S A 106:4012-7.

Kopito RR (2000) Aggresomes, inclusion bodies and protein aggregation. Trends Cell Biol 10:524-530.

Krebs MR, Bromley EH, Donald AM (2005) The binding of thioflavin-T to amyloid fibrils: localisation and implications. J Struct Biol 149:30-7.

Kremer JJ, Pallitto MM, Sklansky DJ, Murphy RM (2000) Correlation of β-amyloid aggregate size and hydrophobicity with decreased bilayer fluidity of model membranes. Biochemistry 39:10309-18.

Krishnan R, Lindquist SL (2005) Structural insights into a yeast prion illuminate nucleation and strain diversity. Nature 435:765-72.

Krishnan R, Goodman JL, Mukhopadhyay S, Pacheco CD, Lemke EA, Deniz AA, Lindquist S (2012) Conserved features of intermediates in amyloid assembly determine their benign or toxic states. Proc Natl Acad Sci U S A 109:11172-7.

Kristiansen M, Graversen JH, Jacobsen C, Sonne O, Hoffman HJ, Law SK, Moestrup SK (2001) Identification of the haemoglobin scavenger receptor. Nature 409:198-201.

Kubota H (2009) Quality control against misfolded proteins in the cytosol: a network for cell survival. J Biochem 146:609-16.

Labrador-Garrido A, Bertoncini CW, Roodveldt C (2011) The Hsp70 chaperone system in Parkinson´s disease. In Etiology and Pathophysiology of PD, pp. 221-246. InTech, Vienna, Austria.

Lachmann HJ and Hawkins PN (2006) Systemic amyloidosis. Curr Opin Pharmacol 6:214-220.

Ladiwala AR, Dordick JS, Tessier PM (2011) Aromatic small molecules remodel toxic soluble oligomers of amyloid β through three independent pathways. J Biol Chem 286:3209-18.

Ladiwala AR, Litt J, Kane RS, Aucoin DS, Smith SO, Ranjan S, Davis J, Vannostrand WE, Tessier PM (2012) Conformational differences between two amyloid β oligomers of similar size and dissimilar toxicity. J Biol Chem 287:24765-73

Ladiwala AR, Bhattacharya M, Perchiacca JM, Cao P, Raleigh DP, Abedini A, Schmidt AM, Varkey J, Langen R, Tessier PM (2012) Rational design of potent domain antibody inhibitors of amyloid fibril assembly. Proc Natl Acad Sci U S A 109:19965-70.

Laemmli UK (1970) Cleavage of structural proteins during the assembly of the head of bacteriophage T4. Nature 227:680-85.

Lai Y, Stange C, Wisniewski SR, Adelson PD, Janesko-Feldman KL, Brown DS (2006) Mitochondrial heat shock protein 60 is increased in cerebrospinal fluid following pediatric traumatic brain injury. Dev Neurosci 28:336-41.

Lakowicz JR (1999) Effects of sample geometry. in Principles of fluorescence spectroscopy 2nd edn.(ed. Lakowicz, J.R.) p. 54 (Kluwer Academic / Plenum Publishers, New York).

Lambert MP, Viola KL, Chromy BA, Chang L, Morgan TE, Yu J, Venton DL, Krafft GA, Finch CE, Klein WL (2001) Vaccination with soluble Aβ oligomers generates toxicity-neutralizing antibodies. J Neurochem 79:595-605.

Lancaster GI, Moller K, Nielsen MB, Secher NH, Febbraio MA, Nybo L (2004) Exercise induces the release of heat shock protein 72 from the human brain in vivo. Cell Stress Chaperones 9:276-80.

Larson J, Lynch G, Games D, Seubert P (1999) Alterations in synaptic transmission and long-term potentiation in hippocampal slices from young and aged PDAPP mice. Brain Res 840:23-35.

Lee J, Culyba EK, Powers ET, Kelly JW (2011). Amyloid-β forms fibrils by nucleated conformational conversion of oligomers. Nat Chem Biol 7:602-9.

Lesné S, Koh MT, Kotilinek L, Kayed R, Glabe CG, Yang A, Gallagher M, Ashe KH (2006) A specific amyloid-β protein assembly in the brain impairs memory. Nature 440:352-7.

LeVine H (1995) Thioflavine T interaction with amyloid β-sheet structures. Amyloid 2:1-6.

Levinthal C (1968) Are there pathways for protein folding? J Chim Phys 65:44-5.

Li X, Masliah E, Reixach N, Buxbaum JN (2011) Neuronal production of transthyretin in human and murine Alzheimer's disease: is it protective? J Neurosci 31:12483-90.

Lie JT, Hammond PI (1988) Pathology of the senescent heart: anatomic observations on 237 autopsy studies of patients 90 to 105 years old. Mayo Clinic Proc 63:552-64.

Link CD (1995) Expression of human beta-amyloid peptide in transgenic Caenorhabditis elegans. Proc Natl Acad Sci U S A 92:9368-72.

Litvinovich SV, Brew SA, Aota S, Akiyama SK, Haudenschild C, Ingham KC (1998) Formation of amyloid-like fibrils by self-association of a partially unfolded fibronectin type III module. J Mol Biol 280:245-58.

Liu L and Murphy RM (2006) Kinetics of inhibition of β-amyloid aggregation by transthyretin. Biochemistry 45:15702-9.

Liu S, Tobias R, McClure S, Styba G, Shi Q, Jackowski G (1997). Removal of endotoxin from recombinant protein preparations. Clin Biochem 30:455-63.

Lomas DA and Carrell RW (2002) Serpinopathies and the conformational dementias. Nat Rev Genet 3:759-68.

Lu T, Pan Y, Kao SY, Li C, Kohane I, Chan J, Yankner BA (2004) Gene regulation and DNA damage in the ageing human brain. Nature 429:883-91.

Luca S, Yau WM, Leapman R, Tycko R (2007) Peptide conformation and supramolecular organization in amylin fibrils: constraints from solid-state NMR. Biochemistry 46:13505-22.

Lue LF, Kuo YM, Roher AE, Brachova L, Shen Y, Sue L, Beach T, Kurth JH, Rydel RE, Rogers J (1999) Soluble amyloid β peptide concentration as a predictor of synaptic change in Alzheimer's disease. Am J Pathol 155:853-62.

Magrane J, Rosen KM, Smith RC, Walsh K, Gouras GK, Querfurth HW (2005) Intraneuronal β-amyloid expression downregulates the Akt survival pathway and blunts the stress response. J Neurosci 25:10960-9.

Mangialasche F, Solomon A, Winblad B, Mecocci P, Kivipelto M (2010) Alzheimer's disease: clinical trials and drug development. Lancet Neurol 9:702-16.

Mannini B, Cascella R, Zampagni M, van Waarde- Verhagen M, Meehan S, Roodveldt C, Campioni S, Boninsegna M, Penco A, Relini A, Kampinga H, Dobson CM, Wilson M, Cecchi C, Chiti F (2012) Molecular mechanisms used by chaperones to reduce the toxicity of aberrant protein oligomers. Proc Natl Acad Sci U S A 109:12479-84

Marcon G, Plakoutsi G, Canale C, Relini A, Taddei N, Dobson CM, Ramponi G, Chiti F (2005) Amyloid formation from HypF-N under conditions in which the protein is initially in its native state. J Mol Biol 347:323-35.

Martinez-Vicente M, Sovak G, Cuervo AM (2005) Protein degradation and aging. Exp Gerontol 40:622-33.

Martinon F and Tschopp J (2004) Inflammatory caspases: linking an intracellular innate immune system to autoinflammatory diseases. Cell 117:561-74.

Martins IC, Kuperstein I, Wilkinson H, Maes E, Vanbrabant M, Jonckheere W, Van Gelder P, Hartmann D, D'Hooge R, De Strooper B, Schymkowitz J, Rousseau F (2008) Lipids revert inert Aβ amyloid fibrils to neurotoxic protofibrils that affect learning in mice. EMBO J 27:224-33.

Masliah E, Rockenstein E, Veinbergs I, Mallory M, Hashimoto M, Takeda A, Sagara Y, Sisk A, Mucke L (2000) Dopaminergic loss and inclusion body formation in α-synuclein mice: implications for neurodegenerative disorders. Science 287:1265-9.

Massey AC, Kiffin R, Cuervo AM (2006) Autophagic defects in aging: looking for an "emergency exit"? Cell Cycle 5:1292-6.

Masters SL and O'Neill LA (2011) Disease-associated amyloid and misfolded protein aggregates activate the inflammasome. Trends Mol Med 17:276-82.

Mastrangelo IA, Ahmed M, Sato T, Liu W, Wang C, Hough P, Smith SO (2006) High-resolution atomic force microscopy of soluble Aβ42 oligomers. J Mol Biol 358:106-19.

McGeer PL, Itagaki S, Boyes BE, McGeer EG (1988) Reactive microglia are positive for HLA-DR in the substantia nigra of Parkinson's and Alzheimer's disease brains. Neurology 38:1285-91.

McGeer PL, Rogers J, McGeer EG (2006) Inflammation, anti-inflammatory agents and Alzheimer disease: the last 12 years. J Alzheimers Dis 9:271-76.

McLean CA, Cherny RA, Fraser FW, Fuller SJ, Smith MJ, Beyreuther K, Bush AI, Masters CL (1999) Soluble pool of Aβ amyloid as a determinant of severity of neurodegeneration in Alzheimer's disease. Ann Neurol 46:860-6.

Michel GP and Starka J (1986) Effect of ethanol and heat stresses on the protein pattern of Zymomonas mobilis. J Bacteriol 165:1040-2.

Missmahl HP and Hartwig M (1953) Optical polarization studies of amyloid substance. Virchows Arch 1953; 324:489-508.

Mizushima N, Levine B, Cuervo A, Klionsky D (2008) Autophagy fights disease through cellular self-digestion. Nature 451:1069-75.

Moechars D, Dewachter I, Lorent K, Reversé D, Baekelandt V, Naidu A, Tesseur I, Spittaels K, Haute CV, Checler F, Godaux E, Cordell B, Van Leuven F (1999) Early phenotypic changes in transgenic mice that overexpress different mutants of amyloid precursor protein in brain. J Biol Chem 274:6483-92.

Monsellier E and Chiti F (2007) Prevention of amyloid-like aggregation as a driving force of protein evolution. EMBO Rep 8:737-42.

Morimoto RI (2008) Proteotoxic stress and inducible chaperone networks in neurodegenerative disease and aging. Genes Dev 22:1427-38.

Morimoto RI and Cuervo AM (2009) Protein homeostasis and aging: taking care of proteins from the cradle to the grave. J Gerontol A Biol Sci Med Sci. 64:167-70.

Morley JF, Brignull HR, Weyers JJ, Morimoto RI (2002) The threshold for polyglutamine-expansion protein aggregation and cellular toxicity is dynamic and influenced by aging in Caenorhabditis elegans. Proc Natl Acad Sci USA 99:10417-22.

Morris AM, Watzky MA, Finke RG (2009) Protein aggregation kinetics, mechanism, and curve-fitting: a review of the literature. Biochim Biophys Acta 1794:375-97.

Mosmann T (1983) Rapid colorimetric assay for cellular growth and survival: application to proliferation and cytotoxicity assays. J Immunol Methods 65:55-63.

Muchowski PJ, Schaffar G, SittlerA, Wanker EE, Hayer-Hartl MK, Hartl FU (2000) Hsp70 and Hsp40 chaperones can inhibit self-assembly of polyglutamine proteins into amyloid-like fibrils. Proc Natl Acad Sci USA 97:7841-6.

Muchowski PJ and Wacker JL (2005) Modulation of neurodegeneration by molecular chaperones. Nat Rev Neurosci 6:11-22.

Naiki H, Hashimoto N, Suzuki S, Kimura S, Nakakuki K, Gejyo F (1997) Establishment of a kinetic model of dialysis-related amyloid fibril extension in vitro. Amyloid 4:223-232.

Nash B, Thomson CE, Linington C, Arthur AT, McClure JD, McBride MW, Barnett SC (2011) Functional duality of astrocytes in myelination. J Neurosci 31:13028-38.

Nelson R, Sawaya MR, Balbirnie M, Madsen AØ, Riekel C, Grothe R, Eisenberg D (2005) Structure of the cross-β spine of amyloid-like fibrils. Nature 435:773-8.

Nelson R and Eisenberg D (2006) Structural models of amyloid-like fibrils. Adv Protein Chem 73:235-82.

Nilsberth C, Westlind-Danielsson A, Eckman CB, Condron MM, Axelman K, Forsell C, Stenh C, Luthman J, Teplow DB, Younkin SG, Näslund J, Lannfelt L (2001) The 'Arctic' APP mutation (E693G) causes Alzheimer's disease by enhanced Aβ protofibrilformation. Nat Neurosci 4:887-93.

Nilsson MR (2004) Techniques to study amyloid fibril formation in vitro. Methods 34:151-60.

Novitskaya V, Bocharova OV, Bronstein I, Baskakov IV (2006) Amyloid fibrils of mammalian prion protein are highly toxic to cultured cells and primary neurons. J Biol Chem 281:13828-36.

Oda T, Wals P, Osterburg HH, Johnson SA, Pasinetti GM, Morgan TE, Rozovsky I, Stine WB, Snyder SW, Holzman TF (1995) Clusterin (apoJ) alters the aggregation of amyloid beta-peptide (A beta 1-42) and forms slowly sedimenting A beta complexes that cause oxidative stress. Exp Neurol 136:22-31.

Ojha J, Masilamoni G, Dunlap D, Udoff RA, Cashikar AG (2011) Sequestration of toxic oligomers by HspB1 as a cytoprotective mechanism. Mol Cell Biol 31:3146-57.

Olofsson A, Ippel JH, Wijmenga SS, Lundgren E, Ohman A (2004) Probing solvent accessibility of transthyretin amyloid by solution NMR spectroscopy. J Biol Chem 279:5699-707.

Olzscha H, Schermann SM, Woerner AC, Pinkert S, Hecht MH, Tartaglia GG, Vendruscolo M, Hayer-Hartl M, Hartl FU, Vabulas RM (2011) Amyloid-like aggregates sequester numerous metastable proteins with essential cellular functions. Cell 144:67-78.

Oma Y, Kino Y, Sasagawa N, Ishiura S (2005) Comparative analysis of the cytotoxicity of homopolymeric amino acids. Biochim Biophys Acta 1748:174-9.

O'Neill LA (2004) TLRs: Professor Mechnikov, sit on your hat. Trends Immunol 25:687-93.

Orrenius S, Zhovotovsky B, Nicotera P (2003) Regulation of cell death: the calciumapoptosis link. Nat Rev 4:552-65.

Orte A, Birkett NR, Clarke RW, Devlin GL, Dobson CM, Klenerman D (2008) Direct characterization of amyloidogenic oligomers by single-molecule fluorescence. Proc Natl Acad Sci U S A 105:14424-9.

Ousman SS, Tomooka B, van Noort JM, Wawrousek EF, O'Connor K, Hafler DA (2007) Protective and therapeutic role for αB-crystallin in autoimmune demyelination. Nature 448:474-9.

Pagano K, Bemporad F, Fogolari F, Esposito G, Viglino P, Chiti F, Corazza A (2010) Structural and dynamics characteristics of acylphosphatase from Sulfolobus solfataricus in the monomeric state and in the initial native-like aggregates. J Biol Chem 285:14689-700.

Panayi GS and Corrigall VM (2008) BiP, an anti-inflammatory ER protein, is a potential new therapy for the treatment of rheumatoid arthritis. Novartis Found Symp 291:212-6.

Parker JA, Arango M, Abderrahmane S, Lambert E, Tourette C, Catoire H, Neri C (2005) Resveratrol rescues mutant polyglutamine cytotoxicity in nematode and mammalian neurons. Nat Genet 37:349-50.

Pavliček Z and Ettrich R (1999) Chaperone-like activity of human haptoglobin: similarity with α-crystallin. Collect Czechoslov Chem Commun 64:717-25.

Pedersen JS, Christensen G, Otzen DE (2004) Modulation of S6 fibrillation by unfolding rates and gatekeeper residues. J Mol Biol 341:575-88.

Pedersen JS, Dikov D, Flink JL, Hjuler HA, Christiansen G, Otzen DE (2006) The changing face of glucagon fibrillation: structural polymorphism and conformational imprinting. J Mol Biol 355:501-23.

Pellistri F, Bucciantini M, Relini A, Nosi D, Gliozzi A, Robello M, Stefani M (2008) Nonspecific interaction of prefibrillar amyloid aggregates with glutamatergic receptors results in Ca2+ increase in primary neuronal cells. J Biol Chem 283:29950-60.

Perry VH and Gordon S (1988) Macrophages and microglia in the nervous system. Trends Neurosci 11:273-77.

Petersen RC (2010) Alzheimer's disease: progress in prediction. Lancet Neurol 9:4-5.

Pickart CM (2000) Ubiquitin in chains. Trends Biochem Sci 25:544-8.

Pickart CM and Cohen RE (2004) Proteasomes and their kin: proteases in the machine age. Nat Rev Mol Cell Biol 5:177-87.

Plakoutsi G, Bemporad F, Calamai M, Taddei N, Dobson CM, Chiti F (2005) Evidence for a mechanism of amyloid formation involving molecular reorganisation within native-like precursor aggregates. J Mol Biol 351:910-22.

Poon S, Rybchyn MS, Easterbrook-Smith SB, Carver JA, Pankhurst GJ, Wilson MR (2002) Mildly acidic pH activates the extracellular molecular chaperone clusterin. J Biol Chem 277:39532-40.

Powers ET, Morimoto RI, Dillin A, Kelly JW, Balch WE (2009) Biological and chemical approaches to diseases of proteostasis deficiency. Annu Rev Biochem 78:959-91.

Powers JM, Schlaepfer WW, Willingham MC, Hall BJ (1981) An immunoperoxidase study of senile cerebral amyloidosis with pathogenetic considerations. J Neuropathol Exp Neurol 40:592-612.

Pozo D, Anderson P, Gonzalez-Rey E (2009) Induction of alloantigen-specific human T regulatory cells by vasoactive intestinal peptide. J Immunol 183:4346-59.

Prusiner SB (1982) Novel proteinaceous infectious particles cause scrapie. Science 216:136-44.

Qi W, Zhang A, Patel D, Lee S, Harrington JL, Zhao L, Schaefer D, Good TA, Fernandez EJ (2008) Simultaneous monitoring of peptide aggregate distributions, structure, and kinetics using amide hydrogen exchange: application to Aβ(1-40) fibrillogenesis. Biotechnol Bioeng 100:1214-27.

Ramshini H, Parrini C, Relini A, Zampagni M, Mannini B, Pesce A, Saboury AA, Nemat-Gorgani M, Chiti F (2011) Large proteins have a great tendency to aggregate but a low propensity to form amyloid fibrils. PLoS One 6:e16075.

Ransohoff RM and Brown MA (2012) Innate immunity in the central nervous system. J Clin Invest 122:1164-71.

Raine CS (1994) Multiple sclerosis: immune system molecule expression in the central nervous system. J Neuropathol Exp Neurol 53:328-37.

Reixach N, Foss TR, Santelli E, Pascual J, Kelly JW, Buxbaum JN (2008) Human-murine transthyretin heterotetramers are kinetically stable and non-amyloidogenic. A lesson in the generation of transgenic models of diseases involving oligomeric proteins. J Biol Chem 25: 2098-107.

Relini A, Torrassa S, Rolandi R, Gliozzi A, Rosano C, Canale C, Bolognesi M, Plakoutsi G, Bucciantini M, Chiti F, Stefani M (2004) Monitoring the process of HypF fibrillization and liposome permeabilization by protofibrils. J Mol Biol 338:943-57.

Relini A, Torrassa S, Ferrando R, Rolandi R, Campioni S, Chiti F, Gliozzi A (2010) Detection of populations of amyloid-like protofibrils with different physical properties. Biophys J 98:1277-84.

Renkawek KL, Voorter CE, Bosman GJ, van Workum FP, de Jong WW (1994) Expression of αB-crystallin in Alzheimer's disease. Acta Neuropathol (Berl) 87:155–60.

Richter-Landsberg C and Goldbaum O (2003) Stress proteins in neural cells: functional roles in health and disease. Cell Mol Life Sci 60:337–49.

Ritossa P (1962) Problems of prophylactic vaccinations of infants. Riv Ist Sieroter Ital 37:79-108.

Ritter C, Maddelein ML, Siemer AB, Lührs T, Ernst M, Meier BH, Saupe SJ, Riek R (2005) Correlation of structural elements and infectivity of the HET-s prion. Nature 435:844-8.

Rogers J, Strohmeyer R, Kovelowski CJ, Li R (2002) Microglia and inflammatory mechanisms in the clearance of amyloid β peptide. Glia 40:260-9.

Roodveldt C, Christodoulou J, Dobson CM (2008) Immunological features of α-synuclein in Parkinson's disease. J Cell Mol Med 12:1820-9.

Roodveldt C, Bertoncini CW, Andersson A, van der Goot AT, Hsu ST, Fernández-Montesinos R, de Jong J, van Ham TJ, Nollen EA, Pozo D, Christodoulou J, Dobson CM (2009) Chaperone proteostasis in Parkinson's disease: stabilization of the Hsp70/alpha-synuclein complex by Hip. EMBO J 28:3758-70.

Roodveldt C, Labrador-Garrido A, Gonzalez-Rey E, Fernandez-Montesinos R, Caro M, Lachaud CC, Waudby CA, Delgado M, Dobson CM, Pozo D (2010) Glial innate immunity generated by non-aggregated alpha-synuclein in mouse: differencesbetween wild-type and Parkinson's disease-linked mutants. PLoS One 5:e13481.

Roodveldt C, Labrador-Garrido A, Izquierdo G, Pozo D (2011) α-Synuclein and the immune system in Parkinson's Disease. In Towards New Therapies for Parkinson's Disease, pp.57-76. InTech, Vienna, Austria.

Rosano C, Zuccotti S, Bucciantini M, Stefani M, Ramponi G, Bolognesi M (2002) Crystal structure and anion binding in the prokaryotic hydrogenase maturation factor HypF acylphosphatase-like domain. J Mol Biol 321:785-96.

Roseman MA (1988) Hydrophilicity of polar amino acid side-chains is markedly reduced by flanking peptide bonds. J Mol Biol 200:513-22

Sabate R, de Groot NS, Ventura S (2010) Protein folding and aggregation in bacteria. Cell Mol Life Sci 67:2695-2715.

Saiki M, Honda S, Kawasaki K, Zhou D, Kaito A, Konakahara T, Morii H (2005) Higher-order molecular packing in amyloid-like fibrils constructed with linear arrangements of hydrophobic and hydrogen-bonding side-chains. J Mol Biol 348:983-98.

Saridaki T, Zampagni M, Mannini B, Evangelisti E, Taddei N, Cecchi C, Chiti F (2012) Glycosaminoglycans (GAGs) suppress the toxicity of HypF-N prefibrillar aggregates. J Mol Biol 421:616-30.

Satyal SH, Schmidt E, Kitagawa K, Sondheimer N, Lindquist S, Kramer JM, Morimoto RI (2000) Polyglutamine aggregates alter protein folding homeostasis in Caenorhabditis elegans. Proc Natl Acad Sci USA 97:5750-5.

Sawaya MR, Sambashivan S, Nelson R, Ivanova MI, Sievers SA, Apostol MI, Thompson MJ, Balbirnie M, Wiltzius JJ, McFarlane HT, Madsen AØ, Riekel C, Eisenberg D (2007) Atomic structures of amyloid cross-β spines reveal varied steric zippers. Nature 447:453-7.

Schaffar G, Breuer P, Boteva R, Behrends C, Tzvetkov N, Strippel N, Sakahira H, Siegers K, Hayer-Hartl M, Hartl FU (2004) Cellular toxicity of polyglutamine expansion proteins: mechanism of transcription factor deactivation. Mol Cell 15:95-105.

Schiene C and Fischer G (2000) Enzymes that catalyse the restructuring of proteins. Curr Opin Struct Biol 10:40-5.

Schwarzman AL, Gregori L, Vitek MP, Lyubski S, Strittmatter WJ, Enghilde JJ, Bhasin R, Silverman J, Weisgraber KH, Coyle PK (1994) Transthyretin sequesters amyloid beta protein and prevents amyloid formation. Proc Natl Acad Sci U S A 91:8368-72.

Sekijima Y, Wiseman RL, Matteson J, Hammarström P, Miller SR, Sawkar AR, Balch WE, Kelly JW (2005) The biological and chemical basis for tissue-selective amyloid disease. Cell 121: 73–85.

Selkoe DJ (2003) Folding proteins in fatal ways. Nature 426:900-4.

Selkoe DJ (2008) Soluble oligomers of the amyloid β-protein impair synaptic plasticity and behavior. Behav Brain Res 192:106-13.

Selkoe DJ (2011) Resolving controversies on the path to Alzheimer's therapeutics. Nat Med 17:1060-5.

Seong SY and Matzinger P (2004) Hydrophobicity: an ancient damage-associated molecular pattern that initiates innate immune responses. Nat Rev Immunol 4:469-78.

Serio TR, Cashikar AG, Kowal AS, Sawicki GJ, Moslehi JJ, Serpell L, Arnsdorf MF, Lindquist SL (2000) Nucleated conformational conversion and the replication of conformational information by a prion determinant. Science 289:1317-21.

Serpell LC, Berriman J, Jakes R, Goedert M, Crowther RA (2000) Fiber diffraction of synthetic α-synuclein filaments shows amyloid-like cross-β conformation. Proc Natl Acad Sci U S A 97:4897-902.

Sharma S, Chakraborty K, Müller BK, Astola N, Tang YC, Lamb DC, Hayer-Hartl M, Hartl FU (2008) Monitoring protein conformation along the pathway of chaperonin-assisted folding. Cell 133:142-53.

Sherman MY and Goldberg AL (2001) Cellular defenses against unfolded proteins: a cell biologist thinks about neurodegenerative diseases. Neuron 29:15-32

Shirahama T, Skinner M, Westermark P, Rubinow A, Cohen AS, Brun A, Kemper TL (1982) Senile cerebral amyloid. Prealbumin as a common constituent in the neuritic plaque, in the neurofibrillary tangle, and in the microangiopathic lesion. Am J Pathol 107:41-50.

Sirangelo I, Malmo C, Iannuzzi C, Mezzogiorno A, Bianco MR, Papa M, Irace G (2004) Fibrillogenesis and cytotoxic activity of the amyloid-forming apomyoglobin mutant W7FW14F. J Biol Chem 279:13183-9.

Smith MH, Ploegh HL, Weissman JS (2011) Road to ruin: targeting proteins for degradation in the endoplasmic reticulum. Science 334:1086-90

Soprano DR, Herbert J, Soprano KJ, Schon EA, Goodman DS (1985) Demonstration of transthyretin mRNA in the brain and other extrahepatic tissues in the rat. J Biol Chem 25:11793-8.

Sousa MM, Cardoso I, Fernandes R, Guimarães A, Saraiva MJ (2001) Deposition of transthyretin in early stages of familial amyloidotic polyneuropathy: evidence for toxicity of nonfibrillar aggregates. Am J Pathol 159:1993-2000.

Stauder AJ, Dickson PW, Aldred AR, Schreiber G, Mendelsohn FA, Hudson P (1986) Synthesis of transthyretin (pre-albumin) mRNA in choroid plexus epithelial cells, localized by in situ hybridization in rat brain. J Histochem Cytochem 34:949-52.

Stefani M and Ramponi G (1995) Acylphosphate phosphohydrolases. Life Chem Rep 12:271-301.

Stefani M and Dobson CM (2003) Protein aggregation and aggregate toxicity: new insights into protein folding, misfolding diseases and biological evolution. J Mol Med (Berl). 81:678-99.

Stefani M (2010) Biochemical and biophysical features of both oligomer/fibril and cell membrane in amyloid cytotoxicity. FEBS J 277:4602-13.

Streit WJ (2002) Microglia as neuroprotective, immunocompetent cells of the CNS. Glia 40:133-9.

Strle K, Zhou JH, Shen WH, Broussard SR, Johnson RW, Freund GG, Dantzer R, Kelley KW (2001) Interleukin-10 in the brain. Crit Rev Immunol 21:427-49.

Sunde M and Blake C (1997) The structure of amyloid fibrils by electron microscopy and X-ray diffraction. Adv Protein Chem 50:123-59.

Tagawa K, Marubuchi S, Qi ML, Enokido Y, Tamura T, Inagaki R, Murata M, Kanazawa I, Wanker EE, Okazawa H (2007) The induction levels of heat shock protein 70 differentiate the vulnerabilities to mutant huntingtin among neuronal subtypes. J Neurosci 27:868-80.

Takata K, Kitamura Y, Tsuchiya D, Kawasaki T, Taniguchi T, Shimohama S (2003) Heat shock protein-90-induced microglial clearance of exogenous amyloid-β_{1-42} in rat hippocampus in vivo. Neurosci Lett 344:87-90.

Tam S, Geller R, Spiess C, Frydman J (2006) The chaperonin TRiC controls polyglutamine aggregation and toxicity through subunit-specific interactions. Nat Cell Biol 8:1155-62.

Tanskanen M, Peuralinna T, Polvikoski T, Notkola IL, Sulkava R, Hardy J, Singleton A, Kiuru-Enari S, Paetau A, Tienari PJ (2008) Senile systemic amyloidosis affects 25% of the very aged and associates with genetic variation in alpha2-macroglobulin and tau: A population-based autopsy study. Ann Med 40:232-9.

Tatini F, Pugliese AM, Traini C, Niccoli S, Maraula G, Eddami T, Mannini B, Pedata F, Casamenti F, Chiti F. Misfolded protein oligomers formed by a model protein mimic the effect of Aβ oligomers on synaptic plasticity involved in Alzheimer's disease. (unpublished).

Török M, Milton S, Kayed R, Wu P, McIntire T, Glabe CG, Langen R (2002) Structural and dynamic features of Alzheimer's Aβ peptide in amyloid fibrils studied by site-directed spin labeling. J Biol Chem 277:40810-5.

Tycko R (2003) Insights into the amyloid folding problem from solid-state NMR. Biochemistry 42:3151-9.

van Eden W (2008) XToll, a recombinant chaperonin 10 as an anti-inflammatory immunomodulator. Curr Opin Investig Drugs 9:523-33.

van Noort JM, Van Sechel AC, Bajramovic JJ, El Ouagmiri M, Polman CH, Lassmann H (1995) The small heat-shock protein αB-crystallin as candidate autoantigen in multiple sclerosis. Nature 375:798-801.

van Noort JM (2008) Stress proteins in CNS inflammation. J Pathol 214:267-75.

Vanags D, Williams B, Johnson, B, Hall S, Nash P. Taylor A, Weiss J, Feeney D (2006) Therapeutic efficacy and safety of chaperonin 10 in patients with rheumatoid arthritis: a double-blind randomized trial. Lancet 368:855-63.

Viitanen PV, Gatenby AA, Lorimer GH (1992) Purified chaperonin 60 (groEL) interacts with the nonnative states of a multitude of Escherichia coli proteins. Protein Sci 1:363-9.

Voellmy R, Boellmann F (2007) Chaperone regulation of the heat shock protein response. Adv Exp Med Biol 594:89-99.

Vilar M, Chou HT, Lührs T, Maji SK, Riek-Loher D, Verel R, Manning G, Stahlberg H, Riek R (2008) The fold of α-synuclein fibrils. Proc Natl Acad Sci USA 105:8637-42.

Walter P and Ron D (2011) The unfolded protein response: from stress pathway to homeostatic regulation. Science 334: 1081-6.

Walter S and Buchner J (2002) Molecular chaperones--cellular machines for protein folding. Angew Chem Int Ed Engl 41:1098-113.

Wang J, Dickson DW, Trojanowski JQ, Lee VM (1999) The levels of soluble versus insoluble brain Aβ distinguish Alzheimer's disease from normal and pathologic aging. Exp Neurol 158:328-37.

Wang Y, Whittall T, McGowan E, Youson J, Kelly C, Bergmeier LA (2005) Identification of stimulating and inhibitory epitopes within the heat shock protein 70 molecule that modulate cytokine production and maturation of dendritic cells. J Immunol 174:3306-16.

Waudby CA, Knowles TP, Devlin GL, Skepper JN, Ecroyd H, Carver JA, Welland ME, Christodoulou J, Dobson CM, Meehan S (2010) The interaction of alphaB-crystallin with mature alpha-synuclein amyloid fibrils inhibits their elongation. Biophys J 98:843-51.

Weibezahn J, Schlieker C, Tessarz P, Mogk A, Bukau B (2005) Novel insights into the mechanism of chaperone-assisted protein disaggregation. Biol Chem 386:739-44.

Westermark P, Benson MD, Buxbaum JN, Cohen AS, Frangione B, Ikeda S, Masters CL, Merlini G, Saraiva MJ, Sipe JD (2007) A primer of amyloid nomenclature. Amyloid 14:179-83.

White JT and Kelly JW (2001) Support for the multigenic hypothesis of amyloidosis: the binding stoichiometry of retinol-binding protein, vitamin A, and thyroid hormone

influences transthyretin amyloidogenicity in vitro. Proc Natl Acad Sci USA 98:13019-24.

Wilhelmus MMM, de Waal RMW, Verbeek MM (2007) Heat shock proteins and amateur chaperones in amyloid-β accumulation and clearance in Alzheimer's disease. Mol Neurobiol 35:203-16.

Williams B, Vanags D, Hall S, McCormack C, Foley P, Weiss J, Johnson B, Latz E Feeney D (2008) Efficacy and safety of chaperonin 10 in patients with moderate to severe plaque psoriasis: evidence of utility beyond a single indication. Arch Dermatol 144:683-5.

Wilson MR and Easterbrook-Smith SB (1992) Clusterin binds by a multivalent mechanism to the Fc and Fab regions of IgG. Biochim Biophys Acta 1159:319-26.

Wilson MR, Yerbury JJ, Poon S (2008) Potential roles of abundant extracellular chaperones in the control of amyloid formation and toxicity. Mol Biosyst 4:42-52.

Winkelmann J, Calloni G, Campioni S, Mannini B, Taddei N, Chiti F (2010) Low-level expression of a folding-incompetent protein in Escherichia coli: search for the molecular determinants of protein aggregation in vivo. J Mol Biol 398:600-13.

Winner B, Jappelli R, Maji SK, Desplats PA, Boyer L, Aigner S, Hetzer C, Loher T, Vilar M, Campioni S, Tzitzilonis C, Soragni A, Jessberger S, Mira H, Consiglio A, Pham E, Masliah E, Gage FH, Riek R (2011) In vivo demonstration that α-synuclein oligomers are toxic. Proc Natl Acad Sci U S A 108:4194-9.

Wisniewski T, Castano E, Ghiso J, Frangione B (1993) Cerebrospinal fluid inhibits Alzheimer beta-amyloid fibril formation in vitro. Ann Neurol 34:631-3.

Wogulis M, Wright S, Cunningham D, Chilcote T, Powell K, Rydel RE (2005) Nucleation-dependent polymerization is an essential component of amyloid-mediated neuronal cell death. J Neurosci 25:1071-80.

Wyatt AR, Yerbury JJ, Ecroyd H, Wilson MR (2013) Extracellular Chaperones and Proteostasis. Annu Rev Biochem [Epub ahead of print].

Yerbury JJ, Rybchyn M, Easterbrook-Smith SB, Henriques C, Wilson MR (2005) The acute phase protein haptoglobin is a mammalian extracellular chaperone with an action similar to clusterin. Biochemistry 44:10914-25.

Yerbury JJ, Poon S, Meehan S, Thompson B, Kumita JR, Dobson CM, Wilson MR (2007) The extracellular chaperone clusterin influences amyloid formation and toxicity by interacting with prefibrillar structures. FASEB J 21:2312-22.

Yerbury JJ, Kumita JR, Meehan S, Dobson CM, Wilson MR (2009) α2-macroglobulin and haptoglobin supress amyloid formation by interacting with prefibrillar protein species. J Biol Chem 284:4246-52.

Yerbury JJ and Wilson MR (2010) Extracellular chaperones modulate the effects of Alzheimer's patient cerebrospinal fluid on $A\beta_{1-42}$ toxicity and uptake. Cell Stress Chaperones. 15:115-21.

Young JC, Agashe VR, Siegers K, Hartl FU (2004) Pathways of chaperone-mediated protein folding in the cytosol. Nat Rev Mol Cell Biol 5:781-91.

Yura T, Tobe T, Ito K, Osawa T (1984) Heat shock regulatory gene (htpR) of Escherichia coli is required for growth at high temperature but is dispensable at low temperature. Proc Natl Acad Sci U S A. 81:6803-7.

Zampagni M, Cascella R, Casamenti F, Grossi C, Evangelisti E, Wright D, Becatti M, Liguri G, Mannini B, Campioni S, Chiti F, Cecchi C (2011) A comparison of the biochemical modifications caused by toxic and non-toxic protein oligomers in cells. J Cell Mol Med 15:2106-16.

Zhang Q, Powers ET, Nieva J, Huff ME, Dendle MA, Bieschke J, Glabe CG, Eschenmoser A, Wentworth P Jr, Lerner RA, Kelly JW (2004) Metabolite-initiated protein misfolding may trigger Alzheimer's disease. Proc Natl Acad Sci U S A 101:4752-7.

Zhang W, Wang T, Pei Z, Miller DS, Wu X, Block ML, Wilson B, Zhang W, Zhou Y, Hong JS, Zhang J (2005) Aggregated alpha-synuclein activates microglia: a process leading to disease progression in Parkinson's disease. FASEB J 19:533-42.

Acknowledgements

The PhD has been a special period for me, mostly because of the people that I've met and worked with. First of all, my professor Fabrizio Chiti. I would really like to thank him for being scientifically and humanly supportive and for teaching me to have an open minded approach to research. Silvia Campioni, because she gave me the foundation on which to build this PhD and has always been there for me, as a teacher and as a friend. Cintia Roodveldt and David Pozo for welcoming in their lab and making me feel at home during my stay in Seville.

A huge thank goes to Estefania and Matilde, that have shared with me hours and hours working in the lab with passion, dedication and a lot of laughter. I owe more than I can say in words to my amazing friends and colleagues that I have been so lucky to meet: the sunny and encouraging Camilla, Francesca generous and full of original ideas, Neda smart and with a big heart, Edda being able to make me smile even in the worst situations. The wise "fatherly" Bemporad and Tommaso willing to give his time for helping me even at the very last moment.

I wish to thank my big family, my grandparents, Deanna and Lorenza, Roberto for being my personal informatics engineer, Bianca, Giulio, Marco, Elena, Alessandro and Gabriele for becoming promptly familiar with the bibliography cited in this thesis.

Finally, my father and my mother for their love and patience.